2012

GIS-based urban land use characterization and population modeling with subpixel information measured from remote sensing data

Quan Tang
Louisiana State University and Agricultural and Mechanical College, qtang3@lsu.edu

GIS-BASED URBAN LAND USE CHARACTERIZATION AND POPUALTION MODELING WITH SUBPIXEL INFORMTION MEASURED FROM REMOTE SENSING DATA

A Dissertation

Submitted to the Graduate Faculty of the
Louisiana State University and
Agricultural and Mechanical College
in partial fulfillment of the
requirements for the degree of
Doctor of Philosophy

in
The Department of Geography and Anthropology

by
Quan Tang
B.M., China Agricultural University, 2005
M.S., Chinese Academy of Sciences, 2008
M.S., Louisiana State University, 2011
August 2012

Acknowledgments

This dissertation would not be made possible without the patient and valuable advice, guidance, and support from my academic advisor, Dr. Lei Wang. His well-developed research philosophy, from formulating the research question to journal article writing, has been influencing me all the time. I am deeply grateful to him. Thanks are also extended to the other three committee members for their advice and help on my doctoral research. Specifically, I would like to thank Dr. Fahui Wang for his advice on the population modeling research and his hospitality throughout my four-year Ph.D life. I thank Mr. Dewitt Braud for his help on the image mosaicking and Dr. Bin Li for his data mining class that led me to the door of machine learning. I thank Dean's representative Dr. Kenneth A. Rose for his advice made during my proposal defense and the final defense.

I also want to thank the department secretary Ms. Dana C. Sanders for her consistent patience and kindness in processing my paperwork and answering my questions regarding international students. I owe a lot to my fellow students of Department of Geography and Anthropology at LSU for their help and support on my study and research, and most importantly, for the good time we get together.

My biggest grateful appreciation goes to my family members. I am very grateful to my parents and in-laws for their everlasting mental support. I thank my wife, Jing Li, for her understanding, support, and encouragements along the way.

Finally, I would like to acknowledge that my Ph.D study and the research are financially supported by LSU Flagship Assistantship for 2008~2012 academic years and Department of Geography and Anthropology.

Table of Contents

List of Tables

List of Figures

Abstract

This dissertation provides deeper understanding on the application of Vegetation-Impervious Surface-Soil (V-I-S) model in the urban land use characterization and population modeling, focusing on New Orleans area.

Previous research on the V-I-S model used in urban land use classification emphasized on the accuracy improvement while ignoring the discussion of the stability of classifiers. I developed an evaluation framework by using randomization techniques and decision tree method to assess and compare the performance of classifiers and input features. The proposed evaluation framework is applied to demonstrate the superiority of V-I-S fractions and LST for urban land use classification. It could also be applied to the assessment of input features and classifiers for other remote sensing image classification context.

An innovative urban land use classification based on the V-I-S model is implemented and tested in this dissertation. Due to the shape of the V-I-S bivariate histogram that resembles topological surfaces, a pattern that honors the Lu-Weng's urban model, the V-I-S feature space is rasterized into grey-scale image and subsequently partitioned by marker-controlled watershed segmentation, leading to an urban land use classification. This new approach is proven to be insensitive to the selection of initial markers as long as they are positioned around the underlying watershed centers.

This dissertation links the population distribution of New Orleans with its physiogeographic conditions indicated by the V-I-S sub-pixel composition and the land use information. It shows that the V-I-S fractions cannot be directly used to model the population distribution. Both the OLS and GWR models produced poor model fit. In

contrast, the land use information extracted from the V-I-S information and LST significantly improved regression models. A three-class land use model is fitted adequately. The GWR model reveals the spatial nonstationarity as the relationship between the population distribution and the land use is relatively poor in the city center and becomes stronger towards the city fringe, depicting a classic urban concentric pattern. It highlighted that New Orleans is a complex metropolitan area, and its population distribution cannot be fully modeled with the physiogeographic measurements.

Chapter 1 Introduction

Urban is a complex dynamic dissipative system, characterized by massive energy and heat exchange with the outside environment and frequent modifications due to the human occupation and activity. Urban analysis is one of the most fascinating and challenging realms in remote sensing and geographic information science (GIS). The urban land use pattern and the urban population distribution represent the physical and socioeconomic environment of an urban area, revealing the urban structure from two distinct aspects. The knowledge about the urban land use and land cover (LULC) provides indispensable input for a variety of studies including urban planning, urban climate, urban hydrology and urban landscape, etc. However, reliable urban land characterization in a quick and repetitive manner still present challenges due to the heterogeneity and complexity of urban physical environment. Urban population distribution is also an essential feature for urban analysis. However, the demographic survey and update is a time-consuming and costly undertaking that involves tremendous field work and human resources. In the United States, the national demographic data is collected via the decennial census survey by the United States Census Bureau (USCB). In some developing counties, such a census survey system may not even exist. This large census interval and gap hinges researches and applications that require demographic input.

These two urban features are also associated with each other. On one hand, human activities impact and alter the urban landscape (such as, urbanization and suburbanization,

Kaplan et al. 2008) and also produce the so-called urban head island (UHI, Kim 1992, Voogt 2003, Weng 2009). On the other hand, miscellaneous urban landscape and different living environments, in return, also play important roles in directing or reflecting the immigration of population. Recent literature has witnessed a growing interest and application of using physiogeographic conditions derived from remotely sensed signals in modeling the urban population. This dedicated dissertation works on the advances in the development of quick and reliable methods to characterize urban land use patterns and the urban population distribution modeling based on the subpixel information and land use information.

1.1 Literature Review

1.1.1 Urban land characterization

The urban landscape is composed of dynamic and complex land use features. The remote sensing image classification has been widely employed to obtain historical and present the LULC conditions (Anderson et al. 1976, Jensen 2007). Although being referred to interchangeably, the concept of "land use" (LU) and the concept of "land cover" (LC) are intrinsically distinct with respect to the natural and anthropogenic urban landscape. LC refers to the physical properties of the earth surface, which can be directly identified from the spectral characteristics; while LU, mostly being associated with large scale researches, represents a higher level understanding of the earth surface and is inferred from the land cover composition and configuration (Mesev 2010). Normally, a LU class (e.g. information class) is from by a certain spatial composition and arrangement of several LC classes (e.g. spectral class) (Herold et al. 2003). Previously, only spectral information obtained from remotely sensed images (such as the band

spectral reflectance/radiance, band ratio, vegetation indices, etc.) was used for LULC classification, which mainly produced LC classes. In addition, the process of assigning pixel to a certain "spectral class" is ambiguous. For instance, a pixel spectrally resembling the forest class might actually be enclosed in the "commercial" land use area, e.g. a small tree-stand isolated in the central business district (CBD) area. The "salt-and-pepper" appearance from traditional image classification methods was also produced in this manner. They are all due to the lack of consideration of the spatial configuration and arrangement of pixels, especially when high-resolution images are used. To solve the problem, there have been three ways suggested in the literature to embrace spatial information in urban land use classification:

- Spectral mixture (sub-pixel analysis) techniques with medium resolution image (Adams et al. 1995, Li and Zhao 2003, Lu and Weng 2004, Lu and Weng 2005, Lu and Weng 2006, Ridd 1995, Souza et al. 2005, Ward et al. 2000);
- To use textures and spatial metrics calculated from individual pixel and its neighbors in high resolution images (Berberoglu et al. 2000, Carr 1996, Chica-Olmo and Abarca-Hernández 2000, Emerson et al. 2005, Franklin and Peddle 1990, Gong et al. 1992, Haralick et al. 1973, Herold et al. 2003, Herold et al. 2002, Lark 1996, Lu et al. 2010, Myint 2003, Myint and Lam 2005a, Myint et al. 2006, Wu et al. 2006);
- To use image object produced by aggregating pixels instead of single pixel as the basic unit for classification, so spatial arrangement and configuration of these pixels in image objects could be derived and used (Baatz and Schäpe 2000, Myint et al. 2011, Wang et al. 2004, Xu and Li 2010, Zhou and Troy 2008).

Poorly selected classifiers also produced problems. Parametric classifier, such as the widely-used Bayesian approach (e.g. maximum likelihood classifier, MLC), requires homogeneity and normality assumptions. Yet selections of training samples and classes that satisfy these assumptions remained a challenge (Myint and Lam 2005a).

1.1.1.1 Vegetation-Impervious Surface-Soil model

The V-I-S model (Ridd 1995) has brought the investigation and mapping of urban landscape into a new era. V-I-S model assumes that urban land use patterns are formed by different configuration of three primitive components, namely, Vegetation and Impervious Surface and Soil. V-I-S fractions are generally derived from the medium resolution image and reflect the biophysical and morphological composition and configuration of the urban land use patterns (Figure 1.1). Due to the heterogeneity issue of the Impervious Surface component and the fact that the V-I-S model didn't include the Shade/Shadow component that is incurred by tall buildings and trees (Weng and Quattrochi 2007) , the V-I-S model is also adjusted in different study areas, giving rise to several similar models. Among them were V(egetation), L(ow Albedo) and H(igh Albedo) model (Small 2001); V(egetation), L(ow Albedo), H(igh Albedo) and S(hade) model (Weng et al. 2006, Wu and Murray 2003); S(ubstrate),V(egetation) and D(ark Surface) model (Small and Lu 2006). Subsequent classifications based on the V-I-S fractions were proven to be more accurate for quantifying the urban morphology and characterizing the urban landscape (Lu and Weng 2006, Weng et al. 2007, Weng and Quattrochi 2007). V-I-S model and its variants were utilized extensively in urban landscape mapping(Hu and Weng 2009, Lu et al. 2003, Lu and Weng 2004, Lu and Weng 2005, Lu and Weng 2006, Rashed et al. 2001, Rashed et al. 2003, Small 2001, Small and Lu 2006, Weng and Hu

2008), urban sprawl analysis (Kaya et al. 2004, Li and Zhao 2003, Madhavan et al. 2001, Phinn et al. 2002, Ward et al. 2000, Yang et al. 2003b) and urban heat island (UHI) studies (Weng 2001, Weng et al. 2007, Weng et al. 2006, Weng et al. 2004, Yuan and Bauer 2007).

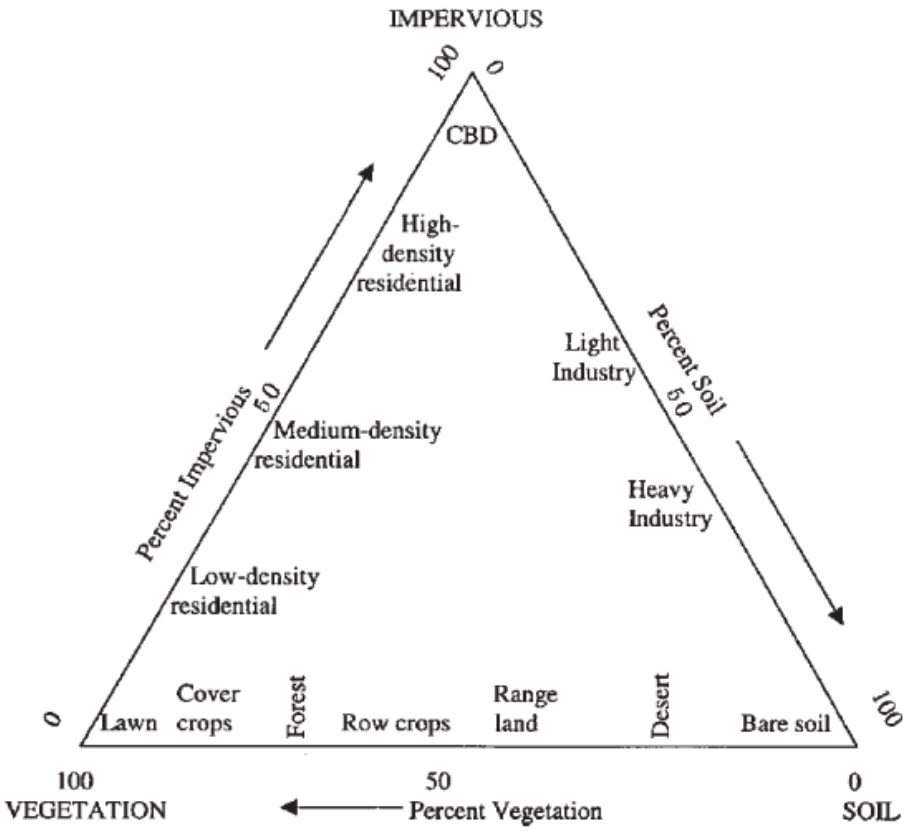

Figure 1-1 Ternary feature space visualization of V-I-S model and its relation to urban land use (Source: Ridd 1995)

1.1.1.2 Textures and Spatial Metrics

Conventional spectral based classification techniques have been criticized for its lack of consideration of spatial configuration and arrangement of image's pixel. Textures derived from remote sensing images have bridged the hole, providing the spatial information for the classification. The most frequently used texture is the Grey Level Co-occurrence Matrix (GLCM, Haralick et al. 1973). GLCM-based textures have been

extensively used in assisting the urban LULC classification (Franklin et al. 2000, Franklin and Peddle 1989, 1990, Gong et al. 1992, Herold et al. 2003, Lu et al. 2010, Ravikumar 2008, Van Coillie et al. 2007). Semi-variance is another texture statistics that describes the spatial variability and models the dependence and correlation of pixels with its neighborhoods respect to distance and direction (Chica-Olmo and Abarca-Hernández 2000, Lark 1996). Lark derived a statistic that incorporates the difference of DN values of pixels separated by particular spatial interval (lag) and direction, which later made important contribution to the discrimination of land cover classes (Lark 1996). Semi-variances at different lag could be fitted using theoretical functions, producing so-called variogram to reveal the spatial autocorrelation (Lloyd 2006). Research effects have been devoted in utilizing coefficients of fitted theoretical variogram functions and the semi-variances at various lags as texture measures in assisting characterizing urban land use and land cover pattern (Berberoglu et al. 2000, Carr 1996, Chen and Gong 2004, Chica-Olmo and Abarca-Hernández 2000, Lark 1996, Maillard 2003, Wu et al. 2006).

While texture measurements are based on the continuous grey-level pixels, spatial metrics is mostly based on a categorical patch-based representation of the urban landscape (Herold et al. 2003). Usually, a patch is a clump of aggregated pixels as a homogeneous region. The minimum spatial unit for classification is composed of several adjacent patches, called land use regions (Herold et al. 2003). The landscape metrics (aka spatial metrics) were derived to measure the arrangement and configuration of patches and pixels in each land use region for classification (Gustafson 1998, Mcgarigal et al. 2002). Spatial metrics describe the configurations and patterns of urban landscape and are useful for urban land characterization (Herold et al. 2003, Herold et al. 2002). For

example, Herold et al. (2003) developed a spatial-metrics-based technique for land use classification. Given the fact that the land use object is composed of land cover objects, Herold firstly classified the IKONOS image to generate land cover objects (aka patches) of three kinds (e.g. buildings, green vegetation and the rest) using object-oriented classification. Then, ancillary data was used to aggregate the land cover objects into land use regions, which are the basic spatial units for the subsequent land use classification. Seven GLCM-based textures and 22 spatial metrics measurements were derived for each land use region. The final classification demonstrated the successfulness of the incorporation of conventional textural statistics and spatial metrics. Spatial metrics were also used in investigating other urban phenomenon, such as population distribution (Liu et al. 2006).

1.1.1.3 Object oriented approach

The object-oriented classification method developed recently is capable of generating more accurate LULC classes due to its consideration of spatial configuration and arrangement of pixels. The object-oriented classification introduces multi-resolution image segmentation and further develops a hierarchical network of image objects at various scales. Image segmentation is a bottom-to-up region-growing process that depends on the color (spectral), shape (spatial compactness and smoothness), texture and contextual information and aggregates pixels into homogenous image object primitives (Baatz and Schäpe 1999, 2000, Benz et al. 2004), which are the basic units for the subsequent classification. The scale parameter defines the stop criteria for merging the pixels or small image objects into larger ones (Baatz and Schäpe 1999, 2000, Benz et al. 2004). A high scale parameter would lead to large image objects with excessive

heterogeneity (under-segmentation) whilst a low scale parameter would lead to many tiny image objects (over segmentation) that ar**e** no different from individual pixels as they cannot capture meaningful spatial and spectral homogeneity. Therefore, selecting the scale parameter is crucial in image segmentation. The heterogeneity of every image object is dependent on the spectral color and shape of that image object. The ratio of their contribution to heterogeneity is defined by the color and shape parameter (Baatz and Schäpe 2000). The optimum output of the image segmentation is the maximized intra-object homogeneity and inter-object heterogeneity. After the image segmentation, a rule-based fuzzy classification (similar to traditional pixel-based decision-tree classification) or a nearest neighbor (NN) classification (similar to traditional pixel-based supervised classification) or a combination of both will follow using these image objects instead of single pixel (Baatz and Schäpe 1999, 2000, Benz et al. 2004). The member functions in fuzzy classification determine that to what extent a certain image object should be classified to a certain class by using expert knowledge.

Object-oriented classification has been applied widely on remote sensing images with high spatial resolution, such as IKONOS and QuickBird. A variety of spectral (e.g. band ratio, vegetation indices, texture, etc.) and spatial (e.g. shape, area, elongation, perimeter, roundness, etc.) attributes of image objects were used to determine the fuzzy rules for classification. For instance, a rectangle-shaped medium-sized image object with low Normalized Difference Vegetation Index (NDVI) derived from high resolution images should be classified as “rooftop” instead of “transportation road” or “parking lot” (Hu and Weng 2010b). Nevertheless, the spectral resemblance of these three categories would make them otherwise not separable if spatial information is not considered. In the

literature, representative applications of object-oriented classification include but not are limited to: urban impervious surface mapping (Hu and Weng 2010b, Li et al. 2010a, Yuan and Bauer 2006, Zhou and Wang 2008), LULC mapping(Geneletti and Gorte 2003, Myint et al. 2011, Shackelford and Davis 2003, Xu and Li 2010, Zhou and Troy 2008), change detection (Walter 2004), building extraction and damage detection (Li et al. 2010b, Liu et al. 2005), mangroves mapping (Myint et al. 2008, Wang et al. 2004), forest mapping (Van Coillie et al. 2007), shrub encroachment monitoring (Laliberte et al. 2004) and more.

1.1.2 Urban population modeling

Demographic data is mainly collected to match with the political administrative divisions (such as, census tract, census block, etc). However, this does not necessarily mean the underlying phenomenon matches with these arbitrary definitions of areas (Eicher and Brewer 2001). Early population modelers were interested in disaggregating population to finer spatial unit and probably also re-aggregate them into another (target layer). The former leads to "dasymetric mapping" (without re-aggregation) and the latter (with re-aggregation) is called "areal interpolation". Nowadays, remote sensing provides an efficient and repetitive way to derive physiogeographic variables that are related to population to predict population distribution using regressions. More advanced population regression models may consider the spatial pattern and spatial nonstationarity.

1.1.2.1 Areal interpolation and dasymetric mapping

The most-developed areal interpolation technique is the weighted areal interpolation (Goodchild et al. 1993, Goodchild and Lam 1980, Lam 1983). The weighted areal interpolation performs spatial intersect firstly between the source layer and the target

layer, producing spatial segments and partitioning the population in the source spatial features proportionally to the area. The resultant population for the target spatial feature is calculated as the sum of population in the constituent spatial segments. Although the assumption of proportionality is ideal, weighted areal interpolation needs no ancillary data inputs and is easy to implement in a GIS environment.

"Dasymetric mapping" refers to techniques that disaggregate spatial data into finer zones in a fashion that maximizes the inter-zonal heterogeneity and maximizes the intra-zonal heterogeneity. Ancillary information is generally required to do so (usually, land use information). It departs from the "areal interpolation" method as the disaggregation process is not based on the area and there is no re-aggregation process. Dasymetric mapping is a remedy to the problematic assumption of an even distribution of population regardless of the underlying land use patterns. Land use information was used in the dasymetric mapping of population by Wright (1936) in his seminal paper when GIS was not even an ubiquitous tool. Wright categorized the land use types into "populated" and "unpopulated" and distributed the population only to the "populated" area to produce a more reasonable demographic map. This binary case was later extended by Mennis (2003) and Langford (2006) in three-class applications. Frequent and efficient dasymetric estimation of population was made feasible when satellite and aerial images assist by providing land use information through image processing and classification. The drawback of dasymetric mapping is that the average population density for each land use class is assumed to be fixed and need to be estimated through regressions or directly required from the previous empirical studies, meaning that dasymetric mapping neglected the possible heterogeneity within land use classes (Liu 2003, Maantay et al. 2007).

In addition to polygonal approach, the pixel-based dasymetric mapping was also studied since remote sensing images played an important role as the data source. Pixel based estimations generate the population surface and are believed to be one of the solutions to the *modifiable areal unit problem* (MAUP) that was always encountered in the polygonal dasymetric mapping practices (Harvey 2002a, Mennis 2003). Tobler (1979) proposed a "pycnophylactic interpolation" approach to conduct volume-preserving interpolation of smooth surface for areal measurement. He adopted a lattice of point superimposed on the polygon feature, and by using iterative calculations he adjusted the values assigned to each point in the lattice preserving the sum for each polygon-defined region (pycnophylactic property) whilst enhancing the smoothness. This method was extended by replacing the lattice with the Triangular Irregular Network (TIN) (Rase 2001). Although TIN introduced the difficulty in implementation, it had the advantages in delineating polygons more precisely, especially for irregular polygons. Tobler's method and the like were mathematical smoothing techniques that didn't use any other ancillary data input for population estimation and thus compromised their reliability. Other population surface generation endeavors using dasymetric techniques can be found in Martin (1989), Langford and Unwin (1994) and Mennis (2003).

1.1.2.2 Conventional regression

Modern and more robust population modeling methods prefer statistical tools. The rationale is the underlying relationship between the population distribution and the socioeconomic and physiogeographic conditions of residential areas. Linear regression models establish the empirical relationship between population/population density (or their transformations) and multiple predictive variables. The increasing availability and

resolution of remote sensing images provide the ancillary data for population estimation besides census data. Physiogeographic information extracted from the remote sensing images was widely used in the regressions on population. Among them were spectral reflectance (Hsu 1973, Iisaka and Hegedus 1982, Lo 1995), night-time illumination (Dobson et al. 2000, Lo 2001, Sutton 1997), vegetation indices (Li and Weng 2005), land use and land cover (Dobson et al. 2000, Langford et al. 1991, Lo 1995, Mennis 2003, Yuan et al. 1997), sub-pixel fractions (Li and Weng 2005, Lu and Weng 2006, Morton and Yuan 2009), textures (Li and Weng 2005, Liu et al. 2006), temperature (Li and Weng 2005) and spatial metrics (Liu 2003). Harvey (2002b) developed a method in which the population count for individual TM pixel was updated by iteratively using an OLS (Ordinary Least Square) calibration until convergence is achieved. His method used band reflectance and band-to-band ratio as the predictive variables in the regression. Liu et al. (2006) used three different indicators of texture: the GLCM, semi-variance, and spatial metrics in predicting the population at a homogenous urban patches level for the Santa Barbara and highlighted that spatial metrics was the superior predictor. Previous studies on the population regression showed that the estimations tend to be subjected to relative large bias (underestimation of high population densities and overestimation of low population densities) when population density is at its extremes (e.g. very high or very low, Harvey 2002a, Li and Weng 2005). Three remedies were reported in the literature to deal with this problem: stratification, scaling and pixel-based regression. Li and Weng (2005) used multiple linear regressions to estimate the population density for the city of Indianapolis, Indiana and found out the model fit was improved after a stratification based on the population density into three categories (low, medium and high residential).

Lo (2003) divided the census tracts of Atlanta into two groups (the periphery and the center) to improve the population estimation. The allometric models were developed for each group for two time periods (1990 and 1997) and slight improvement of the model accuracy was achieved after the stratification. Yuan et al. (1997) employed the regional regression and scaling techniques to improve the estimation performances. Harvey (2002a) compared the zone-based approach (Census Collection Districts of Australian cities) and pixel-based approach (TM imagery). The pixel-based approach utilized the untransformed TM six bands in the regression in an iterative manner and was more robust at the extremes of population density. Similar work and consistent conclusion can be found in Wu and Murray (2005).

1.1.2.3 Considering the spatial dependency and spatial nonstationarity

In a geographical research, the variable of interest usually demonstrates the spatial dependency and spatial nonstationarity; hence the conventional linear regression as a global analysis is incapable of capturing the local variation and characteristics (Brunsdon et al. 1998, Foody 2003, Fotheringham et al. 2002, Fotheringham et al. 1998). Population distribution is spatially auto-correlated. To address the issue of spatial autocorrelation, spatial dependence and spatial heterogeneity of the relationship in the context of the geographical research, two spatial analysis methods, namely, geographically weighted regression (GWR) and spatial autoregressive regression, were employed in a variety of applications.

Geographically weighted regression (GWR) is a well-established regional regression technique developed by Fotheringham et al. (1998) that assigns weights to individual observation according to their distances to the local regression location. It follows that

estimated coefficients of GWR model vary spatially. Geographical patterns, local patterns and local goodness-of-fit can be mapped and compared in a GIS environment. Many successful researches using GWR in all kinds of geographical scales followed. Other than the population modeling, the application of GWR can also be found in regional development mechanism studies (Yu 2006), urban growth (Mark et al. 2008), NDVI-rainfall relations (Foody 2003) and so on.

Attempts of applying GWR or regional regression in population estimation were new tracks in the literature recently. Yuan et al. (1997) conducted a land-use based dasymetric mapping globally in the entire study area in Arkansas as a whole and for its regional four individual counties. Three out of the four county models were found to outperform the global model in terms of goodness of fit. Langford (2006) reported a better regional regression models between population and land cover as opposed to a global approach and confirmed the spatial nonstationarity in his study. Yu and Wu (2004) used both GWR and OLS to estimate the local segregation index at census group level using variable extracted from the ETM+ imagery, demonstrating that GWR was able to capture local patterns. Liu et al. (2006) utilized GWR on population with spatial metrics and the population density for Santa Barbara south coastal urban area. The slope estimate varied geographically for all the spatial metrics used. High R^2 was found at low and intermediate populated areas. Lo (2008) fitted both of the OLS and GWR based on a four-class land use model and reported a 28% increase of the model performance for local GWR model. It was also revealed in his study that a regional regression approach based on the census tracts aggregated by counties was superior to the global OLS model.

Autocorrelation and spatial dependence are always violations of regular regression assumptions. Spatial econometrics is an analogous discipline to the classical Econometrics (Anselin 1988), and temporal autocorrelation and spatial autocorrelation are analogous counterparts in these two disciplines. There are three major spatial autoregressive regression models (Baller et al. 2001, Fotheringham et al. 2000): spatial lag model, spatial error model and spatial autoregressive moving average model. Chi and Zhu (2008) gave a comprehensive review of many aspects and issues that relate to the application of spatial autoregressive regression in demographic analysis in the context of ESDA (Exploratory Spatial Data Analysis). Griffith and Wong (2007) used spatial autoregressive regression to deal with the spatial autocorrelation problem with case studies on the 20 largest metropolitan areas in the US according to the 2000 census, and reports good fits for both mono-centric and polycentric cities.

1.2 Problem statement and research hypothesis

Several research gaps can be found in the practice of urban land use mapping. Although as reported in the current literature, V-I-S fractions and LST were proven to be more accurate in characterizing the urban landscape and qualifying the urban morphology due to their consideration of the land cover mixture characteristics of the urban land use, there was a scarcity of studies focusing on the stability of classifiers built on V-I-S fractions and LST. Although the superiority of V-I-S fractions over the multispectral reflectance as input features in urban land use classification was well identified, current explorations and discussions only emphasized the accuracy improvement, seldom was their superiority viewed comprehensively from both accuracy and model stability. Moreover, classification methods applied with V-I-S fractions were conventional

approaches, namely, the MLC(Lu et al. 2003, Lu and Weng 2004, Lu and Weng 2005, Lu and Weng 2006, Rashed et al. 2001), and decision tree(Lu and Weng 2004, Rashed et al. 2001), failing to embrace other promising modern classifiers, such as the support vector machine (SVM) and the ensemble classifiers, that attracted interests in the remote sensing science community. All of these research gaps also hold true for land surface temperature (LST) variable used as input for characterizing urban land use. LST derived from thermal bands was also found closely related to urban biophysical characteristics, and was applied to studies on UHI, LULC mapping and urban sprawl (Lo et al. 1997, Weng 2001, Weng 2009, Weng et al. 2007). The accuracy and stability performance of the collaboration of V-I-S fractions and LST in the urban land use classification remained an unanswered yet interesting question. Given the success and popularity of object-oriented classification in the recent literature, the study on applying object-oriented classification based on V-I-S fractions and LST was also uncommon; and the optimal classifier and the stability of object-oriented classification in this context were unknown to the urban remote sensing researchers.

The second problem lies in the population modeling with remote sensing data. Although V-I-S fraction images have been used in regression with urban population and success applications were reported extensively, it is still questionable if such models can be generalized to other places in the world.

I have the following hypotheses to be tested in the research:

1. The superiority of classifiers can be evaluated by using a randomization approach and the Kappa-error diagram by the evaluation framework introduced in chapter 2. This hypothesis is tested in chapter 3.

2. The superiority of input features for image classification can be evaluated by looking at the tree depth and complexity. This hypothesis is tested in chapter 3.

3. The urban land use classes can be extracted from applying watershed segmentation on the V-I-S feature space image. This hypothesis is tested in chapter 4.

4. The use of V-I-S fractions and land use information extracted from remote sensing images can result in efficient regression models for modeling and predicting urban population distribution in New Orleans. The relationship between urban population distribution and these physiogeographic measurements exhibits spatial nonstationarity. These hypotheses are tested in chapter 5.

1.3 Research design

1.3.1 Study area

This research uses New Orleans as the study area. New Orleans is the largest city in the Louisiana State and is a metropolitan area with modern industrial and ethnic development despite of its geographical location being around a hurricane-threatened community. New Orleans is in the subtropical environment and undergoes evident UHI effect, especially in the warm weather due to large amounts of paved and dark colored surfaces and the greenhouse gas release in urban communities (Baseline Greenhouse Gas Emission Profile, 2001). The dynamic land use of New Orleans made it a good place for urban LULC studies.

New Orleans is sandwiched between the Lake Pontchartrain, Mississippi River and the Gulf of Mexico. The topography of New Orleans resembles a bowl with the northern part having the lowest elevation. The flow of the Mississippi river across the city resembles an up-side-down Ω symbol. The major part of the city is also below the sea

level. All of these drawbacks made New Orleans exposed to a variety of periodic natural disasters, such as hurricanes, flooding and storm surge. The population of New Orleans experienced massive decline during the last decade due to the natural hazards (especially Hurricane Katrina). These natural hazards have resulted in a large displacement of New Orleans' residents of different race, age and socioeconomic status (Fussell et al. 2010, Groen and Polivka 2009). A challenging opportunity is to study the urban population and population decline and its relationship with community vulnerability reflected from the socioeconomic and physiogeographic conditions, so to help better understanding of disaster prevention, vulnerability, and resilience of the coastal communities. Modern geospatial technologies from GIS and remote sensing have laid a solid foundation for such a research.

1.3.2 Methods and data flows

Multiple GIS, remote sensing, and statistical methods are adopted in this research. Based on a randomization technique in statistics, I constructed an evaluation framework for selecting optimal input feature and classifiers (algorithm) for land use and land cover classification. The evaluation framework put emphasize on the discussion of stability of classifiers. Such an evaluation framework can provide valuable guidance to land use and land cover classification in remote sensing.

By using the evaluation framework, multiple combinations of input data (band reflectance, V-I-S fraction images, and LST) and algorithms (maximum likelihood classifier, support vector machine, classification tree, random forest, etc.) are compared and evaluated in the study area by using the Landsat TM data. The interest is to test whether or not the use of V-I-S fraction images and LST could significantly improve the

accuracy and stability of supervised classification in both pixel-based and object-based approaches as opposed to the conventional spectral reflectance variables in the urban land use classification.

In this research I developed an innovated approach of land use classification as the marker-controlled watershed segmentation in the V-I-S feature space (e.g., histogram). This method extends Ridd's V-I-S model (Ridd 1995) and Lu-Weng's urban land use model (Lu and Weng 2006), by collapsing land cover classes (V-I-S) to land use classes in a triangulated coordinate system in the V-I-S feature space. This is the first realization of the conceptual urban feature space triangle models for land use classification. Watershed segmentation defines "watersheds" from the pixel clusters, which are a nature form of urban land use structures in the V-I-S feature space. Markers are used to control the number of "watersheds" to avoid over-segmentation. This watershed-segmentation based approach is data driven and easy to implement.

It is interesting to know if the V-I-S image fractions or the derived LULC information from the preceding analysis can be used as explanatory variables to estimate population in New Orleans. If it holds true, it is possible to use remote sensing to fuse intercensal gaps of population data, and therefore to facilitate the study of population dynamics and people's migration pattern. First, the global Ordinate Least Square (OLS) regression is evaluated. The residual map of the OLS regression would reveal if there is any spatial nonstationarity in the model. If strong spatial nonstationarity is identified, a local regression model (e.g., GWR) would be preferred.

Figure 1.2 displays the methodology and the data flow of this research.

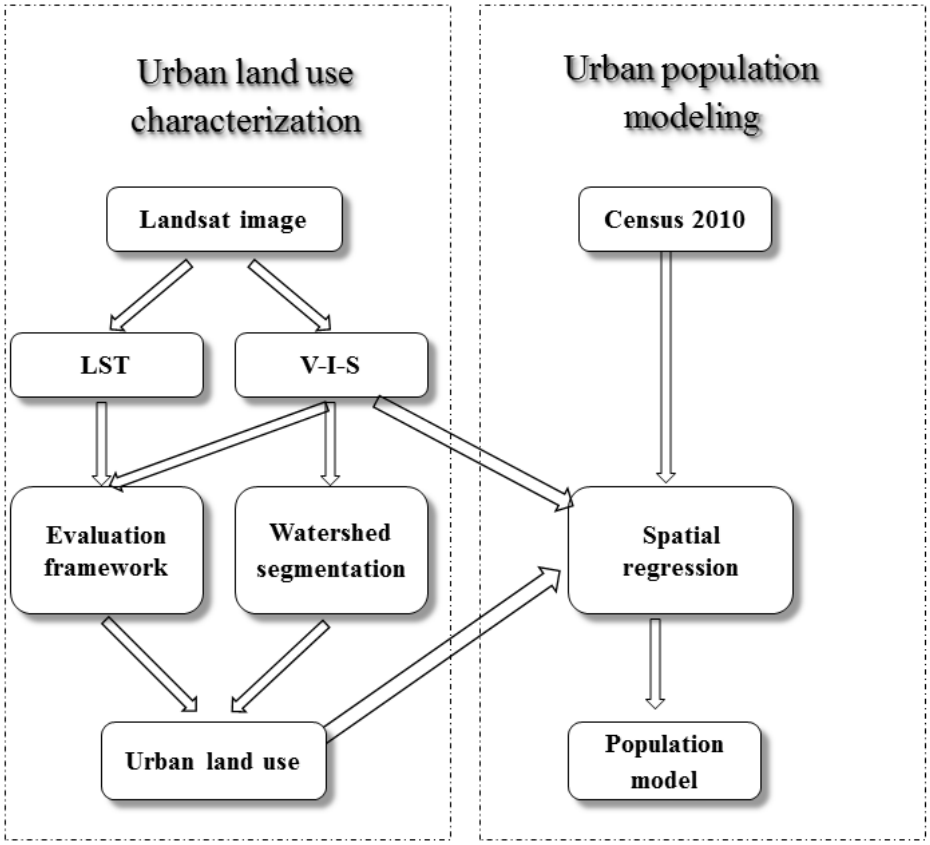

Figure 1-2 Research design and data flows

The objectives of this research are:

1. to establish several reliable remote sensing image classification methodologies for urban land use characterization;
2. to select an appropriate regression model for urban population from remotely sensed information;
3. and to study the pattern of population distribution and relate it to the V-I-S fractions and land use information.

Specifically, upon finishing the dissertation, the following research questions are to be answered:

1. Is the evaluation framework capable of providing comprehensive assessment of V-I-S fractions and LST in urban land use mapping?
2. In addition to the accuracy improvement, would the incorporation of V-I-S fractions and LST also be able to improve the stability of classifier?
3. Are there optimal classifiers associated with the V-I-S fractions and LST or their combination as input?
4. According to the evaluation framework, would the object-oriented classification benefit the accuracy or stability? What is the optimal classifier in this context?
5. Would the marker-controlled watershed segmentation in the V-I-S feature space provide a good classification result?
6. Is there a strong association between the 2010 population and V-I-S sub-pixel information and the urban LULC from remote sensing?

1.4 Significance of the research

This dissertation will contribute to the GIS and remote sensing application in urban geography in general and in the following specific aspects:

- This research extends the V-I-S urban remote sensing model and classification by introducing an innovative comprehensive evaluation framework for guiding the selection of classifiers and input data. The significance of the evaluation framework is that, in addition to the traditionally performed accuracy assessment, it can provide the assessment of classifiers' stability. Although the evaluation framework is initially

developed for urban land use research, it could be future extended to the general applications of remote sensing image classification.

- This research is among the few to provide comprehensive comparisons and evaluations of multiple types of input (band reflectance, V-I-S fractions and LST) plus a variety of classifiers (MLC, SVM, decision tree, random forest). The evaluation results and conclusions would guide remote sensing practitioners and urban planners in their future work of urban land use characterization.
- This research is the very first to rasterize the Ridd's V-I-S triangle model (Ridd 1995) and Lu-Weng's triangle model (Lu and Weng 2006) to visualize the V-I-S feature space, which is followed by the development of an innovated method of using marker-controlled watershed segmentation processing algorithm to partition the V-I-S feature space in the rasterized triangle system. The new method can directly transform V-I-S fraction images to urban land use classes that match with the previously defined urban land use conceptual models.
- This research would also shed lights on the understanding of the population distribution in a disaster-prone urban area of New Orleans and relate it to the physiogeographic conditions derived from remote sensing data.

1.5 Chapter organization

The rest of this dissertation is divided into six chapters. Chapter 2 elaborates the evaluation framework to assess the performance of input features and classifiers used in remote sensing image classification. Chapter 3 applies this proposed evaluation framework in the context of both pixel-based classification and object oriented classification to evaluate the benefits of using the V-I-S fractions and LST in urban land

use classification and to reveal the superiority of these inputs. Chapter 4 introduces the developed marker-controlled watershed segmentation in the V-I-S feature space for urban land use classification. Chapter 5 investigates the urban population distribution of New Orleans with the V-I-S sub-pixel information and the land use characterization. Summary of findings and contributions of the dissertation and future research tracks could be found in Chapter 6. Chapter 3~5 can also be regarded as standalone journal-style articles, which are also related to one another under the central topic of the dissertation.

Chapter 2 A comprehensive evaluation framework for assessing classifiers and input features

Previously, comparisons of input features and the classifier selection were limited to the overall classification accuracy or the Kappa statistics. However, it is could be questionable for the accuracy reported from one sample of the data set because the accuracy might be different if another set of training and testing sample data is used. This potential variability in the accuracy brings up the definition of classifiers' stability, namely, a measure of the consistency in classification decisions generated from different samples. This chapter describes the evaluation framework which takes into account for both the classifiers' accuracy and stability. This evaluation framework can also assess the importance of input features in the classification. I also introduce the classifiers that are used and compared in our research. This chapter illustrates tools we used to answer research question 1~4. The application of the framework is in Chapter 3.

2.1 Overview of the evaluation framework

The evaluation framework employs the classification tree technique to evaluate the importance/superiority of input features and the randomization technique to evaluate the classifiers' performance in both accuracy and stability. Figure 2.1(*a*) displays the three criteria for evaluating input features. Specifically, the classification tree structure and the sequence of variable being selected for branch splitting of trees are used to indicate the input feature's superiority. A random forest of trees is considered by using these two criteria to draw conclusions with statistical significance. The increase of the badness-of-fit on the Out-of-Bag (OOB) samples is also employed to reveal the superiority of input features. The evaluation of classifiers is depicted in Figure 2.1(*b*) from two aspects: the

Kappa-Error diagram and the ANOVA test. The following subsections elaborate the evaluation framework in detail.

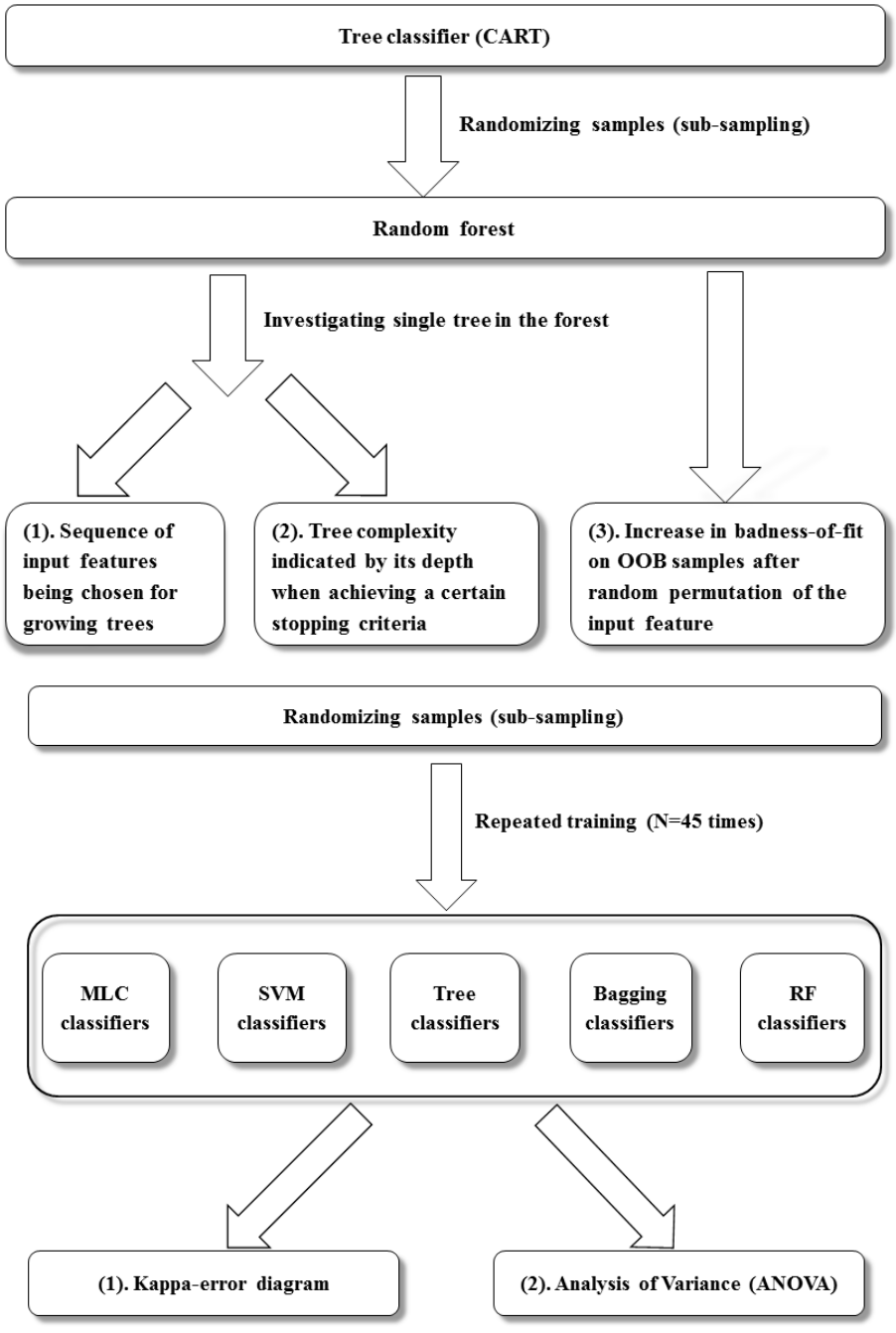

Figure 2-1 Evaluation Framework. (*a*) The evaluation of input features; (*b*) the evaluation of classifiers.

2.1.1 Variable selection sequence and complexity of classification tree (CART)

The first two criteria for evaluating the superiority of input features originated from the Classification and Regression Tree (CART). The CART produces classification rules by recursively seeking the most significant variable and the associated cut-off value for splitting. The fitted tree tends to select variables with great variability and separability in the early splits. The algorithm proceeds until no further splitting can be found to reduce the node impurity (Gini index) or gain information (entropy) by a predefined threshold (controlled by the complexity parameter – *cp*). The gini index and entropy of a given node are defined as:

$$gini\ index = \sum_i\ p_i(1 - p_i) \tag{1}$$

$$entropy = -\sum_{i=1}^{K} p_i\, log p_i \tag{2}$$

where p_i is the portion of class i in the node. Impure node features high gini index and entropy.

This selective splitting mechanism of the tree classifier determines that the sequence of variable chosen for splitting is regarded as an indicator of variables' importance and superiority. A tree's complexity highlighted by its depth and the number of nodes also indicates the capability of input variables in separating designated classes. Generally, trees with more levels (depth) and nodes are due to the inability of the input variable to separate the designed classes. In other words, the simpler a fitted tree is, the superior and more relevant the input variables are.

2.1.2 Randomization technique

Randomization technique is critical in this evaluation framework. Randomizing training samples (called "bootstrapping" if with replacement and "sub-sampling" if

without replacement) creates multiple training datasets through drawing samples with replacement from the original sample pool, and the bootstrap samples are used for producing an ensemble of classifiers (Hastie et al. 2009, pp.249). The contribution of the randomization technique to the evaluation framework is threefold. First, not only can these produced classifiers be considered together to obtain a final classification, but also, and more importantly, they could be investigated individually for the stability assessment of base classifiers that constitute the ensemble. Second, the conclusion regarding the superiority of input features by criteria introduced in Section 2.1.1 could be drawn repeatedly from an ensemble of tree classifiers (random forest); hence, the statistical significance is obtained. Third, randomization provides an innovative Out-of-Bag (OOB) method (Hastie et al. 2009, pp. 593) to look at the variable's importance in the random forest. In the random forest, each tree is built with bootstrap samples. The prediction of a given observation is constructed by averaging only those tree classifiers corresponding to bootstrap samples in which this observation did not appear. Hence, the OOB idea is similar to the N-fold cross validation (Hastie et al. 2009, pp.593). Variable's importance is measured by the increase of the badness-of-fit on OOB samples after a random permutation of the variable's value. Alternatively put, if a given input feature is important, the random permutation would lead to a significant degradation of the model. On the contrary, if a given input feature is not important in the first place at all, the random permutation would not make a big difference on the model fit.

2.1.3 Kappa-Error diagram

Previously, the variability of the overall accuracy was adopted as a measure of stability of classifiers (Huang et al. 2002). However, this indicator still casts problems

because classifiers with similar overall accuracy might still have discrepant or even distinct classification results; hence it is not reasonable to conclude the stability just from consistent accuracy reports. For instance, one certain classifier is trained multiple times (say, three times, producing classifier-1, classifier-2 and classifier-3) using different training data. Due to the use of different training data, the classifier-1 may confuse Class-A and Class-B; the classifier-2 may confuse Class-D and Class-A; and classifier-3 confuses Class-A and Class-D and Class-C. Although these three classifiers may have close overall classification accuracies around, say, 75%, they are making different classification decisions as they confuse different classes. So, in this case, this classifier is not considered as a stable one.

This research introduces the Kappa-Error diagram for the stability assessment. Kappa-Error diagram (Margineantu and Dietterich 1997) is superior to the variability of the overall accuracy as a measure of the stability of classifiers. The Kappa-Error diagram visualizes the accuracy and the stability of a classifier in a single scatter plot. First, n sets of bootstrap samples are produced for fitting a classifier n times, producing $C_n^2 = n(n-1)/2$ pairs of classifiers. Then, the Kappa-Error diagram is constructed by taking the mean error rate of pairwise classifiers on the validation dataset as y and corresponding degree of agreement (indicated by the Kappa statistic as x. The Kappa-error pattern for a stable and accurate classifier will display a compact point cloud located at the lower right corner in the diagram indicating a low error rate and a high Kappa statistic (meaning consistent and stable, see Figure 2.2). Kappa-Error diagram has not been widely adopted in the remote sensing classification applications with only few exceptions, such as

DeFries *et al.* (2000) and Chan *et al.* (2001). The use of Kappa-Error diagram is promoted in this research by demonstrating its value in the classifier evaluation.

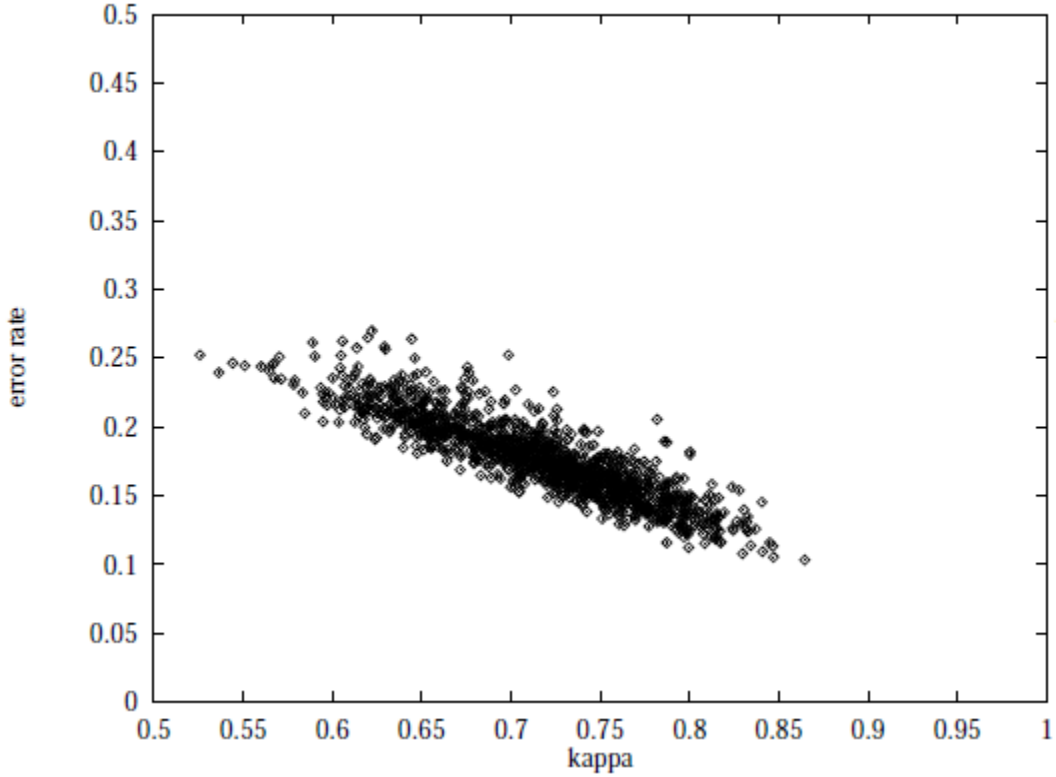

Figure 2-2 Kappa-Error Diagram, image courtesy of Margineantu and Dietterich (1997)

2.2 Classifiers

Other than the aforementioned tree classifier, other four types of classifiers Figure 2.1(*b*) are also investigated for comparisons. They are maximum likelihood classifier (MLC), tree-based ensembles, which include bagging (bootstrapped aggregation) and Random Forest (RF), and support vector machine (SVM).

2.2.1 Maximum likelihood classifier

As a parametric classifier, the MLC relies on multivariate normality assumptions and is mathematically equivalent to the Bayesian Quadratic Discriminant Analysis (QDA). (Richards and Jia 2006, pp. 194-199). It assigns the given pixel to the class when the

posterior probability of that class is a maximum. That the decision rule is quadratic is due to the heterogeneity of the within-class variance matrix.

According Bayesian theorem, we have the posterior probability of pixel x belonging to the class $\omega_i$as the following:

$$p(\omega_i|x) = \frac{p(x,\omega_i)}{p(x)} = \frac{p(x|\omega_i)p(\omega_i)}{p(x)} \quad (3)$$

The decision rule is:

$$x\epsilon w_i, if p(\omega_i|x) > p(\omega_j|x), for\ all\ j \neq i \quad (4)$$

Under the assumption of the multivariate normality and canceling the common factor $p(x)$, we take the log on both sides and get denote:

$$g_i(x) = lnp(\omega_i) - \frac{1}{2}ln|\Sigma_i| - \frac{1}{2}(x - m_i)^T\Sigma_i^{-1}(x - m_i), i = 1,2,3 \dots \dots C \quad (5)$$

where Σ_i is the sample variance-covariance matrix of class i, μ_i is the sample mean vector for class i, ω_i stands for the population i; $p(\omega_i)$ is the prior probability of the class i; C is the number of classes being considered. If assuming equality of the prior probability, which also leads to removing of the ½ as the common factor, one gets:

$$g_i(x) = -ln|\Sigma_i| - (x - \mu_i)^T\Sigma_i^{-1}(x - \mu_i), i = 1,2,3 \dots \dots C \quad (6)$$

The decision rule reduces to:

$$x\epsilon w_i, if\ g_i(x) > g_j(x), for\ all\ j \neq i. \quad (7)$$

After mathematical deduction, the rule can be rewritten as quadratic function:

$$x\epsilon w_i, if\ -\frac{1}{2}x^T\left(\Sigma_i^{-1} - \Sigma_j^{-1}\right)x + \left(\mu_i^T\Sigma_i^{-1} - \mu_j^T\Sigma_j^{-1}\right)x - k > 0,, for\ all\ j \neq i. \quad (8)$$

where

$$k = \frac{1}{2}\ln\left(\frac{|\Sigma_i|}{|\Sigma_j|}\right) + \frac{1}{2}(x^T\Sigma_i^{-1}x - x^T\Sigma_j^{-1}x) \quad (9)$$

MLC is the most popular classifier used by the remote sensing community and is implemented in most remote sensing packages. Yet selections of training samples and classes that satisfy the normality assumptions remained a challenge (Myint and Lam 2005b). Due to its popularity, MLC is used in this research as the benchmark classifier.

2.2.2 Ensemble classifier

Ensemble classifier is a committee formed by fitting a collection of base classifiers and makes classification decisions by a (weighted) majority vote (Hastie et al. 2009, pp. 605). The base classifiers are produced as independent and uncorrelated to each other as possible through randomization to reduce the estimation variation, which generally leads to improved classification performance. I embrace two popular ensembles in this research, namely, bagging and random forest.

Bagging

Bagging stands for "bootstrapped aggregation". Bagging is the most straight forward ensemble method in which a large number of bootstrapped samples were generated from the original training dataset and used to fit the same number of models for later averaging or majority vote. Tree model is not the only but the most used model in bagging method. Since bootstrap is a re-sampling process with replacement; for growing each tree, a certain part of training samples are never used, called Out of Bag (OOB) samples. OOB sample error is a more reasonable way to evaluate the model performance because it is derived from the data that are not used in growing the tree. OOB sample also provides a mechanism to evaluate the variable importance. For each predictor, its importance can be

determined by averaging the increase in prediction error of OOB samples over bagging trees after randomly shuffling the values of that predictor. More technical details about bagging can be found in the seminal paper of Breiman (1996), in which he offered mathematical explanation of the reason for which Bagging works and applied Bagging on both simulated and realistic datasets. He suggested that Bagging can only be used with unstable classifiers as its base, such as tree classifier; it probably would not result in much improvement with stable learners, like SVM (Chan et al. 2001).

Random Forest

Random forest is a general case of Bagging when the base classifier is the single tree classifier. Most of the time, random forest outperforms Bagging as it reduces the correlation between trees classifiers by randomly selecting only a portion (tuning parameter) of predictors from the variable pool for splitting when growing each individual tree. Since classification trees trained use different sets of variables for each branch splitting, the reduction of correlation is achieved and so does the prediction variance. A number of (lowly) correlated trees are produced in this way, forming a random forest. Random forest applied on simulated data indicated that it is able to achieve an adequate performance even if some input variables are noisy or useless (junk variables). The OOB idea is also available in random forest. For more technical details, see Breiman (2001) and Liaw and Wiener (2002).

Random Forest (RF) differs from Bagging method in two aspects. First, it only uses trees as the base classifier; second, only a random subset of all input features is considered in growing a tree classifier. The selected input feature subsets vary over the entire forest, which further reduces the correlation among tress (Breiman 2001).

A band selection mechanism of hyper-spectral remote sensing imagery by using random forest was suggested by Chan and Paelinckx (2008). 25 out of 126 spectral bands of airborne HyMap imagery were selected, spectral location of which indicated the importance of SWIR bands for ecotope classification. Generally speaking, machine learning classifiers were shown to be superior to their conventional counterparts. Gislason et al. (2006) compared several ensemble methods applied on multi-source remote sensing data and concluded that random forest achieves both the best accuracy and the fastest speed. However, inconsistent conclusions regarding the improvement of ensembles on their base classifier were also found in the literature. The improvement of ensembles depends on the dataset (Lawrence et al. 2004), sample size and selected base classifiers (Foody et al. 2007, Joelsson et al. 2005, Lawrence et al. 2006, Wang et al. 2008). Cautions should be taken when applying ensembles. The stability of base classifiers is crucial to the performance of ensembles; ensemble method achieves little improvement if the base classifier is adequately stable (Breiman 1996, Chan et al. 2001, Dietterich 2000).

2.2.3 Support vector machine

SVM is a machine learning technique that seeks the linear (sub) planes as the class boundaries while maximizing the margin between the class boundaries. It turns out the classification decision rule only involves the inner product of partial training datasets that are located at the class boundaries and are so called “support vectors”. In Figure 2.5, they are two hypothetical class plotted in 2-D feature space. The class boundary are the central black line and the two dashed line are parallel to the class boundary and are determined by $\omega x + b = 1$ and$\omega x + b = -1$. The key data points determining the class boundary

are support vectors in grey in Figure 2.5. SVM is a classifier to assign classification label according to:

$$if\ \omega x_i + b > 1, then\ Class\ A\ (y_i = 1);$$

$$if\ \omega x_i + b < -1, then\ Class\ B(y_i = -1); \quad (10)$$

Where x_i is a given vector to be classified and y_i is the class label. The above formula can be combined as:

$$y_i(\omega x_i + b) \geq 1 \quad (11)$$

The margin is the perpendicular distance between the two dashed lines in Figure 2.5, namely, $\frac{\|w\|^2}{2}$, which should be maximized. Hence, the Lagrange form of the SVM is

$$\min_{\omega,b}(\frac{1}{2}\|w\|^2 - \sum_{i=1}^{n}\lambda_i[y_i(\omega x_i + b) - 1]) \quad (12)$$

The dual problem of SVM is:

$$\max_{\lambda_i}(\sum_{i=1}^{n}\lambda_i - \frac{1}{2}\sum_{i=1}^{n}\sum_{j=1}^{n}\lambda_i\lambda_j\, y_i y_j {x_i}^T x_j) = \sum_{i=1}^{n}\lambda_i - \frac{1}{2}\sum_{i=1}^{n}\sum_{j=1}^{n}\lambda_i\lambda_j\, y_i y_j\langle x_i, x_j\rangle \quad (13)$$

Taking derivative of (4) leads to two conditions:

$$\omega = \sum_{i=1}^{n}\lambda_i\, y_i x_i \quad (14)$$

$$\sum_{i=1}^{n}\lambda_i\, y_i = 0 \quad (15)$$

The dual problem can be solved by quadratic programming. Under the KKT condition and Mercer Theorem, the optimal solution is sparse in λ_i, meaning most of the λ_i have to be zero. From Figure 2.3, we see that only those data points (so-called support vectors, rendered in grey color) whose λ_i coefficients are nonzero are contributing to calculating ω. Substituting (2) and (4) in (1), one gets the solution of SVM as the following:

$$class\ label = Sign(\omega x_i + b) = Sign\left(\left(\sum_{k=1}^{n} \lambda_k\, y_k x_k\right) x_i + b\right)$$

$$= Sign\left(\left(\sum_{k=1}^{n} \lambda_k\, y_k x_k\right) x_i + b\right) = Sign\left(\sum_{k=1}^{n} \lambda_k\, y_k \langle x_k, x_i\rangle + b\right)$$

Hence, both the dual and the solution only involve the inner product of support vectors in the training dataset and vectors that need to be classified.

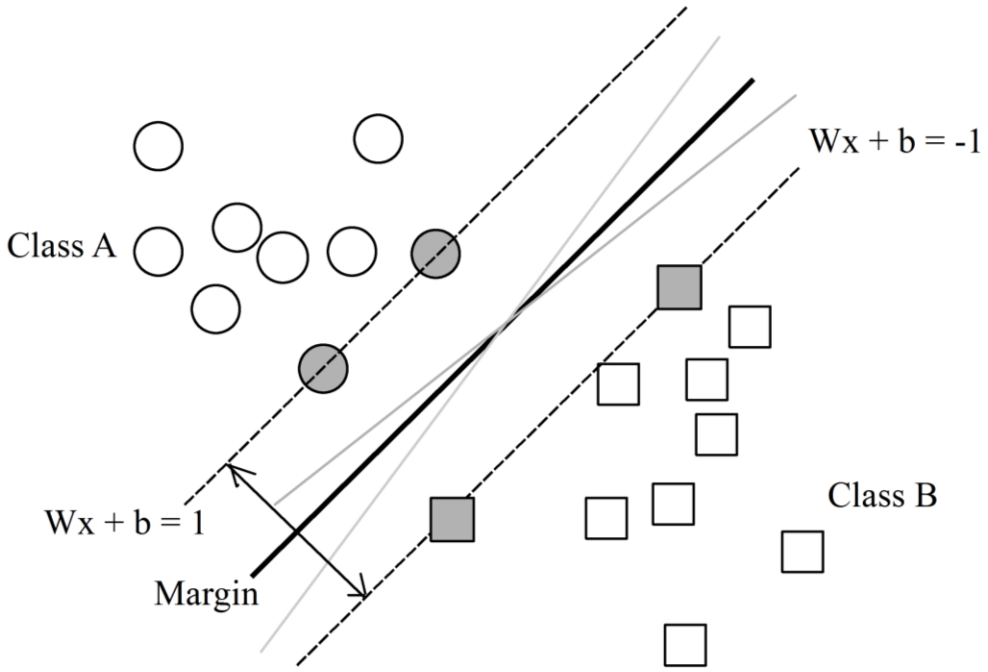

Figure 2-3 Illustration of SVM classifier in a two-class linear separable case; and grey features are the support vectors.

When the data in the original feature space are not linearly separable, SVM adopts a technique called "kernel-trick" (Schölkopf and Smola 2002), which attempts to project datasets into higher dimensional feature space to achieve the linear separability by using kernel mapping functions. This "kernel trick" idea is based on the fact that the regular solutions of SVM only involves the inner product of the support vectors; and kernels can

be regarded as the inner product in the mapped feature space (with higher or even infinite dimensions). Once the kernel is defined, the actual mapping function is implicit and need not to be known (Schölkopf and Smola 2002). The most frequently used kernels include linear kernel (inner product, no mapping), polynomial kernel, and Gaussian kernel, etc. SVM problem can be solved by quadratic programming using Lagrange Multiplier method (Burges 1998, Schölkopf and Smola 2002).

Recent literature has witnessed a growing interest in the application of SVM classifier in the remote sensing image classifications (Brown et al. 1999, Bruzzone and Carlin 2006, Foody and Mathur 2004a, Foody and Mathur 2004b, Huang et al. 2002, Li and Wan 2010, Mathur and Foody 2008, Melgani and Bruzzone 2004, Pal and Foody 2010). SVM has been compared with MLC (Huang et al. 2002), decision tree (Foody and Mathur 2004a, Huang et al. 2002) and neural network (Foody and Mathur 2004a, Huang et al. 2002) and demonstrated its superiority. The classical SVM is two-class SVM (TCSVM), and was extended to be multi-class SVM because remote sensing classification usually deals with more than two classes. Melgani and Bruzzone (2004) evaluated four different multi-class strategies of SVM (e.g. one-against-all, one-against-one, binary hierarchical balanced tree-based and binary hierarchical tree based one-against-all) and showed that the one-against-all and one-against-one strategies had better performance. Spectrally weighted kernels (Guo et al. 2008a) were developed to extend SVM-based methods for hyper-spectral image classification. It was based on the fact that the useful information for classification is not evenly distributed among all spectral bands. One-class SVM (OCSVM) has been an emerging type of SVM recently developed to cater for the requirement for feature detection and one-class classification (Schölkopf and

Smola 2002, Tax and Duin 2004). In OCSVM, only one class is of interest so that analysts need only to train that specific class occurred in the study area. OCSVM projects data into high–dimensional space and uses a hyper-sphere instead of hyper-plane as the decision boundary (Schölkopf and Smola 2002). Sanchez-Hernandez et al. (2007) adopted a series of one-class classifiers including the OCSVM for mapping a specific land-cover class (fens) and the result highlighted the potential of accurate classification. Li et al. (2010b) utilized OCSVM to detect the damaged building class at both pixel-based level and object-based level and the result showed that the object-based level with texture input produced much better results. Other applications of OCSVM can be found in (Guo et al. 2008b, Li and Xu 2010, Li and Guo 2010, Li et al. 2011, MũNoz-Marí et al. 2010). A most recent detailed review of SVM applied in the remote sensing community was furnished by Mountrakis et al. (2010).

The software R in the public domain is used to construct the evaluation framework since it has implemented all the aforementioned classification algorithms (Table 2.1). The reading and writing functions for raster images and shapefile vector files are available in the R package **rgdal**.

Table 2.1 R packages with the implementation of different classification algorithms.

Classification method	R package
Maximum Likelihood Classification	**MASS**
Classification Tree	**rpart**
Random Forest	**randomForest**
Bagging	**randomForest**
Support Vector Machine	**e1071**

2.3 Summary

This chapter elaborates the evaluation framework for assessing the performance of classifiers and different input feature configurations. It serves as the basis for Chapter 3. The evaluation framework borrows tools from the machine learning community. It uses the randomization technique to train classifier multiple times to study their stability, which has been ignored in previous studies. The tree structures are analyzed in the evaluation framework to study the importance of input features. The OOB-based importance mechanism is also used to order the importance of input features. The Kappa-Error diagram is a visualization tool in the framework for compare classifiers.

This framework is not limited to any particular classifier, nor any input variables or classification application. As an example, in chapter 3, we apply this evaluation framework to deeply look at the superiority of V-I-S model and LST in urban land use classification.

Chapter 3 Evaluation of V-I-S fractions and Land Surface Temperature for urban land use classification

3.1 Introduction

In remote sensing of urban land use and land cover (LULC), the most widely used Bayesian approach (or maximum likelihood classifier, MLC) has been criticized for its difficulty in retaining the normality assumption when used with the image spectral bands. Recently, there was a growing interest in the application of non-parametric and assumption-free classifiers. Examples included the decision tree, support vector machine (SVM), and ensemble classifiers (Chan and Paelinckx 2008, Chan et al. 2001, Friedl and Brodley 1997, Gislason et al. 2006, Ham et al. 2005, Joelsson et al. 2005, Lawrence et al. 2006, Lawrence and Wright 2001, Pal and Mather 2003, Yang et al. 2003a). Upon the desire for seeking more relevant input features, the Vegetation-Impervious Surface-Soil (V-I-S) model (Ridd 1995) opened a new avenue for the urban LULC studies and was applied and extended by many others (Lu and Weng 2004, 2006, Phinn et al. 2002, Small 2001, Small and Lu 2006). In addition, land surface temperature (LST) derived from thermal bands was also found closely related to urban biophysical characteristics (Lo et al. 1997, Weng 2009, Weng et al. 2007).

It is of great interest to bridge several research gaps existing in the urban land use classification using the V-I-S model and LST. First, the stability of classifiers built with V-I-S fractions and LST was not explored; Second, current discussions on the superiority of V-I-S fractions and LST were limited to the aspect of accuracy improvement only, and hardly was it scrutinized from other aspects; Third, no comparative studies were found on using V-I-S fractions and LST in training different classifiers in attempt to identify the

best classifier. This chapter applies the evaluation framework introduced in chapter 2 to demonstrate the superiority of V-I-S fractions and LST over the conventional multispectral reflectance in the urban land use classification and to identify the most suitable classifiers for different input feature configurations. The chapter answers the research questions 1~4.

3.2 Study area and data

Several land use classes are identified in the study area of New Orleans. The southwest contains major vegetated areas composed of forest, agricultural land and wetland; the City Park to the south shore of Lake Pontchartrain and the Audubon Park in the uptown neighborhood also have large coverage of vegetation; the residential area is mainly located to the north and southeast of the Mississippi River; commercial and industrial areas are predominantly constructed along the Mississippi river and in the central city. Water areas are evident as the Mississippi River across the city and canals as well as bayous in the southwest.

Baton Route (Figure 3.1), the capital and the second largest city of the Louisiana State is also included as an additional test site to verify major conclusions and to demonstrate the generalizability of the current study. The economy development of Baton Rouge depends on the petrochemical industry. The CBD area is to the north of Baton Rouge and in the north of CBD locate massive amount of oil refineries. The residential areas are mainly established in the east and south of the city. Baton Rouge is a dynamic urban area with a diversity of land use patterns that is similar to New Orleans. These two urban areas are representative of the majority of the U.S. urban environment.

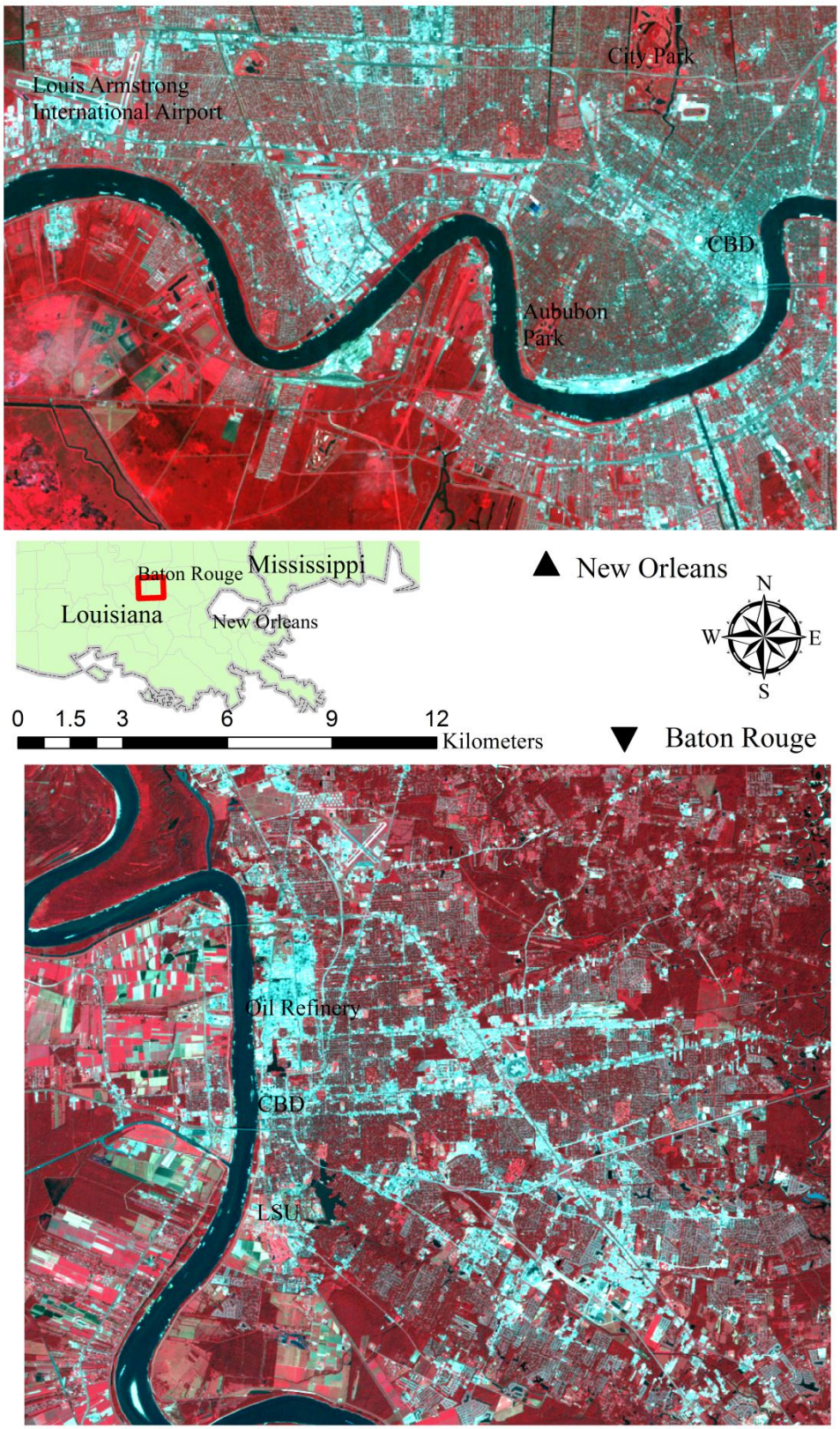

Figure 3-1 Study area of New Orleans and Baton Rouge. (Landsat 22/39 and 23/39)

3.2.1 Data source and classification scheme

The Landsat TM image used in this analysis (Path/Row 39/22 for New Orleans acquired on 22 August 2005 and Path/Row 39/23 for Baton Rouge acquired on 16 October 2005) was acquired on August, 2005, as to expect a better UHI effect than other seasons. The bands 1~5 and 7 were calibrated with the image metadata to compute the spectral reflectance. The 1-m resolution Digital Orthophoto Quarter Quadrangles (DOQQs) acquired in the time of the year was used for validation. A rigorous image co-registration between DOQQs and the TM image was performed in the UTM Zone 15, North American Datum 1983 projection system to ensure the locational accuracy of our analysis. A classification scheme with four classes of "Commercial and Industrial", "Residential", "Vegetated" and "Water" was adopted (Table 3.1). These land use classes are commonly encountered in U.S. urban area.

Table 3.1 Description of Land use classes adopted in this study

Category	Description
Commercial and Industrial	Areas predominantly constructed for human activities associated with commercial and industrial events, including, buildings, parking lot, shopping centers, transportation roads, etc.
Residential	Areas predominantly constructed for human dwelling and residential purpose.
Vegetation	Large homogenous areas of vegetation cover, including forests, forested wetlands, grassland, shrubs, etc.
Water	Mississippi River, lakes, ponds and canals.

Training samples were specified by identifying polygons of homogenous land use areas in the Landsat TM scene in New Orleans, which comprised of 628 pixels of "Commercial and Industrial" land use, 541 pixels of "Residential" land use, 471 pixels of

"Vegetated" land use and 173 pixels as "Water". For Baton Rouge site, the training samples covered 195 pixels of "Commercial and Industrial", 368 pixels of "Residential", 481 pixels of "Vegetation" and 133 pixels of "Water". Random points were generated and V-I-S visually interpreted from the DOQQ to identify the reference data of land use classes.

3.2.2 Feature extraction

The fraction images were derived from the Landsat TM image by using the linear spectral mixture analysis (LSMA) method (Wu and Murray 2003). Endmember selection is the most critical step in the application of V-I-S model. Endmembers can be selected directly from the image or from the data collected from the field trip or from a spectra library. However, image endmember is more favored as it bears consistent systematic errors (due to atmospheric effect and distortions incurred by sensor's motion and underlying topography) and is under the consistent scale with all pixels in the image (Settle and Drake 1993). In addition, it is the most available as compared to the other two approaches for the endmember extraction. Image endmember can be determined in an unsupervised manner. These unsupervised methods Visualize the pixel vectors in the high-dimensional hyperspace to form a point cloud contained in the hyper-dimensional convex. Endmember can be found by iterative projecting (ortho-projection and oblique projection) data vectors. Algorithms falling into this category include Pure Pixel Index (PPI, Boardman et al. 1995), Sequential Maximum Angle Convex Cone (SMACC, Gruninger et al. 2004), Convex Cone Analysis (CCA, Ifarraguerri and Chang 1999) and N-FINDR (Winter 1999). The imperviousness component is the most complicated component in the V-I-S model due to its large heterogeneity and lack of unique

endmembers, leading to bias (Lu and Weng 2006, Weng and Quattrochi 2007). To address this issue, two approaches were reported in the literature. One is Multiple Endmember method (MESMA, Powell et al. 2007, Rashed et al. 2003, Roberts et al. 1998). MESMA seeks more than one endmember for each V-I-S component, especially for the imperviousness component and determines the best endmember combination at a per-pixel level that has the least Root Mean Square Error (RMSE) in the unmixing process. The best endmember combination varies across the entire image scene. Another solution is the spectral normalization method (Hu and Weng 2010a, Morton and Yuan 2009, Voorde et al. 2008, Wu 2004), which reduces the heterogeneity between endmembers through normalization. For example, after the normalization, the spectra of dark vegetation and bright vegetation become more similar; the dark impervious surface and bright impervious surface also achieves a more desirable spectral homogeneity (Wu 2004).

A normalization procedure (Wu 2004) was performed prior to the LSMA in order to reduce the spectra variance of endmembers, followed by Minimum Noise Fraction (MNF) transformation to reduce the data dimensionality and to eliminate noise in the TM image. Endmembers were extracted based on the scatter plots of MNF components. The impervious surfaces were mainly man-made features with high albedo, such as buildings, transportation roads, parking lots, river deck, etc. The spectrum of soil was mixed with that of low albedo features. Vegetation was predominately found as the forests and grassland. LSMA assumes the spectral reflectance profile of the mixed pixel is the linear (weighted) combination of the constituent endmember's spectral reflectance profile and the weight is determined by the fractions (abundance). LSMA is expressed as:

$$\rho(\lambda_i) = \sum_{j=1}^{m} f_i \rho_j(\lambda_i) + \varepsilon(\lambda_i) \quad (1)$$

where m is the number of endmember, which is 3 in this case; i is the band index; f_i is the fraction of j^{th} endmember to be estimated; $\rho(\lambda_i)$ is the pixel reflectance of band i, and i = 1,2,3,4,5,7. The value of f_i is subject to the sum-to-unity constraint:

$$\sum_{j=1}^{m} f_i = 1 \quad (2)$$

This linear spectral unmixing problem can be solved by quadratic programming in Matlab or IDL (Interactive Data Language) that minimizes the square error (SE).

$$\hat{f} = argmin \sum_i [\rho(\lambda_i) - \sum_{j=1}^{m} f_i \rho_j(\lambda_i)]^2] \quad (3)$$

LSMA produced three fraction images: impervious surface + high albedo fraction image (Figure 3.2(*a*)), low albedo + soil fraction image (Figure 3.2(*b*)), and vegetation fraction image (Figure 3.2(*c*)). The overall root mean square error (RMSE) of the LSMA was 0.045.

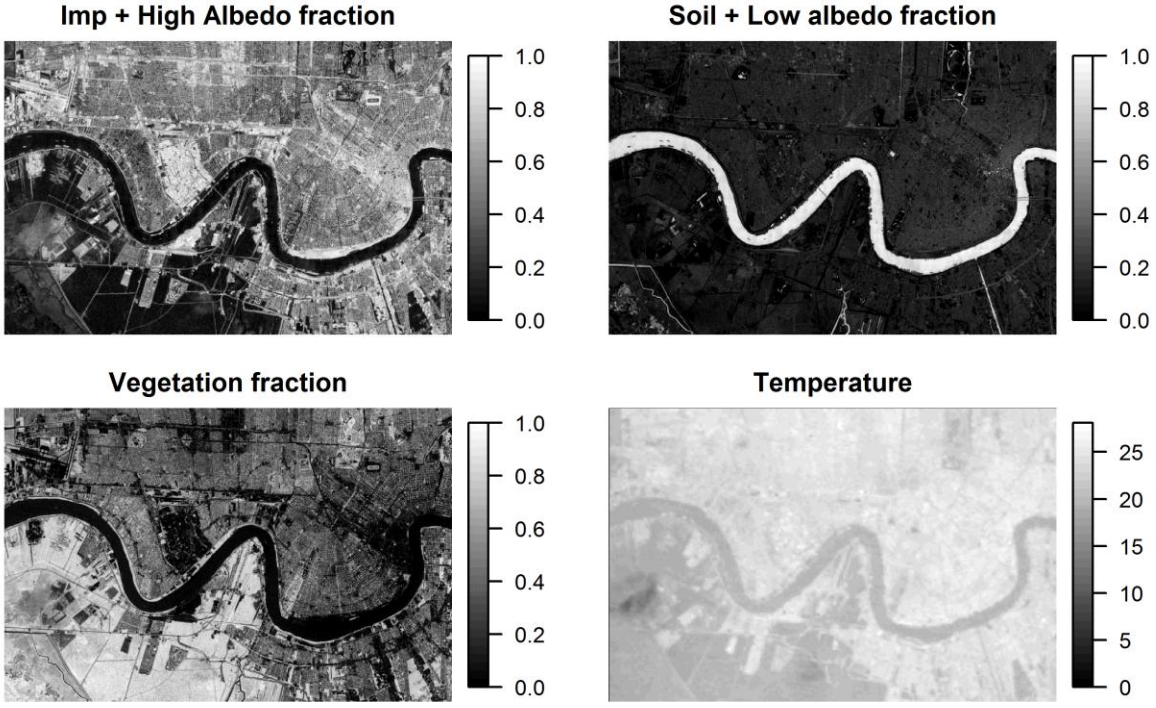

Figure 3-2 V-I-S fraction images and LST image.

Various algorithms were developed to recover the absolute value of LST from thermal infrared (TIR) bands, including the Radiative Transfer Equation (RTE) based algorithm (Berk et al. 1989, Schmugge et al. 1998, Sobrino et al. 2004), mono-window algorithm (Qin et al. 2001) and single-channel algorithm (Jiménez-Muñoz and Sobrino 2003). These models usually require additional data input (water vapor content, etc.) and prior knowledge about the underlying surface for atmospheric correction and emissivity adjustment. However, in this study use of LST is for the classification purpose. Therefore, the relative measurement was sufficient for mapping LST spatial variation and relating it to the LULC patterns (Weng 2009); hence LST was computed by using the standard calibration procedure (Landsat Project Science Office, 2002). The formula for converting radiance to temperature is:

$$T_s = \frac{K_2}{\ln(\frac{K_1}{L_\lambda}+1)} \quad (4)$$

where T_s is the land surface temperature in degree Kelvin; $K_1$and$K_2$are pre.launch calibration constant for Landsat TM with the value of 607.76 K and 1260.56, respectively.

Figure 3.2(*d*) shows the LST image obtained from the TM band 6. The UHI effect was evident in New Orleans during the period of study. The average LST of the southern forest area was much lower than the commercial area.

A ten-dimensional composite input dataset for classification is made by stacking three fraction images, six multispectral reflectance images from TM bands 1 through 5 and 7, and the LST image. Various combinations of these input bands are possible for classification. Specifically, this research is interested in testing the following three commonly used input feature configurations:

1) Six original spectral bands of TM only;

2) V-I-S fractions and LST synergy;

3) Combination of six original spectral bands of TM and V-I-S fractions and LST (the full data dimension, a total of ten bands).

3.3 Pixel based classification

3.3.1 Classification results

The classification results using the six-band multispectral reflectance data (TM band 1.5 and 7) are shown in Figure 3.3. Regardless of the classifier being used, multispectral reflectance input produced evident "salt and pepper" effect as marked in the maps, which is a common problem associated with the pixel-based classification. Two salient misclassification regions were noticed. One was the bayou area with vegetation coverage to the southwest of the scene; and the other was the vegetated area to the north of the southwest canals. Both were misclassified to the "residential" land use. Note that the sliver areas in the southern forest area were misclassified as "residential" as well and those pixels appeared isolated. These misclassifications revealed the incapability of spectral reflectance in distinguishing the urban land use patterns. In contrast, as seen in Figure 3.4, classifiers built with V-I-S fractions and LST were notably improved by alleviating the "salt and pepper" problem, producing reasonable and homogenous vegetated area in the southwest. Table 3.2 and Table 3.3 summarize error matrices of 10 classification scenarios (2 input feature configuration × 5 classifiers). As we can see from these tables, classification accuracy was also improved when using V-I-S fractions and LST instead of the six-band multispectral data.

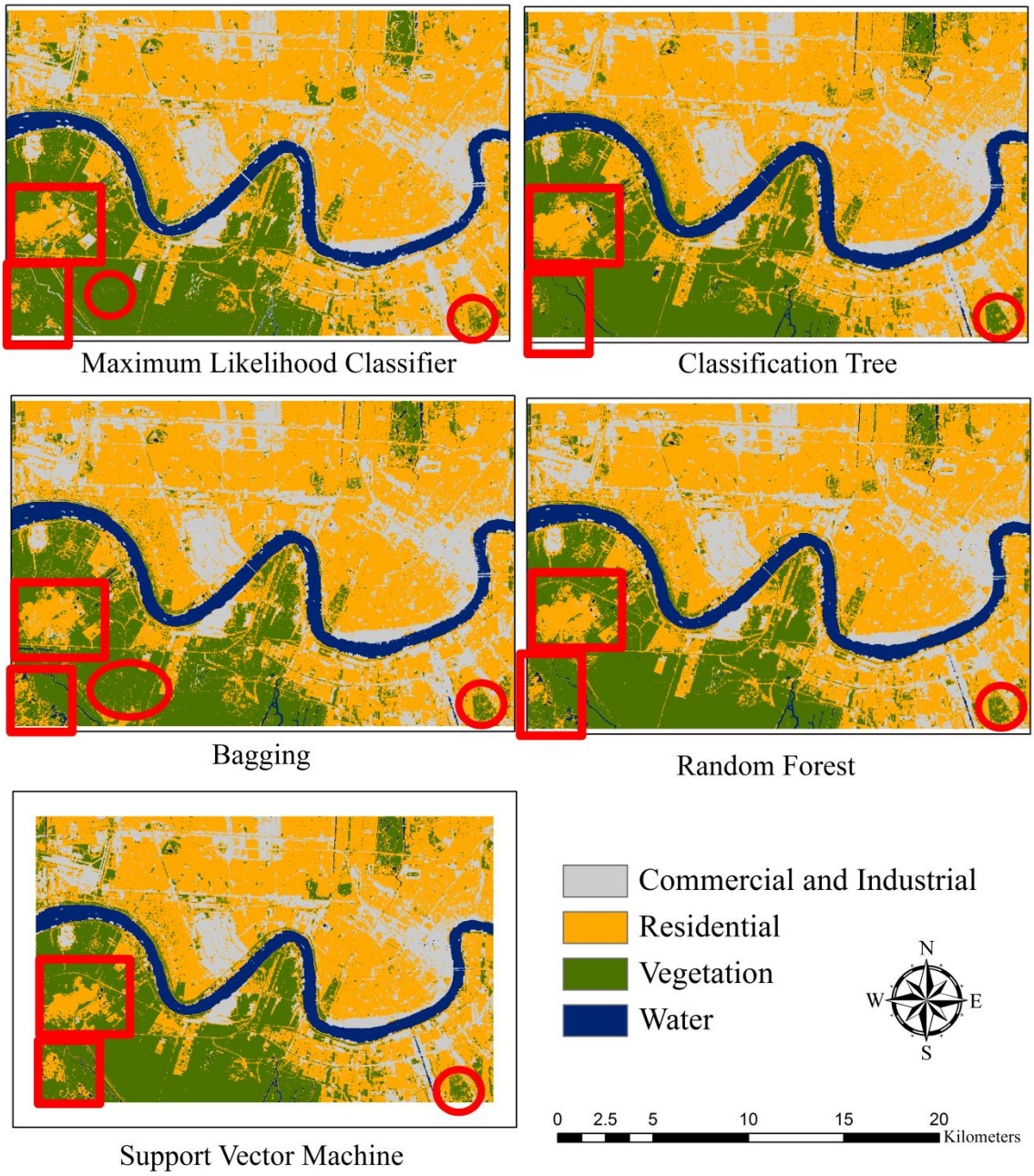

Figure 3-3 Classification results with only multispectral reflectance variable used as the input. Red circles mark the "salt-and-pepper" effect from the image classification. Red rectangles mark the salient misclassification regions.

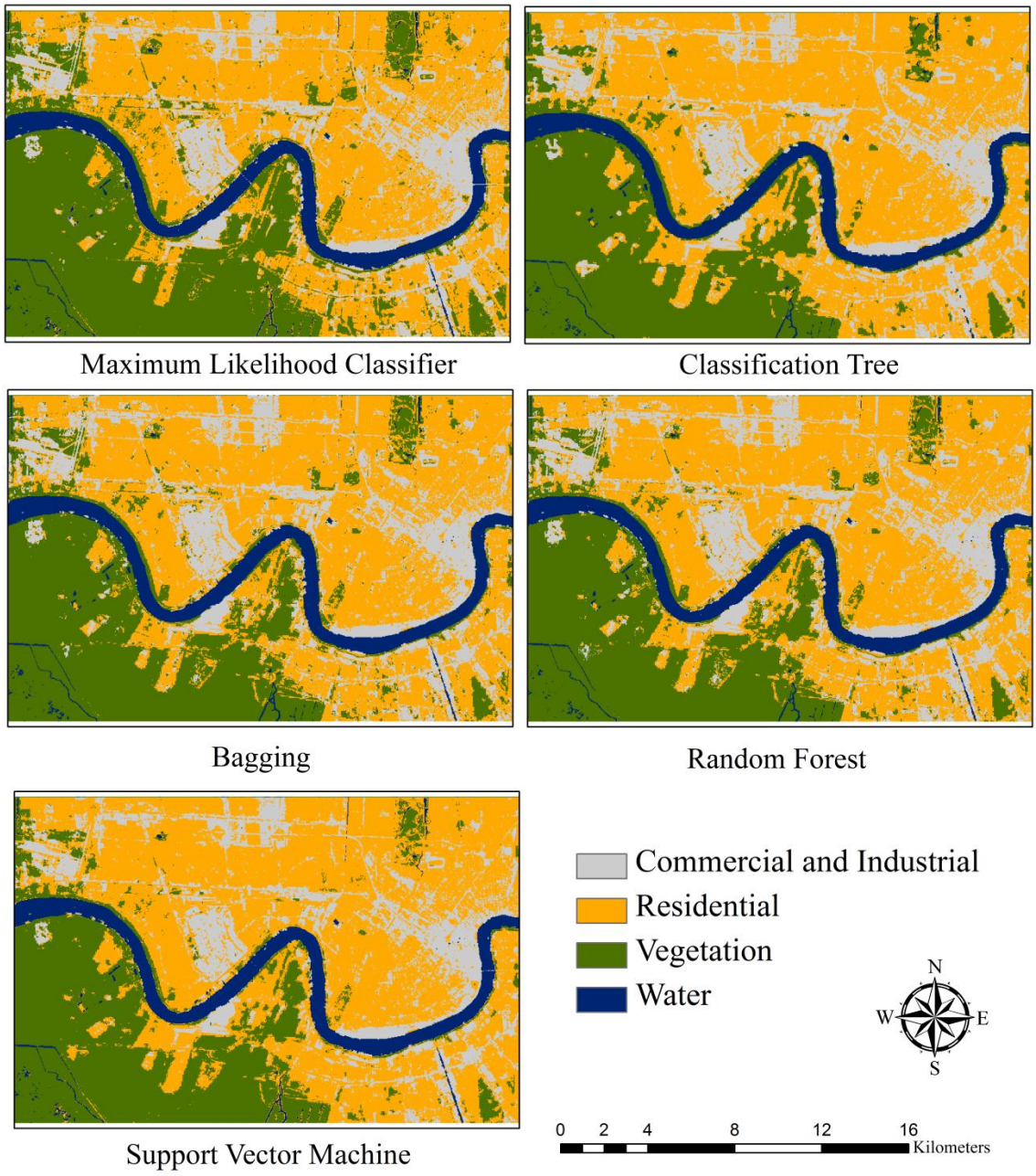

Figure 3-4 Classification results with V-I-S fractions and land surface temperature. As compared to figure 4, the "salt and pepper" problem is alleviated. More homogenous area of vegetated area to the southwest of the study area is produced. The salient misclassification regions in Figure 3.3 are also eliminated.

Table 3.2 Confusion matrices of all classifiers (with spectral band reflectance as the input variables)

	Classified Data	Reference Data				Ref. Totals	Class. Totals	Number Correct	Producer Accuracy	User Accuracy
		Commercial	Residential	Vegetation	Water					
MLC	Commercial	50	7	8	5	97	70	50	0.52	0.71
	Residential	39	110	43	6	123	198	110	0.89	0.56
	Vegetation	8	6	96	2	148	102	96	0.65	0.86
	Water	0	0	1	16	29	17	16	0.55	0.94
Overall accuracy: 0.69; Kappa Statistic: 0.55										
CART	Commercial	50	6	7	1	97	64	50	0.52	0.78
	Residential	41	111	49	5	123	206	111	0.90	0.54
	Vegetation	6	6	91	3	148	106	91	0.61	0.86
	Water	0	0	1	20	29	21	20	0.69	0.95
Overall accuracy: 0.69; Kappa Statistic: 0.55										
Bagging	Commercial	52	5	10	1	97	68	52	0.54	0.76
	Residential	41	114	49	5	123	209	114	0.93	0.55
	Vegetation	4	4	87	3	148	98	87	0.59	0.89
	Water	0	0	2	20	29	22	20	0.69	0.91
Overall accuracy: 0.69; Kappa Statistic: 0.55										
Random Forest	Commercial	52	5	7	1	97	65	52	0.54	0.80
	Residential	41	112	50	6	123	209	112	0.91	0.54
	Vegetation	4	6	89	2	148	111	89	0.60	0.88
	Water	0	0	2	20	29	22	20	0.69	0.91
Overall accuracy: 0.69; Kappa Statistic: 0.55										
SVM	Commercial	51	5	7	0	97	63	51	0.53	0.81
	Residential	38	112	39	7	123	196	112	0.91	0.57
	Vegetation	8	6	101	1	148	116	101	0.68	0.87
	Water	0	0	1	21	29	22	21	0.72	0.95
Overall accuracy: 0.72; Kappa Statistic: 0.60										

Table 3.3 Confusion matrices of all classifiers (with V-I-S fractions and LST as input variables)

	Classified Data	Reference Data				Ref. Totals	Class. Totals	Number Correct	Producer Accuracy	User Accuracy
		Commercial	Residential	Vegetation	Water					
MLC	Commercial	47	10	7	1	97	65	47	0.48	0.72
	Residential	37	109	18	1	123	165	109	0.89	0.66
	Vegetation	12	4	122	8	148	146	122	0.82	0.84
	Water	1	0	1	19	29	21	19	0.66	0.90
Overall Accuracy: 0.75; Kappa Statistic: 0.64										
CART	Commercial	47	11	9	1	97	68	47	0.48	0.69
	Residential	38	108	33	1	123	180	108	0.88	0.60
	Vegetation	11	4	105	8	148	128	105	0.71	0.82
	Water	1	0	1	19	29	21	19	0.66	0.90
Overall Accuracy : 0.70; Kappa Statistic: 0.57										
Bagging	Commercial	51	13	13	1	97	78	51	0.53	0.65
	Residential	36	107	25	1	123	169	107	0.87	0.63
	Vegetation	9	3	109	8	148	129	109	0.74	0.84
	Water	1	0	1	19	29	21	19	0.66	0.90
Overall Accuracy : 0.72; Kappa Statistic: 0.60										
Random Forest	Commercial	52	11	16	1	97	80	52	0.54	0.65
	Residential	37	109	25	1	123	172	109	0.89	0.63
	Vegetation	7	3	106	8	148	124	106	0.72	0.85
	Water	1	0	1	19	29	21	19	0.66	0.90
Overall Accuracy : 0.72; Kappa Statistic: 0.60										
SVM	Commercial	44	9	5	0	97	58	44	0.45	0.76
	Residential	42	111	43	2	123	198	111	0.90	0.56
	Vegetation	10	3	99	7	148	119	99	0.67	0.83
	Water	1	0	1	20	29	22	20	0.69	0.91
Overall Accuracy : 0.70; Kappa Statistic: 0.55										

3.3.2 Evaluation framework-guided selection of input features

As mentioned before, this research is interested in testing three specific combinations of input data: (1) multispectral reflectance only, (2) V-I-S fractions and LST combination, and (3) the composite of (1) and (2).

3.3.2.1 Multispectral reflectance only

All classifiers were trained repeatedly (by $n = 45$ times) with bootstraping samples for producing the Kappa-Error diagram. Figure 3.5(a) shows the accuracy performances of all classifiers trained with different input feature combinations. When used with the multispectral reflectance as the only input feature, all classifiers result in low accuracy (indicated by lowly-elevated green boxes in Figure 3.5(a)). The tree classifier appeared as the most spreaded box, indicating that it is the most unstable classifier when using the spectral reflectance data only. Due to the instability and weakness of the single tree classifier, tree-based ensemble classifiers can improve the stability of individual tree classifiers. However, the improvement was only statistically significant in stability, not much in accuracy as seen from the Analysis of Variance (ANOVA) tests using multiple comparisons with Tukey-Kramar adjustment (Freund and Wilson 2002, pp. 256-257) (Table 3.4). The ANOVA test indicated that the SVM classifier stood out in both accuracy and stability. In the Kappa-Error diagram (Figure 3.6(a)), classifiers trained with band spectral reflectance depicted a more compact point cloud for those tree-based ensemble methods as compared to single tree classifier. Again, the SVM classifier demonstrated its power by arriving at the lower-right corner of the Kappa-Error diagram.

Table 3.4 Multiple comparisons in terms of accuracy and stability of different classifiers trained by band spectral reflectance variables only

Classifier	Accuracy Difference	p-value	Implication
CART-BAGGING	0.8%	0.9994	Randomization achieves no significant accuracy improvement on the single tree classifier.
CART-RF	0.2%	0.9513	
SVM-BAGGING	2.0%	<0.0001	SVM significantly outperforms all other classifiers.
SVM-MLC	2.0%	<0.0001	
SVM-RF	1.9%	<0.0001	
SVM-CART	2.0%	<0.0001	
Classifier	Kappa Difference	p-value	Implication
CART-BAGGING	-0.08	<0.0001	Randomization improves the stability of the single tree classifier significantly.
CART-RF	-0.12	<0.0001	
SVM-BAGGING	0.07	<0.0001	SVM is significantly more stable than any other classifiers, especially as opposed to the single tree classifier.
SVM-CART	0.15	<0.0001	
SVM-RF	0.04	<0.0001	
SVM-MLC	0.02	<0.0001	

3.3.2.2 Synergy of V-I-S fractions and LST

The performance of MLC benefits significantly from replacing the band reflectance input with the V-I-S fraction and LST combination input (see Figure 3.5(*a*) for a clearly elevated blue box for the MLC and Table 3.5 for significant *p-value*s when testing accuracy performance of MLC against other classifiers). The performance was even better than a synergy of V-I-S fractions and LST and all spectral reflectance variables together. A possible explanation is as follows: according to Ridd's V-I-S model (Ridd1995) and Lu-Weng's model (Lu and Weng 2006), certain urban land use type can identified as cluster of points at certain locations in the V-I-S feature space (see Figure 3.7 for our case). Hence, the distribution of V-I-S fractions and LST in the feature space displays several bell-shaped (Gaussian-like) surfaces with each individual peak corresponding to a certain urban land use type, which matches with the MLC's normality assumption, and thus leads to the optimal Bayesian decision boundary of the classes.

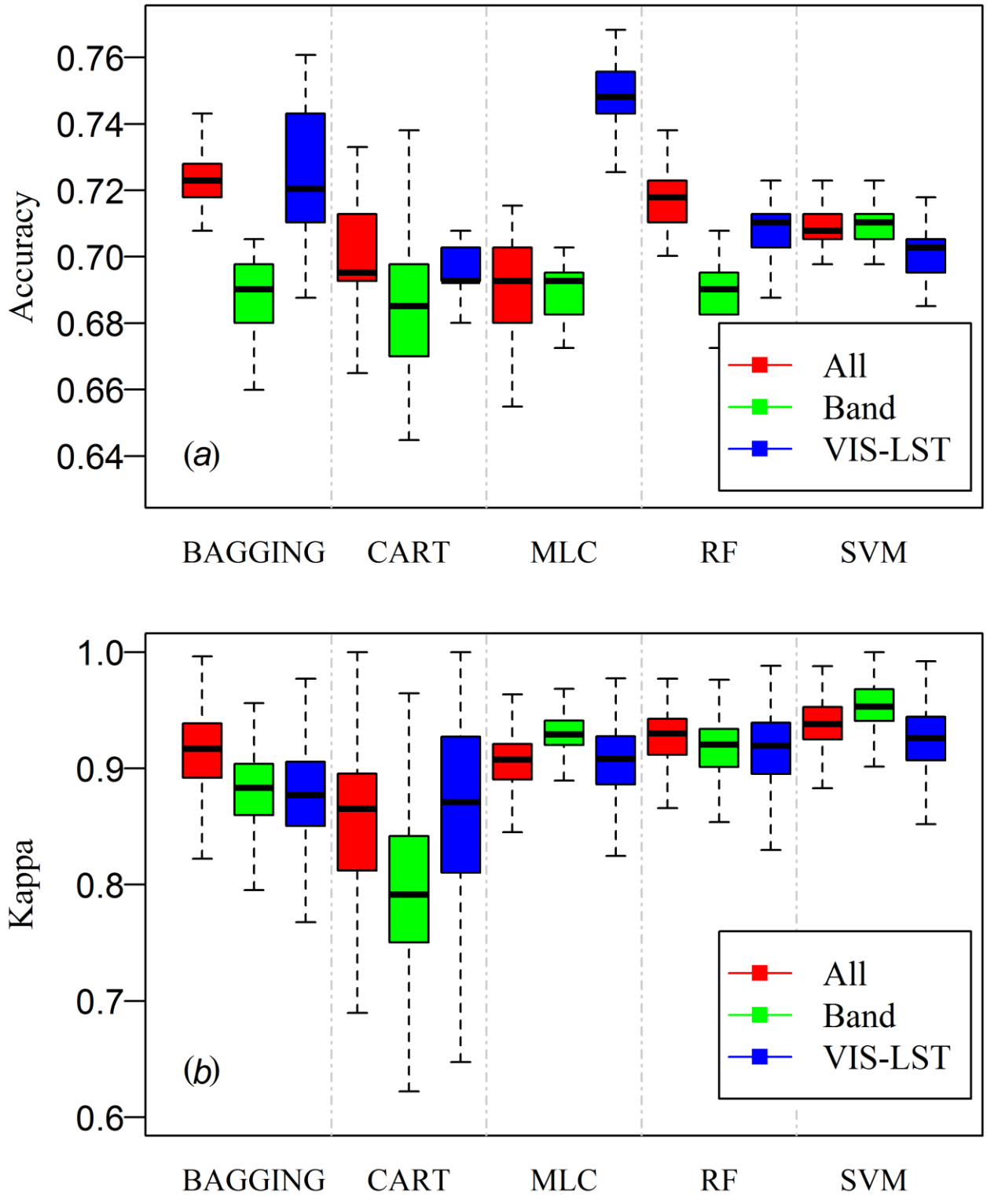

Figure 3-5 Accuracy and stability comparisons of five classifiers for three different input feature configurations (New Orleans, LA).

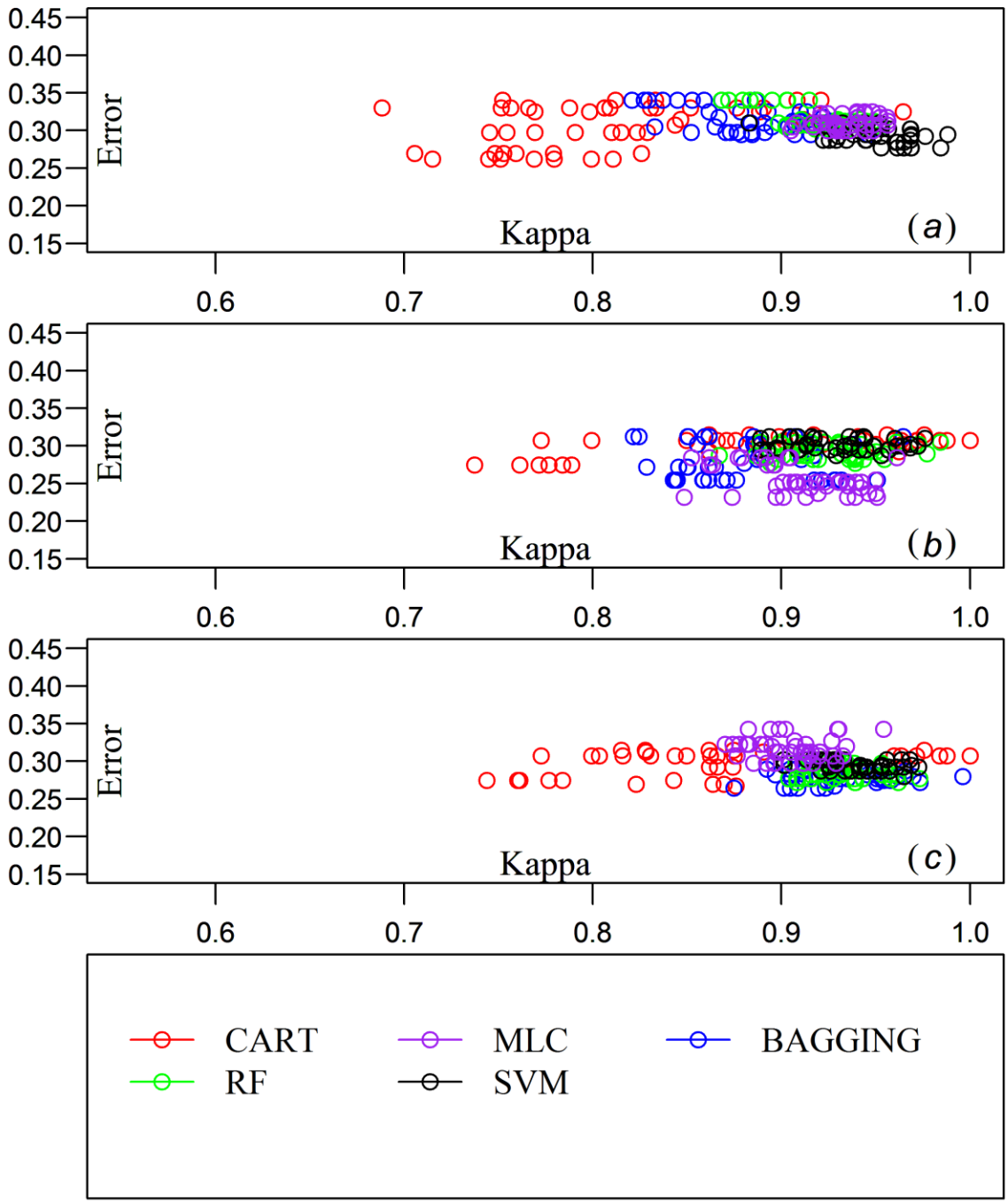

Figure 3-6 Kappa-Error diagrams produced by three different input feature configurations: (*a*). Multispectral reflectance only; (*b*). V-I-S fractions and LST combination; (*c*). Composite of (*a*) and (*b*), e.g., all features being included.

However, the similar pattern cannot be found for the case when the multispectral reflectance is used as the data input. Similar finding was also stated in Pal and Mather (2003): "*the MLC algorithm is preferred unless there is particular reason believing that the data do not follow a Gaussian distribution*". Hence, although being criticized in the literature the MLC stands as a good classifier as long as its basic assumption is met by carefully selecting the input features. In this study, we found that the use of V-I-S fractions and LST data made the normality assumption to be more closely satisfied.

The tree classifiers built with V-I-S fractions and LST had more stability than their counterparts built with the multispectral reflectance input, as highlighted by the fact that the "Accuracy" box for CART was less spread out (Figure 3.6(*a*)) and the "Kappa" box for CART was more elevated (Figure 3.6(*b*)) and a significant *p* value ($p<0.001$) in Table 3.5. The point cloud for the tree classifier was more compact in Figure 3.6 (*b*) than Figure 3.6(*a*). The commonly reported improvement caused by using tree-based ensembles over single tree classifier was, however, not observed (Table 3.6). This result was different from the case when the multispectral reflectance was used. Hence, the improvement of tree-based ensembles over the single tree classifier was not significant because the tree classifier as the base classifier was adequately accurate and stable when trained with V-I-S fractions and LST combinations. This confirms with the conclusion from previous theoretical (Breiman 1996) and empirical studies (Chan et al. 2001). Random forest and Bagging had 1.9% and 3.0% accuracy increase, respectively.

In an urban environment, commercial and industrial areas have evident UHI effect due to the thermal property of underlying surfaces (buildings, transportation network, parking lots, etc) and massive human activities generating extra heat. These areas usually

have higher surface temperatures as opposed to more vegetated areas in the suburban area (forest and grassland, etc). On the contrary, the "Vegetated" areas are less disturbed by human activities, and undergo transpiration through leaves to lower the surface temperature. Hence, LST has the ability to differentiate the vegetated areas from those built-up areas. However, "Water" with high thermal inertia also appears cool in the day time, making it not separable from the "Vegetated" areas by merely using LST. The "Residential" area has intermediate surface temperature in between, so it might be confused with "Commercial and Industrial" land use or "Vegetated" land use depending on the relative amount of vegetation coverage (the "V" component) and man-made materials (the "I" component). The lack of separability in terms of LST was clearly seen in Figure 3.2(*d*). Although these land use classes ("Vegetated" along with "Water", or "Residential" along with "Commercial and Industrial") have similar LSTs, their V-I-S configuration differ considerably. This is where V-I-S fractions input come into play to increase the separability. As such, V-I-S fractions and LST are complementary to each other and make an ideal input data configuration for urban land use classification.

3.3.2.3 Full data dimension

Table 3.7 demonstrated how much gain could be obtained by the addition of V-I-S fractions and LST to the conventional spectral-based classification. MLC received little benefits because the use of spectral reflectance variables, as they violate the assumptions of MLC and the impact was great enough to interfere the use of V-I-S fractions and LST. On the contrary, the tree and tree-based ensembles were enhanced in accuracy due to the addition of V-I-S fractions and LST. The improvement in accuracy for CART, Bagging and random forest was 1.7%, 3.0%, 2.4%, respectively. The best classifier to be used for

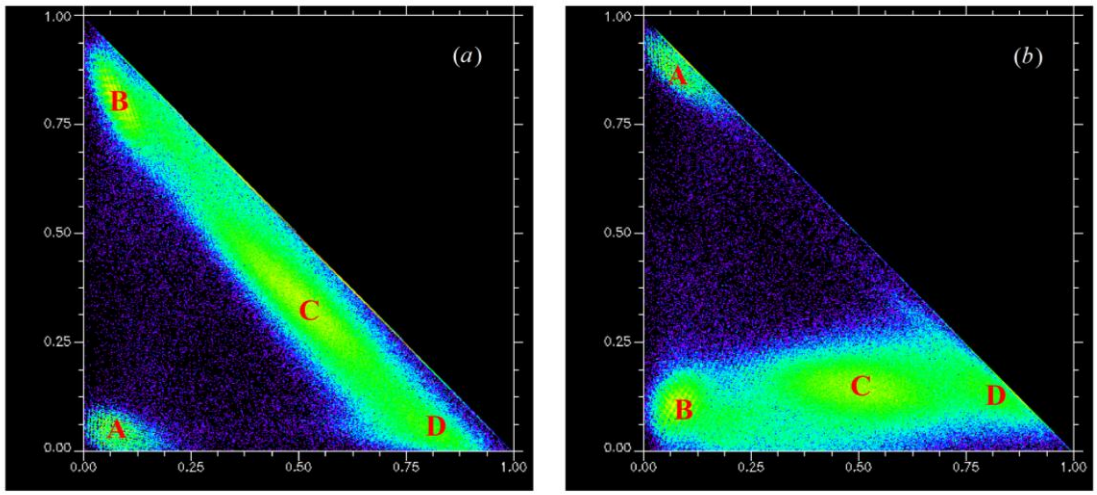

Figure 3-7 Slice density maps of distribution of V-I-S fractions and LST in the study area. The distribution is Gaussian-like and each bump represents a certain land use pattern. (*a*) "Impervious surface" fraction as x and "Vegetation" fraction as y; (*b*) "Impervious surface" fraction as x and "Low Albedo + Soil" fraction as y. Land use classes are labeled with (A) Water; (B) Vegetated; (C) Residential; (D) Commercial.

Table 3.5 Multiple comparisons in terms of accuracy and stability of different classifiers built with V-I-S fractions and LST combination.

Classifier	Accuracy difference	*p*-value	Implication
CART-BAGGING	-2.2%	<0.0001	Ensembles slightly improve accuracy on CART. The base tree classifier was sufficiently stable, making less room for potential improvement.
CART-RF	-1.2%	0.0026	
MLC-BAGGING	2.7%	<0.0001	MLC classifier is the most accurate classifier when built with V-I-S fractions and LST.
MLC-CART	5.0%	<0.0001	
MLC-RF	3.7%	<0.0001	
MLC-SVM	4.3%	<0.0001	
Classifier	Kappa difference	*p*-value	Implication
CART-BAGGING	-0.02	<0.0001	Improvements on stability achieved by ensembles are less than as in Table 3 or even none. The base tree classifier is sufficiently stable, making less or no room for potential improvement.
CART-RF	-0.06	<0.0001	
MLC-BAGGING	0.03	0.0224	MLC classifier is also the top stable classifier when built with V-I-S fractions and LST.
MLC-CART	0.04	0.5475	
MLC-RF	-0.01	<0.0001	
MLC-SVM	0.02	<0.0001	

this input feature configuration was the Bagging method. SVM remained its good performance regardless of the addition of input features.

Table 3.6 Performance comparison between (*a*) V-I-S fractions and LST (*b*) band spectral reflectance only. The differences were calculated by subtracting (*b*) from (*a*).

Classifier	Accuracy difference	*p*-value	Implication
BAGGING	3.0%	<0.0001	Bagging, RF and MLC classifier are improved when band spectral reflectance input is replaced by V-I-S fractions and LST.
CART	0.8%	0.1767	
MLC	6.0%	<0.0001	
RF	1.9%	<0.0001	
SVM	-0.6%	0.6843	
Classifier	Kappa difference	*p*-value	Implication
CART	0.06	<0.0001	More stable trees are produced when trained with V-I-S fractions and LST.

Table 3.7 Performance comparison between (*a*) All input features (*b*) band spectral reflectance only. The differences were calculated by subtracting (*b*) from (*a*).

Classifier	Accuracy difference	*p*-value	Implication
BAGGING	3.0%	<0.0001	Adding V-I-S fractions and LST variable would not enhance the MLC classifier as the assumption still remained violated. Tree classifier gained accuracy; tree-based ensemble classifiers achieved the highest accuracy.
CART	1.7%	<0.0001	
MLC	0.3%	0.9983	
RF	2.4%	<0.0001	
SVM	0.0%	1.0000000	
Classifier	Kappa difference	*p*-value	Implication
BAGGING	0.03	<0.0001	Slight but statistically significant stability improvement is achieved by adding V-I-S fractions and LST.
CART	0.06	<0.0001	
MLC	0.03	<0.0001	
RF	0.01	<0.0001	
SVM	-0.02	<0.0001	

3.3.3 Discussions on the superiority of V-I-S Fractions and LST

In additon to the revealed stability and accuracy improvement, the superority of V-I-S fractions and LST was also explored from other two aspects: (1) the tree structure (e.g. the sequence of variable being selected and the tree size) of single classification tree and trees in the forest; (2) the variable importance determined by OOB samples. The latter

would provide an alternative way for band selection, such as the application in hyper-spectral remote sensing (Chan and Paelinckx 2008).

In our case study, the tree classifier built with the ten-dimension dataset using the "Gini index" criteria picked up all V-I-S fractions and LST (Figure 3.8 (*a*)) in the earlier splits, which, however, only adopted one spectral band reflectance (B5), indicating that the decrease of the overall lack-of-fit could not be achieved much by using spectral reflectance data. The "information gain" criterion was also specified and the fitted tree picked up the V-I-S fractions and LST for their early splits and ignored most of the spectral reflectance variables (Figure 3.8 (*b*)). Tree was pruned to *cp* = 0.001 because beyond this *cp* value little accuracy improvement would result.

Delving into the grown forest to view each single fitted tree further confirmed the relevance of V-I-S fractions and LST with the urban land use classes. All ten input features were used for growing the random forest. The forest size (number of random trees) was set to 500 as with this number the random forest can achieve the least OOB error rate. The increase of the badness-of-fit can be represented by either the decrease in accuracy (equivalent to the increase in OOB error rate) or increase in "node impurity". The greater importance of V-I-S fraction and LST should be observed in Figure 3.9.

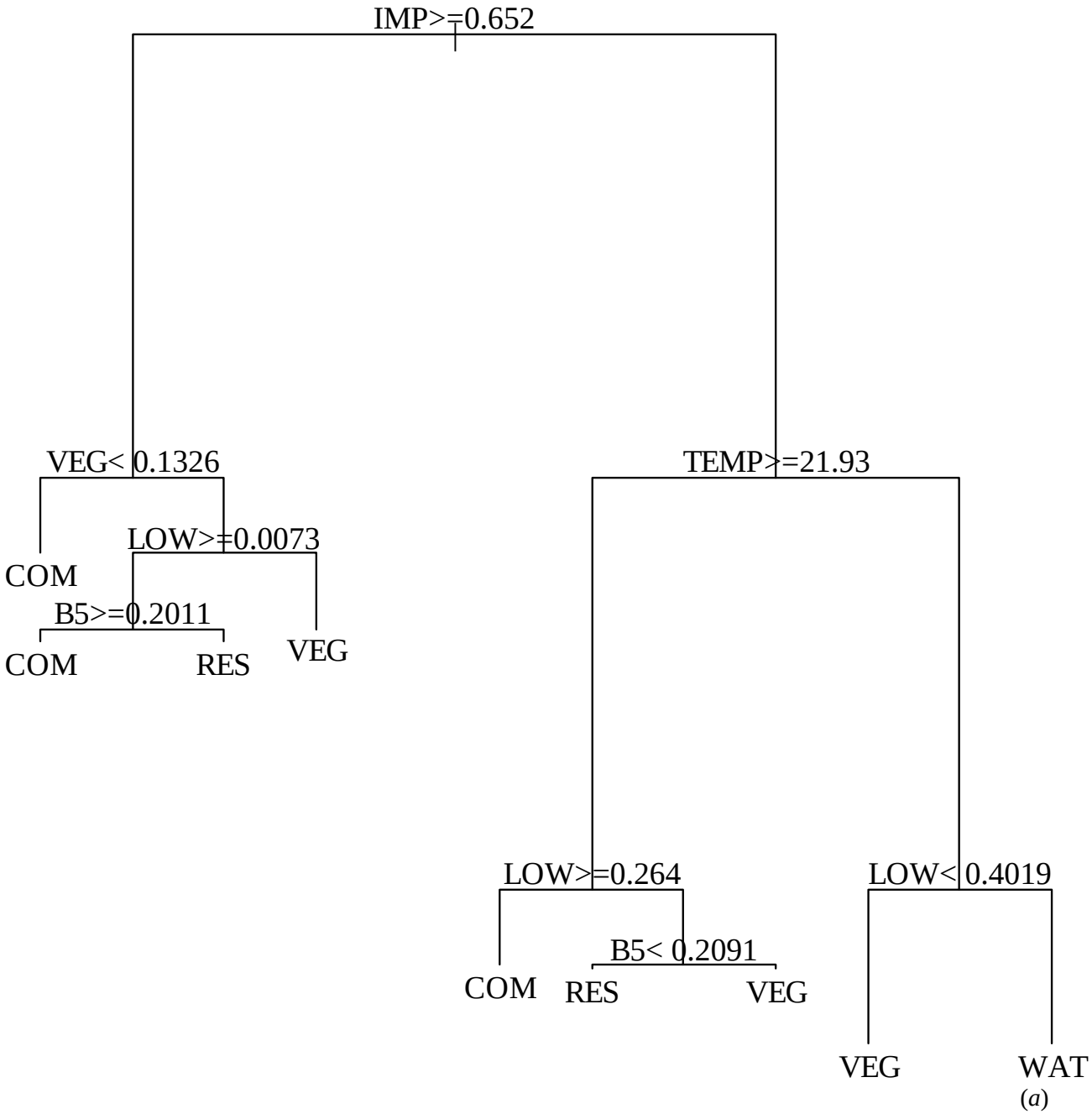

(*a*)

Figure 3-8 (*a*). Tree fitted with *cp*=0.001 and "Gini index" criteria; (*b*). Tree fitted with *cp*=0.001 and "information gain" criteria. (IMP=Impervious Surface fraction, VEG=Vegetation fraction, LOW= Low albedo + Soil fraction, TEMP=LST, COM=Commercial, RES=Residential, VEG=Vegetated, WATER=Water).

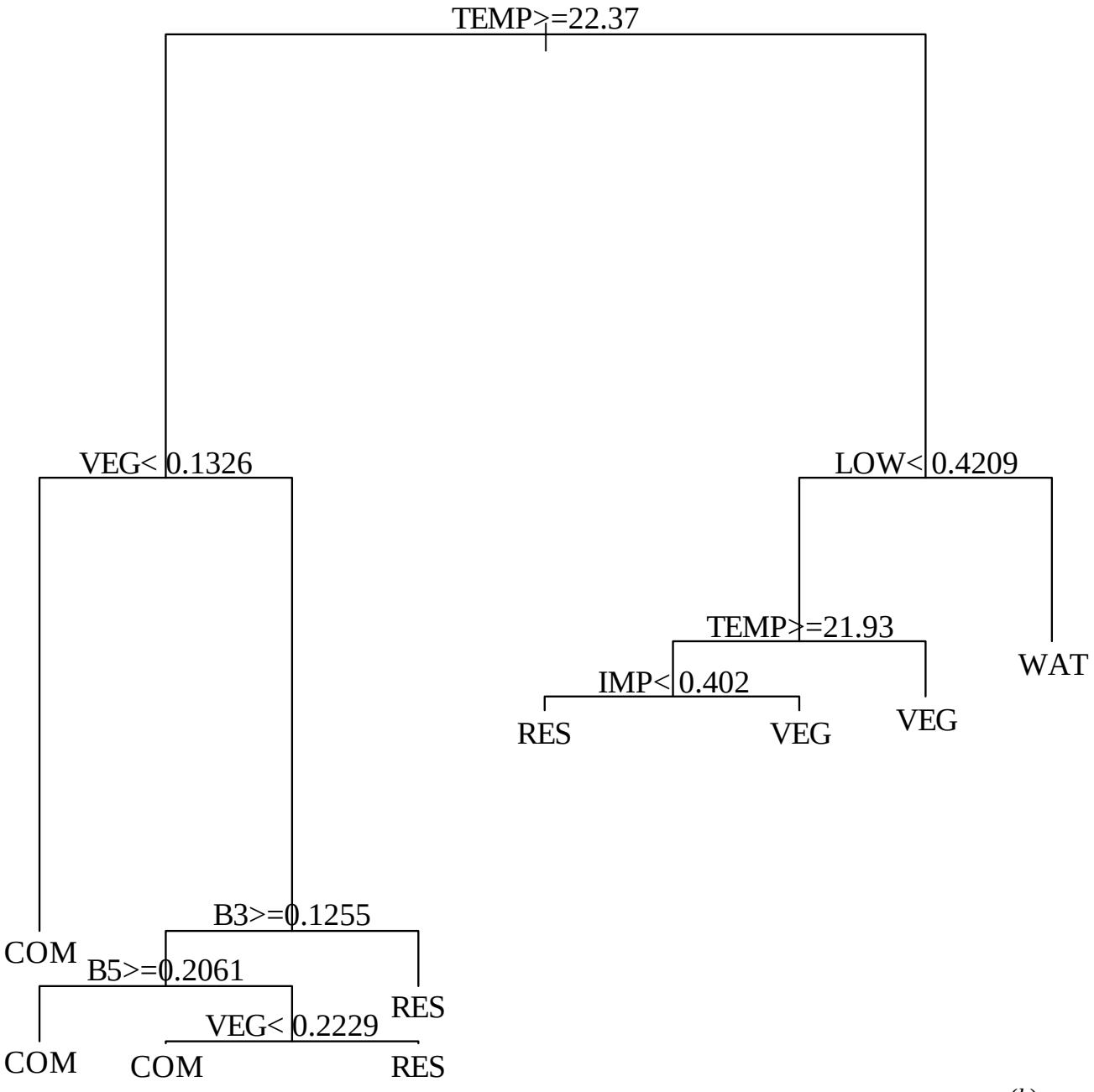

(*b*)

Figure 3.8 Continued.

To evaluate the input feature's superiority with statistical significance, a forest consisting of 500 overfitted trees was grown for individual inspections. The average size of the 500 trees (# of nodes, returned from the R package **randomForest**) when only

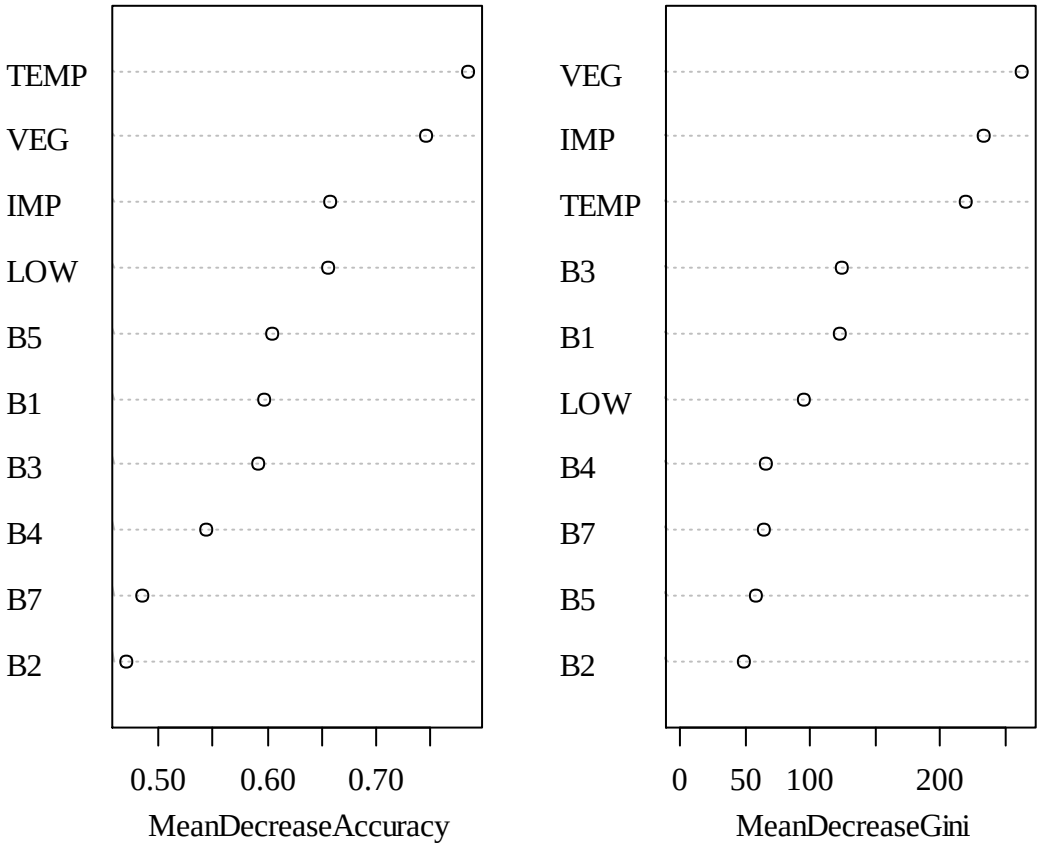

Figure 3-9 Variable importance comparisons based on the increase in the badness-of-fit on OOB samples in random forest. LST is the most important input feature. Band spectral reflectance is less important than the LST and V-I-S fractions in urban land use classification. (IMP=impervious surface fraction, VEG=Vegetation fraction, LOW= Low albedo/Soil fraction, TEMP=LST)

spectral reflectance was used was about 77 nodes; and this number was reduced to 49 when V-I-S fractions and LST were used instead. The ANOVA test returned a significant *p*-value ($p<0.001$). The frequencies of the ten input variables being used as the first five splitting variables are summarized in Table 3.8. The first five splits were generally based on the use of V-I-S fractions and LST, suggesting their superiority over the band reflectance for urban land use studies. Another finding in the analysis was that the

infrared bands (B4, B5 and B7) of Landsat TM carry more information for separating urban land use classes than the visible bands.

Table 3.8 Deep investigation of individual trees in the Bagging method (The random forest method was replaced with the Bagging method to guarantee the fairness. In random forest, the probability of V-I-S fractions and LST being selected for growing a single tree to that of band spectral reflectance is 4:6, which is not fair). A preference on using V-I-S fractions and LST for splitting tree should be noticed.

Input Feature	Root node	2nd node	3rd node	4th node	5th node
B1	72	43	79	8	39
B2	36	10	35	6	10
B3	78	50	52	21	23
B4	0	25	0	68	54
B5	3	21	3	52	36
B7	7	33	15	67	10
VEG	115	96	130	39	106
IMP	148	77	95	23	34
LOW	0	44	19	64	79
TEMP	41	101	72	18	73

3.3.4 Generalizability and limitation

To test the generalizability of the results, the same analysis was also conducted on the test site of Baton Rouge, LA. SVM classifier was still the best classifier among all classifiers being considered for the conventional spectral based classification. Except for SVM, all classifiers were boosted when replacing the band reflectance with V-I-S fractions and LST combination as input features. This was indicated by the prevalently more elevated and less spread blue boxes as compared to their green counterparts (see Figure 3.10). Especially, the improvement was the most significant for MLC classifier. The difference in accuracy for MLC was 0.10 with a significant *p* value. This could be attributed again to the superiority of V-I-S fractions and LST combined input as they have nearly multivariate normal distribution and meet the MLC assumption. Given the V-I-S fractions and LST combination as the input, although MLC was not the best classifier

among five tested classifiers for Baton Rouge test site, it still managed to achieve a comparable level of accuracy to those modern machine learning classifiers.

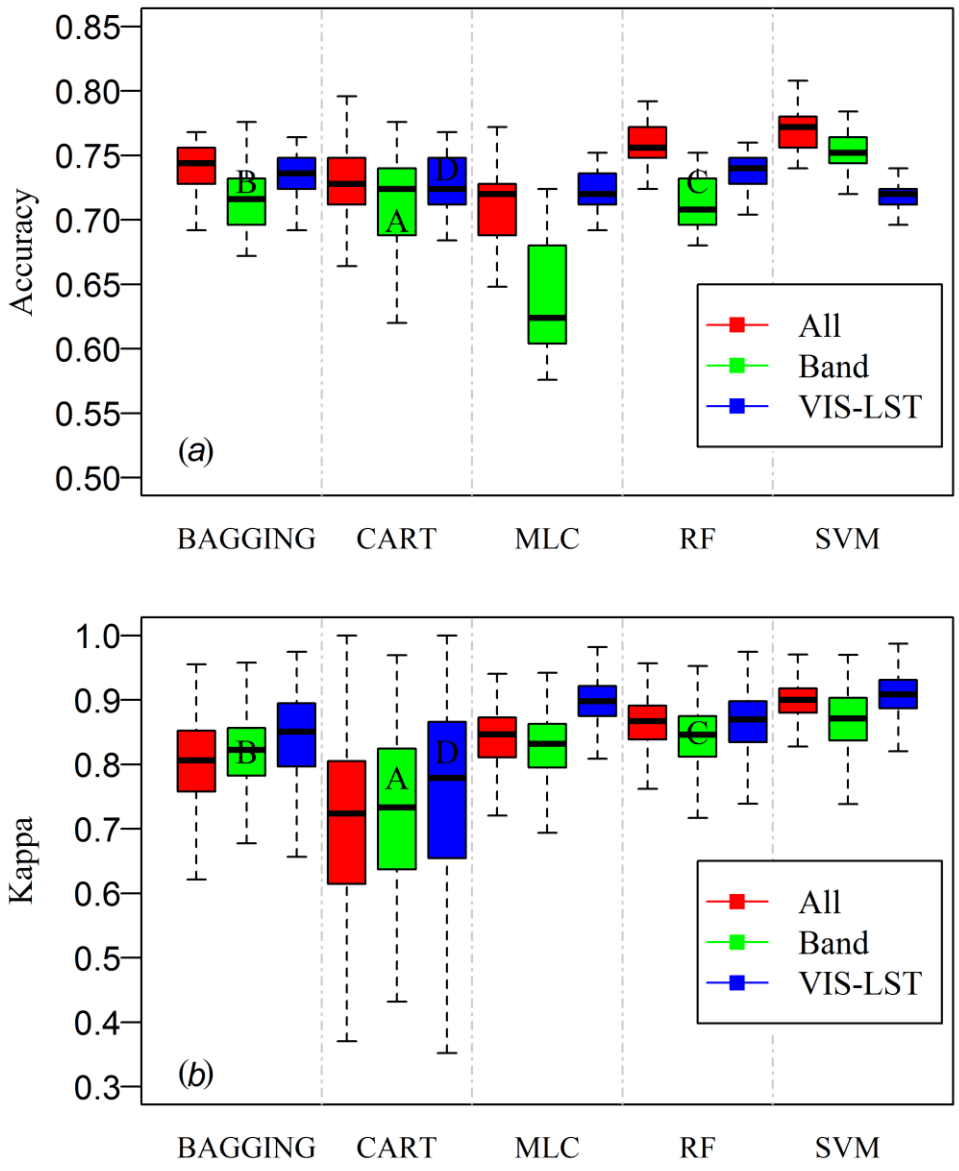

Figure 3-10 Accuracy and stability comparisons of five classifiers for three different input feature configurations (Baton Rouge, LA).

Tree classifier was again made more stable (but not more accurate) by either using ensemble approach or replacing the band reflectance input with the V-I-S fractions and LST, which could be clearly seen in Figure 3.10 (*a*) where the "Accuracy" box B (band

reflectance + Bagging), C (band reflectance + random forest) and D (V-I-S fractions and LST combination + CART) were less spread out than A (band reflectance + CART) as well as in Figure 3.10 (*b*) where the "Kappa" box B (band reflectance + Bagging), C (band reflectance + random forest) and D (V-I-S fractions and LST combination + CART) were more elevated than A (band reflectance + CART). The addition of V-I-S fractions and LST to the multispectral reflectance also improved the tree-based ensemble classifiers significantly, which was also the same as the case for New Orleans. The final classification result is displayed in Figure 3.11.

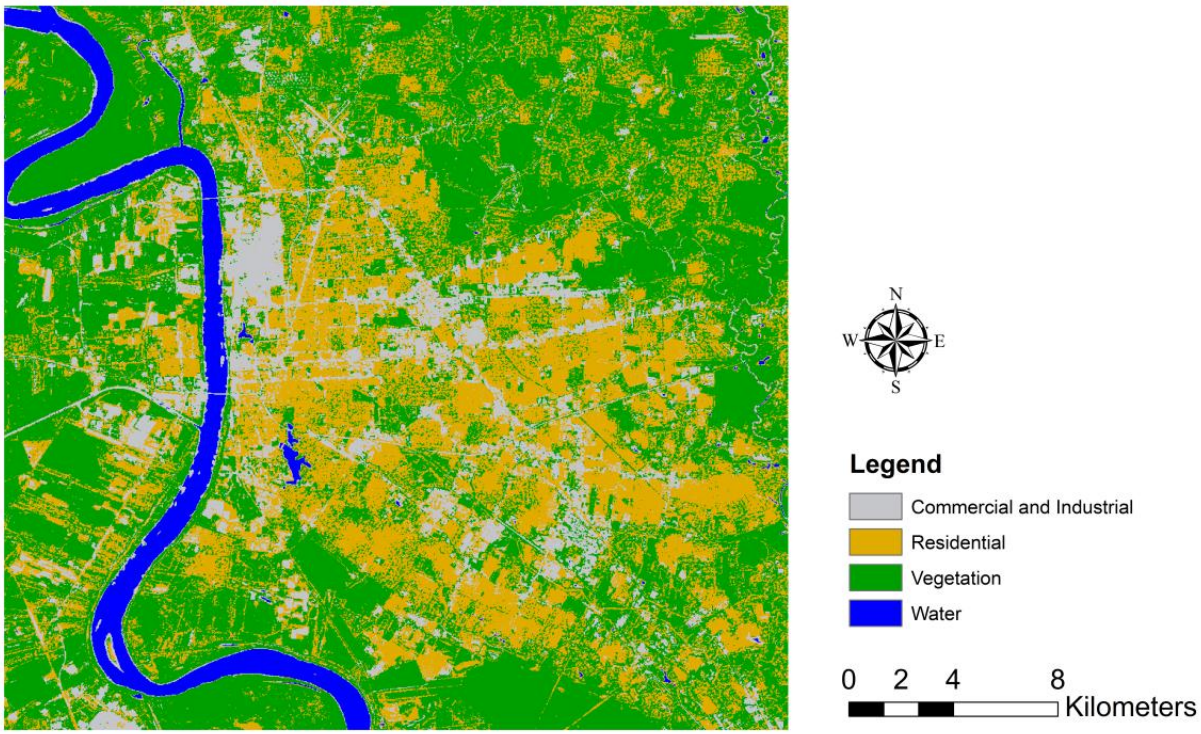

Figure 3-11 Classification of Baton Rouge with MLC+V-I-S+LST input.

The V-I-S model is the most suitable input when the classes of interest have distinguishable differences in their V-I-S structures. This is true for our two study areas and most of the U.S. urban areas where residential parcels are predominantly composed

of individual houses with adequate vegetation coverage. Therefore, the V and I fraction quantities can distinguish different land use classes, e.g. “Residential class” is in between the “Commercial and Industrial class” and “Vegetation class”. However, for some developing countries, such as Haiti and China, the majority of population lives in multi-story apartments and the average vegetation coverage is limited. Hence, the boundary between “Residential class” and “Commercial and Industrial class” becomes fuzzy. Hence, the superiority of V-I-S derived land use classification might be only likely to be applicable in the U.S. urban environment and the like. The conclusion may also be not applicable if a different or more detailed classification schema is to be adopted, such as a breakdown of vegetation class to be “Forest” and “Pasture” class. However, the current classification schema is very common in the literature of the U.S. urban studies. These four land use classes belong to Anderson Level-I classes (Anderson et al. 1976). Given a moderate resolution image, this is a reasonable and applicable land use classification schema. The classification results of this study are useful for a level-II classification with higher spectral/spatial resolution images. For example, the land use class boundary could be used as constraints for the segmentation in a subsequent object-oriented classification with a more detailed classification schema.

3.4 Object oriented approach

3.4.1 Design of research

I also applied the evaluation framework to investigate the superiority of V-I-S fractions and LST in the context of object-oriented classification. Commercial software Definiens (formerly known as “eCognition”) was used to perform the multi-resolution segmentation on the V-I-S+LST composite image. The V-I-S fractions and LST were

stretched from fractional numbers to 0~255 (e.g., 8 bit = 1 byte) so that the software can produce meaningful image objects (the scale parameter has to be set to integers, but the original data scale is in terms of fractions, which is less than 1).

The setting of the scale parameter controls the segmentation and is critical to the analysis. It is interesting to test two specific scale parameters: 15 and 30. A "trial-and-error" approach was adopted to investigate the scale parameter, which indicated a scale parameter between 15~30 was an appropriate range for our data. Scale parameter values outside this range led to obvious either over-segmentation or under-segmentation. This research did not consider the shape or compactness parameter and therefore the default value of 0.5 was applied. The same 800 ×500 image stack of New Orleans was segmented, resulting in 3363 image objects with a scale parameter of 15 and 843 image objects with a scale parameter of 30 (Figure 3.12). The image objects were exported as shapefiles with layer means for V-I-S fractions, LST and band reflectance. Random image object samples were collected to be used as the training dataset.

For accuracy assessment, the same set of 397 points used in previous study was used as the reference data. However, the classification was based on the image objects, the resultant classification results, which were in terms of image objects, cannot be directly used for accuracy assessment due to the scale inconsistency between the reference data and classification result (the former being points and the latter being image objects). As such, the classified image objects, which were in forms of polygon shapefiles, was then converted to raster. The zonal statistics tool was used to extract the assigned classes for each of the 397 test points from the produced raster image. The whole process was automated with a combination of R and Python scripts. Figure 3.13 summaries this work

flow. Only two input feature configurations, namely, band reflectance input only, V-I-S and LST synergic input were compared in this object oriented classification context.

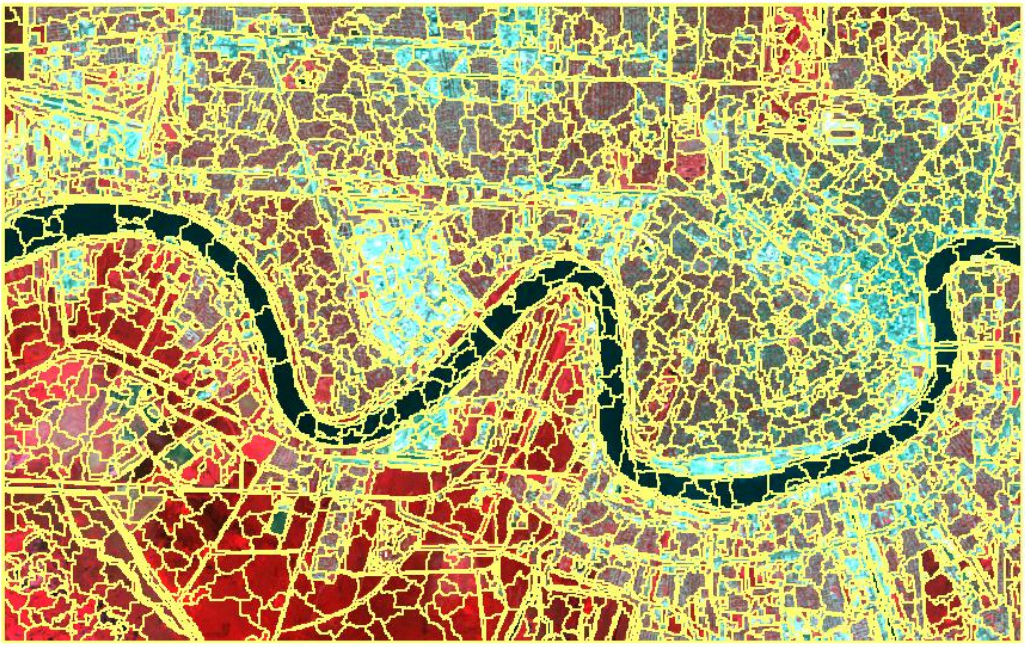

(*a*)

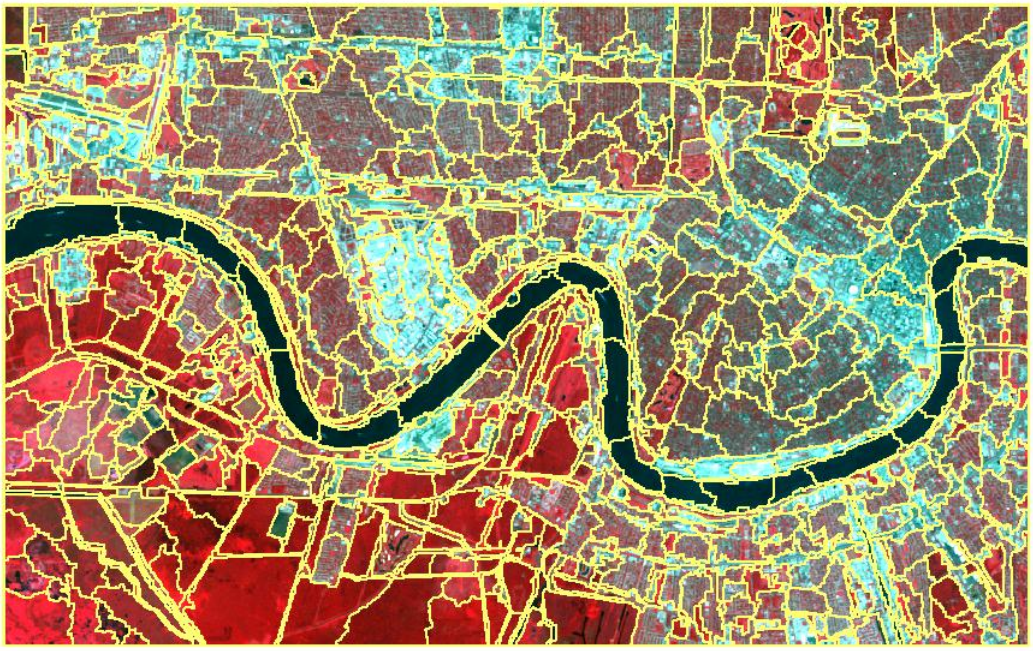

(*b*)

Figure 3-12 Image segmentation from Definiens for New Orleans. (*a*) scale parameter = 15 (*b*) scale parameter =30.

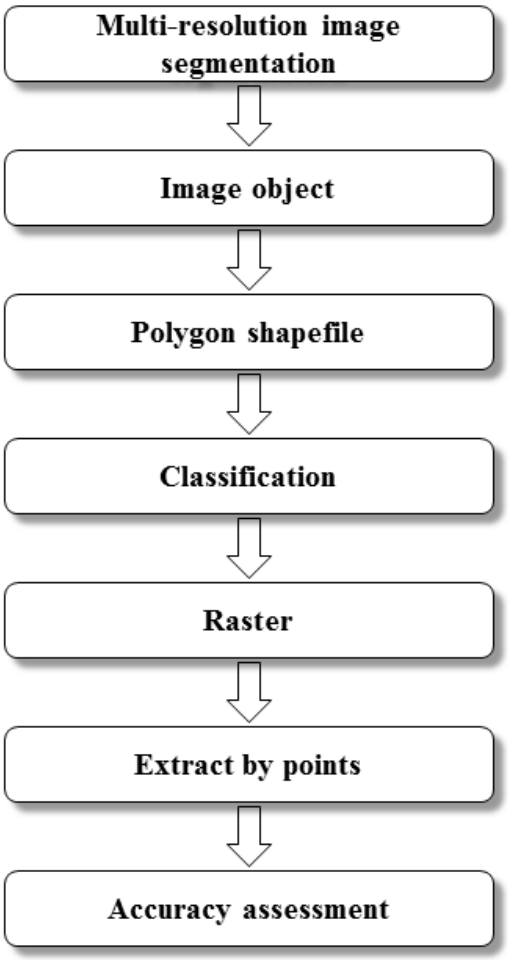

Figure 3-13 Data processing flow for the object oriented classification scenario.

3.4.2 Performance of classifiers

The classification results of five classifiers are summarized in Table 3.9. Figure 3.14 displays the comparison of these classifiers with different input feature configuration when the entire training dataset is used. It is obvious that object oriented classification is superior to the conventional spectral based classification in terms of accuracy. The best scenario is the object-oriented classification using a scale parameter of 30 for segmentation and V-I-S fraction and LST as input features and SVM as the classifier. The overall accuracy was as high as 81%. Figure 3.15 displays the classification result of

the best scenario. Notice that the "salt-and-pepper" effect is further removed by classifying the image in terms of image objects instead of individual pixels.

Table 3.9 Accuracy and Kappa summary of classification result of different set of image objects using different classifiers and input feature configurations. (*a*) scale parameter = 15; (*b*) scale parameter =30.

(*a*)

Multispectral reflectance only			Synergy of V-I-S fractions and LST		
Classifier	Accuracy	Kappa	Classifier	Accuracy	Kappa
MLC	0.81	0.73	MLC	0.80	0.71
CART	0.78	0.69	CART	0.74	0.62
BAGGING	0.78	0.69	BAGGING	0.78	0.68
RF	0.78	0.69	RF	0.78	0.68
SVM	0.78	0.68	SVM	0.80	0.71

(*b*)

Multispectral reflectance only			Synergy of V-I-S fractions and LST		
Classifier	Accuracy	Kappa	Classifier	Accuracy	Kappa
MLC	0.80	0.71	MLC	0.80	0.71
CART	0.74	0.63	CART	0.79	0.70
BAGGING	0.76	0.66	BAGGING	0.79	0.70
RF	0.76	0.65	RF	0.79	0.70
SVM	0.77	0.67	SVM	**0.81**	0.72

From Figure 3.16, tree classifier is again the worst classifier with the lowest accuracy and stability in the object oriented classification scenario when used with the band reflectance as the input. The ensembles improve both the accuracy and the stability of tree classifier. The adoption of V-I-S fractions and LST also benefit the tree classifiers. The SVM classifier is the most robust classifier. The accuracy of MLC doesn't benefit from using V-I-S fractions and LST instead of band reflectance, however, the stability is improved. All of these properties hold true for both scale parameters (Figure 3.16 for scale parameter of 15 and Figure 3.18 for scale parameter of 30). When compared to the pixel based classification case (Figure 3.6), the point cloud is much lower, but not as

significant more to the right as to the low, meaning the benefit of the object oriented classification is more in terms of accuracy than stability.

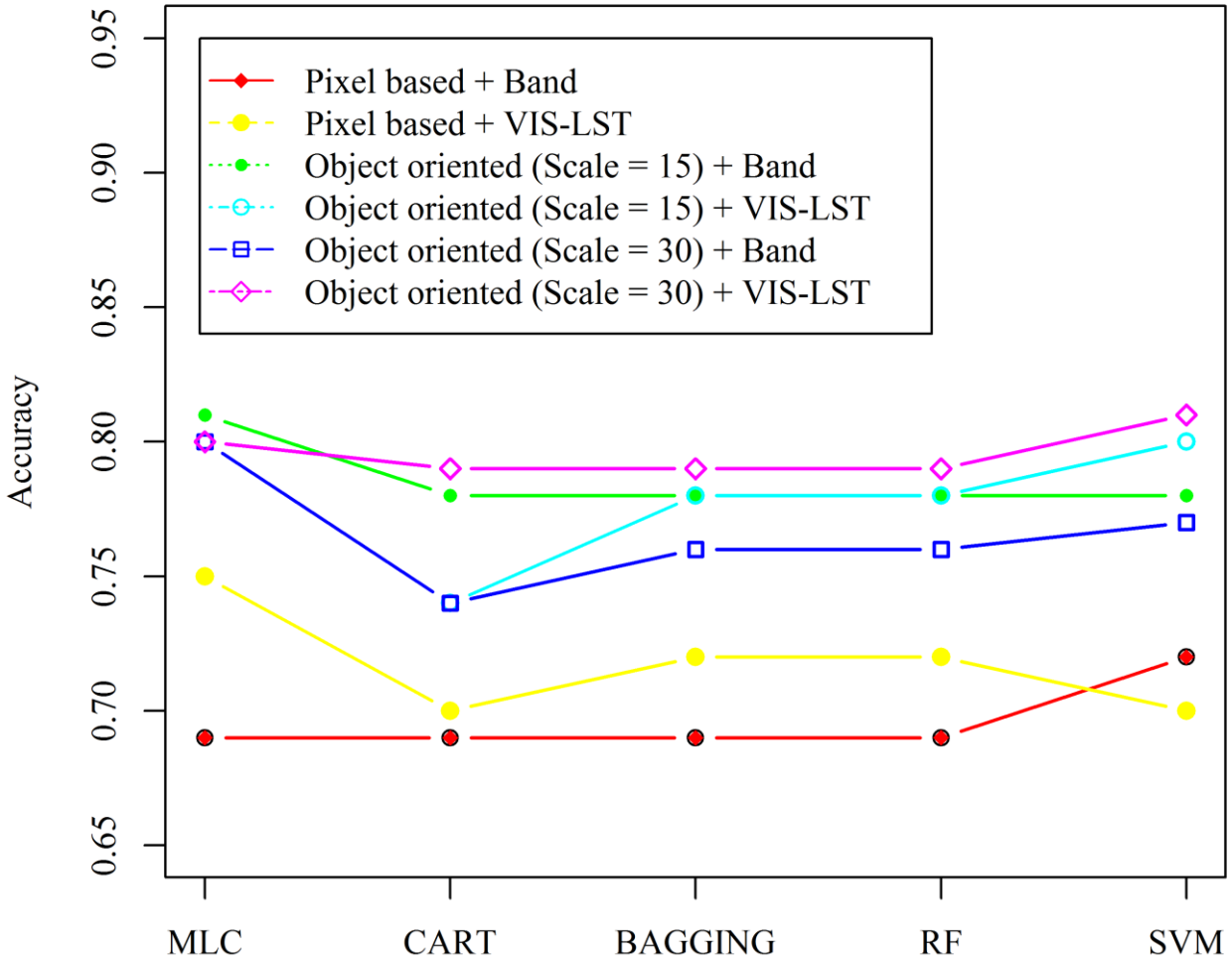

Figure 3-14 Comparisons of classification accuracy with respect to different classifiers and input feature configurations, and different classification principles (pixel-based vs object-oriented classification).

The difference between these two scale parameters is subtle. A clear trend is that the prevalent elevated blue boxes as compared to the green boxes, for both accuracy boxplot and kappa boxplot. The Kappa-Error diagram displays a much more compact cloud points for V-I-S+LST input as compared to band reflectance input (Figure 3.17 for scale parameter of 15 and Figure 3.19 for scale parameter of 30). When compared to the pixel

based classification case (Figure 3.6), the point cloud is much lower, but not as significant more to the right as to the low, meaning the benefit of the object oriented classification is more in terms of accuracy than stability.

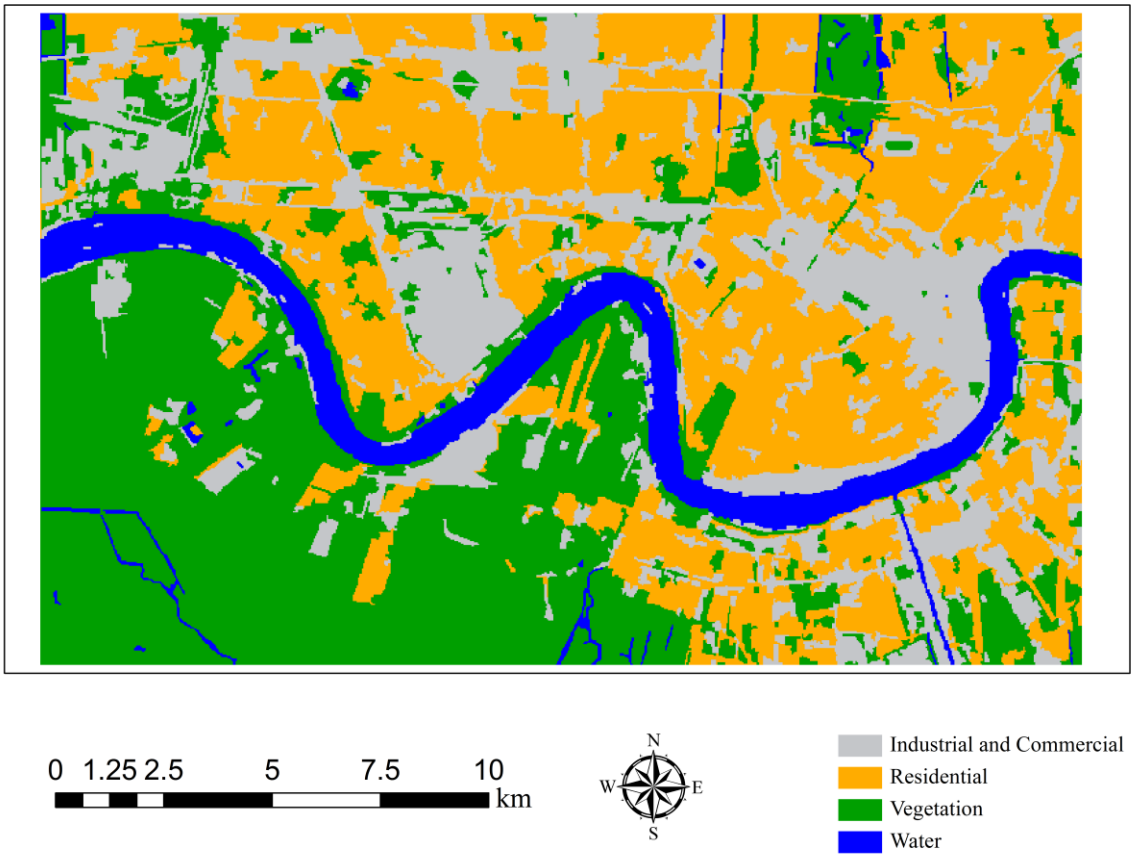

Figure 3-15 Classification result using object oriented method.

The averaged nodes used in tress in the forest were 14 for band reflectance input and 15 for V-I-S in the case of scale parameter = 15. ANOVA test suggested no significant difference between these two different input feature configurations in terms of tree complexity. And 22 vs 23 for the case of scale parameter =30. The higher scale parametercase resulted in slightly more complex trees. However, both cases showed

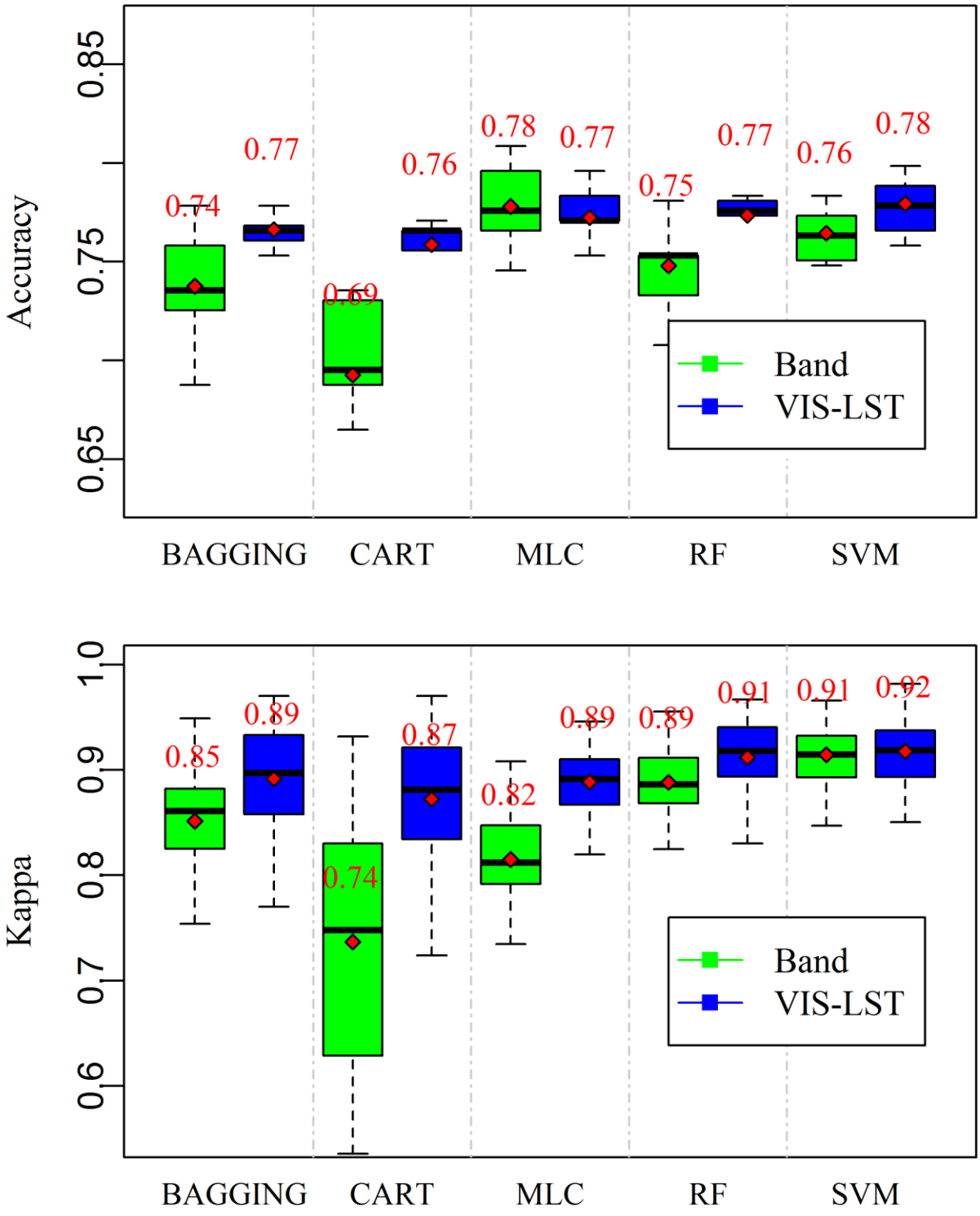

Figure 3-16 (*a*) Accuracy boxplot for scale parameter = 15; (*b*) Kappa boxplot for scale parameter = 15. When compared to figure 3(a), both blue and green boxes are generally elevated from the range [0.7, 0.75] to [0.75, 0.8], indicating the accuracy superiority of object oriented classification.

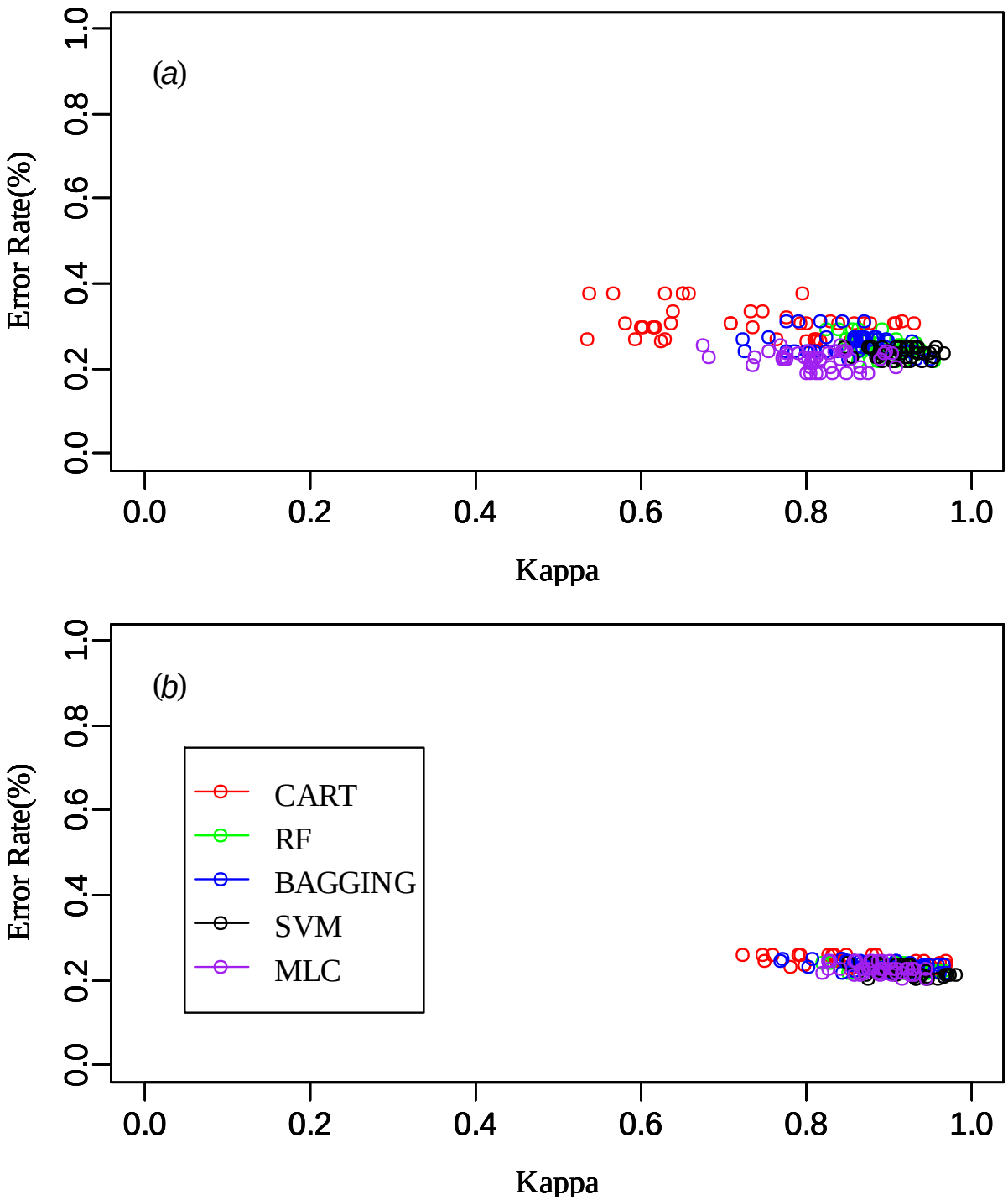

Figure 3-17 Kappa error diagram for scale parameter =15. (*a*) Band reflectance as the input; (*b*) V-I-S+LST as the input. A obvious more compact point cloud for (*b*) than (*a*) should be noticed

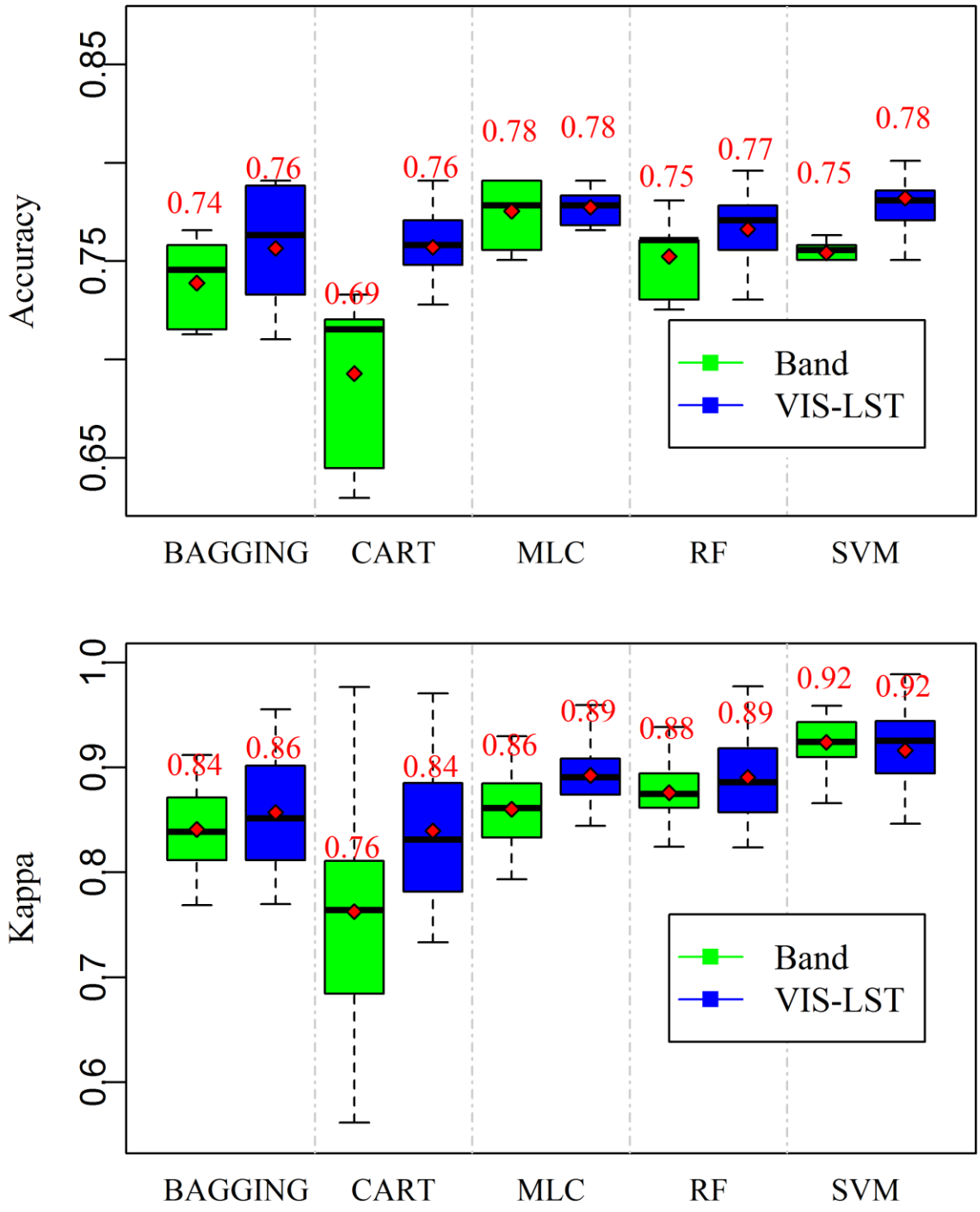

Figure 3-18 (*a*) Accuracy boxplot for scale parameter = 30; (*b*) Kappa boxplot for scale parameter = 30. This figure doesn't show too much difference when compared to its counterpart where scale parameter=15.

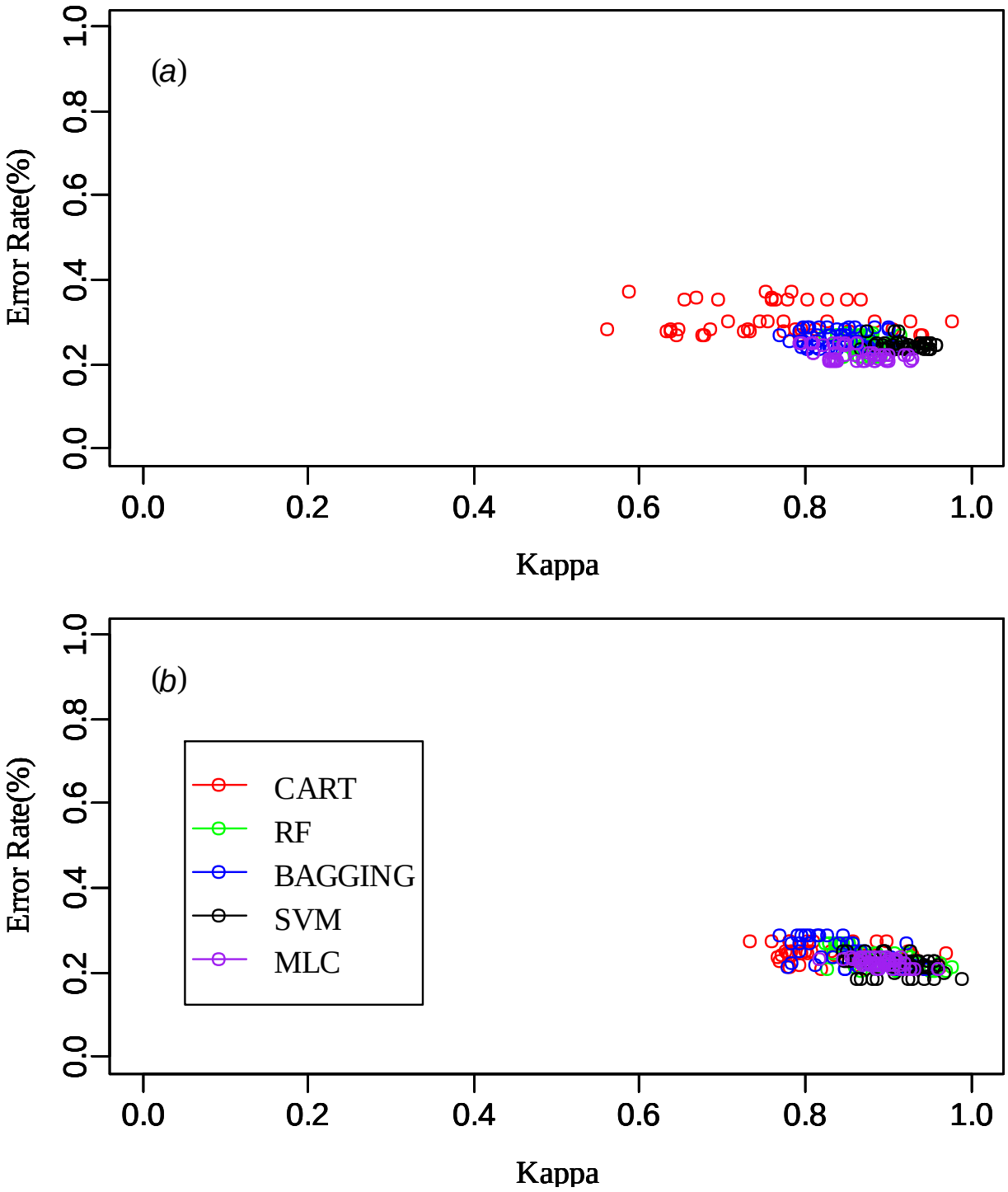

Figure 3-19 Kappa error diagram for scale parameter =30. (*a*) Band reflectance as the input (*b*) V-I-S+LST as the input. A obvious more compact point cloud for (*b*) than (*a*) should be noticed.

significant less complex trees for object oriented classification as compared to pixel based classification (recall that the number is 77 vs 49 for the case of pixel based classification, please refer to page 64 in section 3.3.3).

From Figure 3.20 and Table 3.10, although vegetation fractions and LST was still among the most important ones, the benefit of using V-I-S fractions and LST over band reflectance was reduced in the object-oriented classification as compared to the pixel based classification, which means that the object-oriented approach can compensate the inadequacy of the band reflectance as the input.

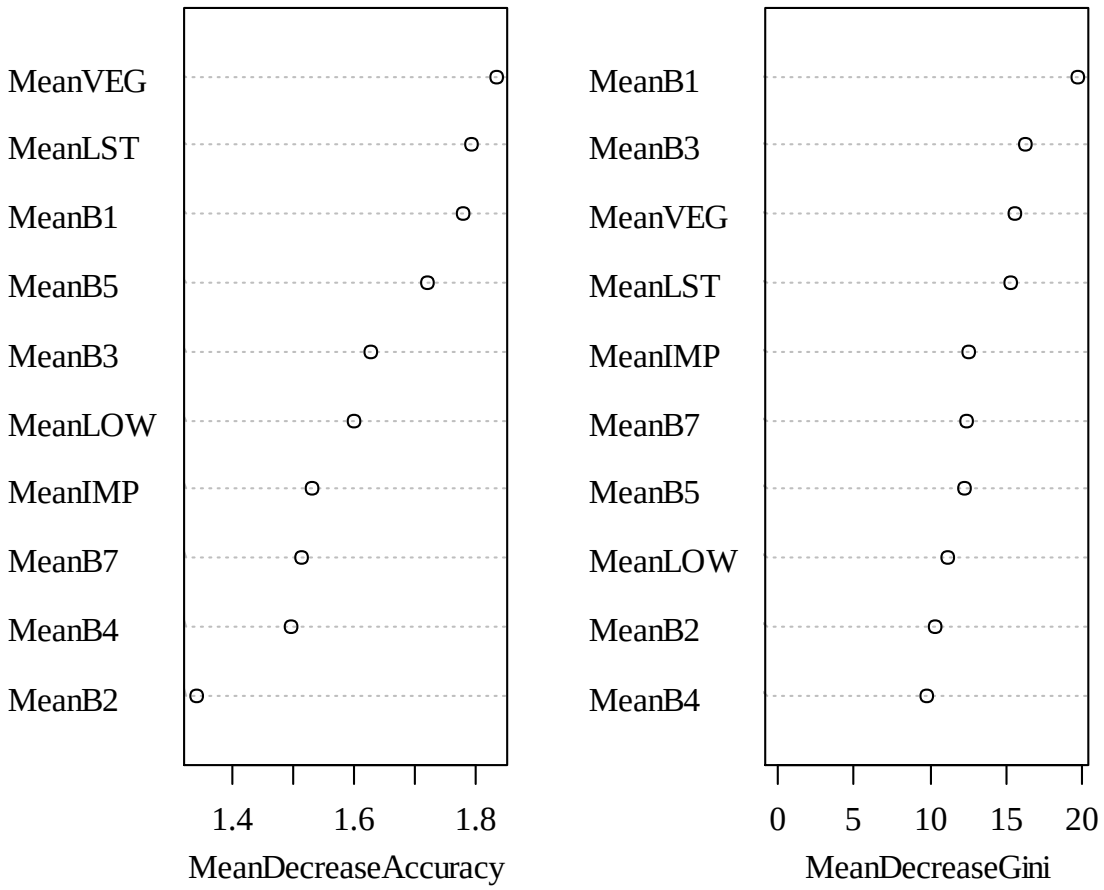

Figure 3-20 Importance of variables from the OOB sample.

Table 3.10 The number of times of each variable being used for first five splits for the 500 trees for the object oriented classification case.

Input Feature	Root node	2nd node	3rd node	4th node	5th node
B1	131	42	26	10	46
B2	75	12	20	21	13
B3	104	44	19	20	27
B4	1	48	3	56	53
B5	8	66	7	61	45
B7	55	27	18	50	38
VEG	34	72	34	45	38
IMP	71	31	19	24	40
LOW	9	53	17	58	46
TEMP	12	96	7	18	57

3.5 Conclusion

The selection of classifiers is closely related to the selection of input features for urban land use classification. In an earlier chapter, this research proposes an evaluation framework based on the classification tree and statistical randomization methods to offer a comprehensive evaluation of the superiority of input features and the performance of classifiers. A case study using the framework showed the superiority of the V-I-S fractions and LST over the direct use of multispectral band reflectance in urban land use classification. The investigations and discussions were made based on (1) the sequence of variable being selected in growing trees; (2) tree complexity; (3) Kappa-Error diagram; (4) increase of badness-of-fit on OOB samples; and (5) ANOVA tests. Four major conclusions can be drawn as following.

First, the analysis results from this research promote the use of V-I-S fraction images and the LST in urban land use studies, because in addition to the improvement on the overall classification accuracy, which was already documented in the previous literature and also confirmed in the present study by using the evaluation framework, the use of V-I-S fractions and LST combination as the input for urban land use classification can: (1)

alleviate the “salt and pepper” problem; (2) is preferred by tree and tree-based ensembles for branch splitting; (3) lead to less complex trees when achieving stopping criteria; (4) improve the stability of tree classifiers; (5) appear nearly normal distribution for urban land use classes and make the parametric MLC a reliable classifier. These advantages of V-I-S fractions and LST revealed from the evaluation framework complete a comprehensive assessment on their superiority in the context of urban land use classification.

Second, the MLC classifier is comparable with the modern statistical learning classifiers or even outperforms them when the V-I-S fractions and LST are used instead of the direct use of spectral bands. This is consistent with previous reports that MLC classifier could be superior to non-parametric methods if the normality assumption is properly met. In this case, the histogram of V-I-S fractions and LST displays adequate normality, and the use of other complex classifiers becomes unnecessary. It is recommended to use MLC classifier in conjunction with V-I-S fractions and LST as the input in urban land use classification due to its adequacy and simplicity. However, the MLC is only suitable when V-I-S fractions and LST are used as the only input features. Replacing them with or including the band reflectance, regardless of enriching the data input, might degrade the multivariate normal distribution and subsequently degrade the MLC classifier.

Third, the direct use of spectral bands is not recommended for any classification approach being considered, except for the SVM, which maintains consistently high classification accuracy and robustness. The tree classifier trained with multispectral band reflectance lacks stability, leaving room for potential improvements through

randomization achieved by tree-based ensembles. Specifically, tree-based ensembles increase the classification stability, but no statistically significant accuracy improvement is found. The SVM achieves the highest overall accuracy and stability when multispectral band reflectance is the only input. Therefore, SVM is recommended for those urban land use studies which do not use the derivation of V-I-S fractions and LST. The addition of V-I-S fractions and LST to the multispectral reflectance contributes to the improvement of ensemble classifiers in the urban land use classification significantly. The tree-based ensemble classifiers and SVM are suitable for the case when the full data dimension is used.

Fourth, the object-oriented classification generally achieves higher accuracy than the pixel based methods. The SVM classifier remains as the best classifier in this scenario. The two different scale parameter used bears little difference in performances. In the application of the urban LULC classification, the conclusion about the accuracy and stability benefit of the V-I-S fractions and LST used as alternative input for pixel based approach also holds true for the object oriented approach. However, the importance of V-I-S fractions and LST revealed from the tree complexity and OOB sample becomes less significant in object-oriented classification.

A general guideline for urban land use classification inferred from this research is that the remote sensing analyst can choose to use either object-oriented method or the transformation from band reflectance to V-I-S images + LST to perform an adequately accurate and reliable classification. If none of them is used, then the SVM classifier is strongly recommended. Despite of the fact that conclusions of this study have minor limitations on locations and classification schema, this research is among the few to

investigate the stability of V-I-S fractions and LST in urban land use classification. The evaluation framework developed could also be applied in other urban environment and considered in the assessment of input features and classifiers in other remote sensing classification endeavors. Future study could be applying the evaluation framework for the assessment of texture variables and object oriented classification in urban land use investigation. A different classification schema may also be considered.

Chapter 4 Urban land use classification through watershed segmentation in the V-I-S feature space

4.1 Introduction

The Vegetation-Impervious Surface-Soil (V-I-S) model (Ridd 1995) has been widely applied in urban landscape studies (Madhavan et al. 2001, Ward et al. 2000, Wu and Murray 2003) and extended by many others (Lu and Weng 2004, Phinn et al. 2002, Small 2001, Small and Lu 2006). Land use/land cover (LULC) classification based on V-I-S fractions has been found to be more accurate than the conventional spectral based classification (Lu and Weng 2004, Rashed et al. 2003). Comparative studies have shown that other than accuracy improvement, using V-I-S fractions could also improve classifiers' stability compared to the conventional band data because sub-pixel fractions quantitatively measure spatial composition of land cover (Tang et al. 2012). The Lu-Weng urban landscape model (Lu and Weng 2004) conceptually partitions the V-I-S ternary feature space (e.g., histogram of frequency of occurrence of each V-I-S fraction combination) to define LULC classes. However, no practical partition of the V-I-S feature space that matches Lu-Weng's triangle was attempted. The V-I-S histogram, if plotted upside down, bears resemblance to topographic depressions. Therefore, the inverse histogram can be partitioned into LULC regions approximating the Lu-Weng's urban model using the watershed segmentation algorithm, which has been widely adopted for partitioning digital image's feature space (Soille 2002) and the filtered gradient (Li and Xiao 2007) of multispectral images for classification. This chapter illustrates the procedure of urban LULC classification through the watershed segmentation in the V-I-S

feature space. The advantages and limitations of this method also are discussed. The chapter answers the research question 5.

4.2 Test sites and remote sensing images

I selected two urban areas for case studies: New Orleans and Baton Rouge in Louisiana, U.S.A. New Orleans (Figure 4.1) is a metropolitan port city traversed by the Mississippi River. The southwest part of New Orleans is undeveloped and comprises forest, agricultural land, and wetlands; the residential area is mainly located to the north and southeast of the Mississippi River; commercial and industrial areas are predominantly constructed along the Mississippi River and in the central city. Baton Rouge (Figure 4.1) is the second largest city and the capital of Louisiana, whose economic development is dominated by the petrochemical industry with large oil refineries constructed in the north of the Central Business District (CBD). The residential areas are mainly established in the east and south of the city. The Mississippi River borders the western edge of the city. These two areas represent the typical southern U.S. urban environment.

Two Landsat 5 Thematic Mapper (TM) images (Path/Row 39/22 for New Orleans acquired on 22 August 2005 and Path/Row 39/23 for Baton Rouge acquired on 16 October 2005) were used for extracting V-I-S fractions. 1-m resolution Digital Orthophoto Quarter Quadrangles (DOQQ) acquired in October 2005 were used as the reference. An image-to-image registration between the DOQQ and TM data was performed using a first-order polynomial transformation and nearest-neighbor resampling to ensure the locational accuracy. The resultant Root Mean Square Error (RMSE) was less than half the size of a TM pixel.

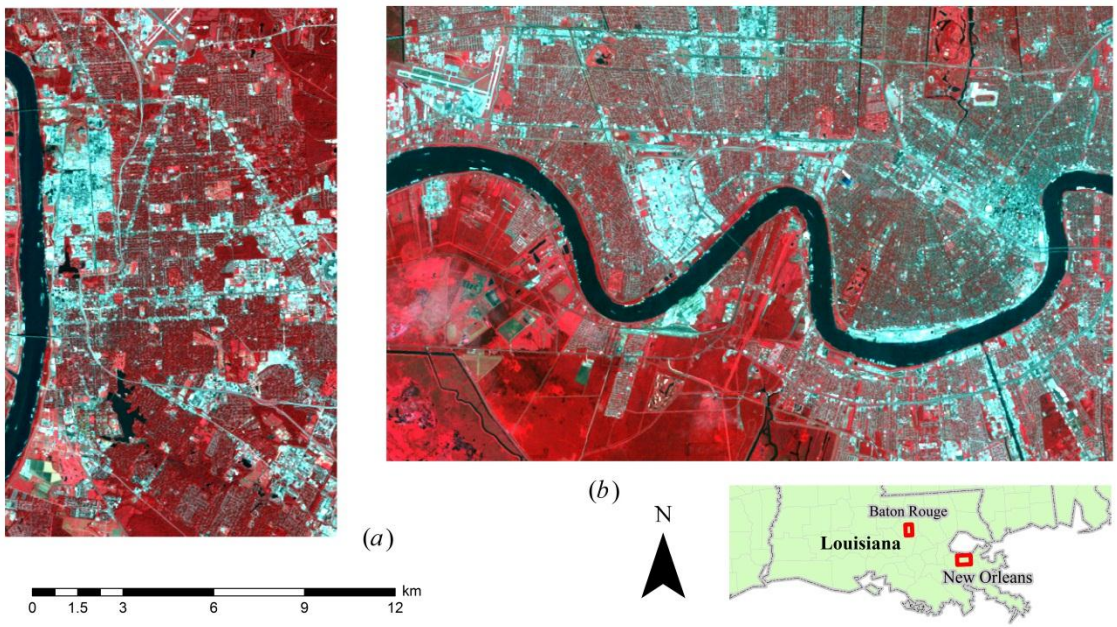

Figure 4-1 Study sites: (a) Baton Rouge and (b) New Orleans. The images are standard false-color composites of Landsat.5 TM. Bright areas are the commercial and industrial areas. Vegetation appears red and the dark linear feature is the Mississippi River. Areas with a fine textural appearance are the residential regions.

4.3 Procedures

The WS-based approach comprises several steps of data processing. A flow chart summarizing the whole procedure is provided in Figure 4.2 and is explained below and the algorithm is implemented by using IDL programming language (Tang 2008).

4.3.1 V-I-S fraction extraction and feature space rasterization

The first step is to extract the V-I-S fraction images, based on which the V-I-S feature space image is to be constructed. The TM data are calibrated to reflectance for bands 1 through 5 and 7. A normalization procedure (Wu 2004) is employed in order to reduce the spectral variance of endmembers prior to the spectral unmixing. The V-I-S fraction images are then derived using the Sequential Maximum Angle Convex Cone Algorithm (SMACC, Gruninger et al. 2004) with the sum-to-unity constraint. SMACC

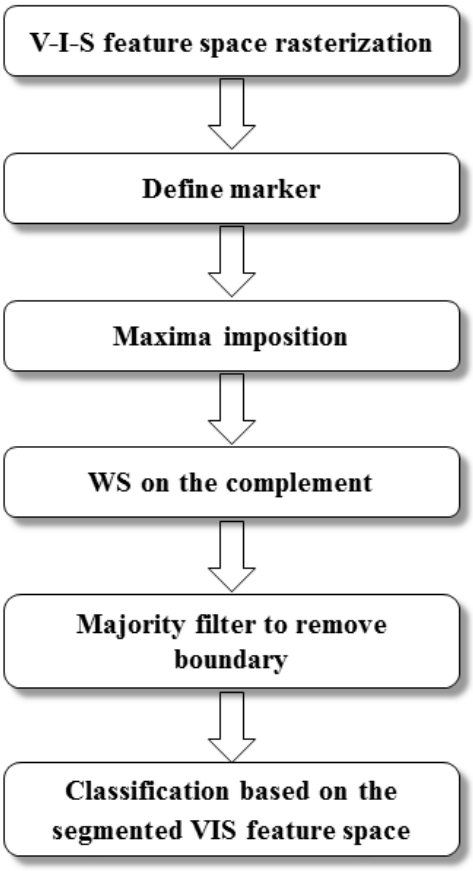

Figure 4-2 Work flow of the proposed watershed segmentation method for LULC classification.

(available in ENVI software) sequentially seeks a set of spectral basis for spectral expansion. The final set of the spectral basis is the endmember spectra and the corresponding expansion coefficients are the endmember fractions. The first basis is set to be the brightest pixel (the longest vector), and the rest of the spectral basis is determined as the longest residual vector after data vectors being approximated by the spectral expansion using the previously found spectral basis (e.g. the pixel with the largest residual norm, namely, the vector with the maximum angle away from the convex

formed by the currently existing set of basis). The expansion coefficients can be updated simultaneously as the spectral basis is sequentially added to the set.

The V-I-S fraction images are then converted to a V-I-S feature space image using a triangle grid system (Figure 4.3) similar to the Lu-Weng's model by equation (1). The entire rasterized feature space consists of 500×434 (434=[500cos(π/3)]) grid pixels, whose values are the count of V-I-S fraction image pixels mapped to the relevant pixel's location in the triangle grid system.

$$X = 500(f_1 + f_2/2)$$

$$Y = 500\cos(\pi/3)(1 - f_2) \qquad (1)$$

where f_1 and f_2 are the fraction of the Impervious Surface and the fraction of Soil, respectively. (X, Y) is the coordinate in the grid system. The V-I-S feature space image of the New Orleans data displays four underlying LULC classes (Figure 4.4*a*). The case for the Baton Rouge data has the same pattern (Figure 4.4*b*).

4.3.2 Marker controlled watershed segmentation

By treating an image as a topographic surface with underlying watersheds, WS simulates an immersion process which progressively floods the surface to find watersheds (Vincent and Soille 1991). The watershed boundaries are at where floodwater from adjacent watersheds meets. If feature space image is turned upside down, the cluster peaks will become depressions, which can be treated as identified watersheds in the WS algorithm. However, because in the general concept of LULC classification classes are peaks of feature space image, we still use the regular unflipped image in all illustrations. Hence, the term "minima" in the original WS algorithm is presented as "maxima" in the V-I-S feature space here.

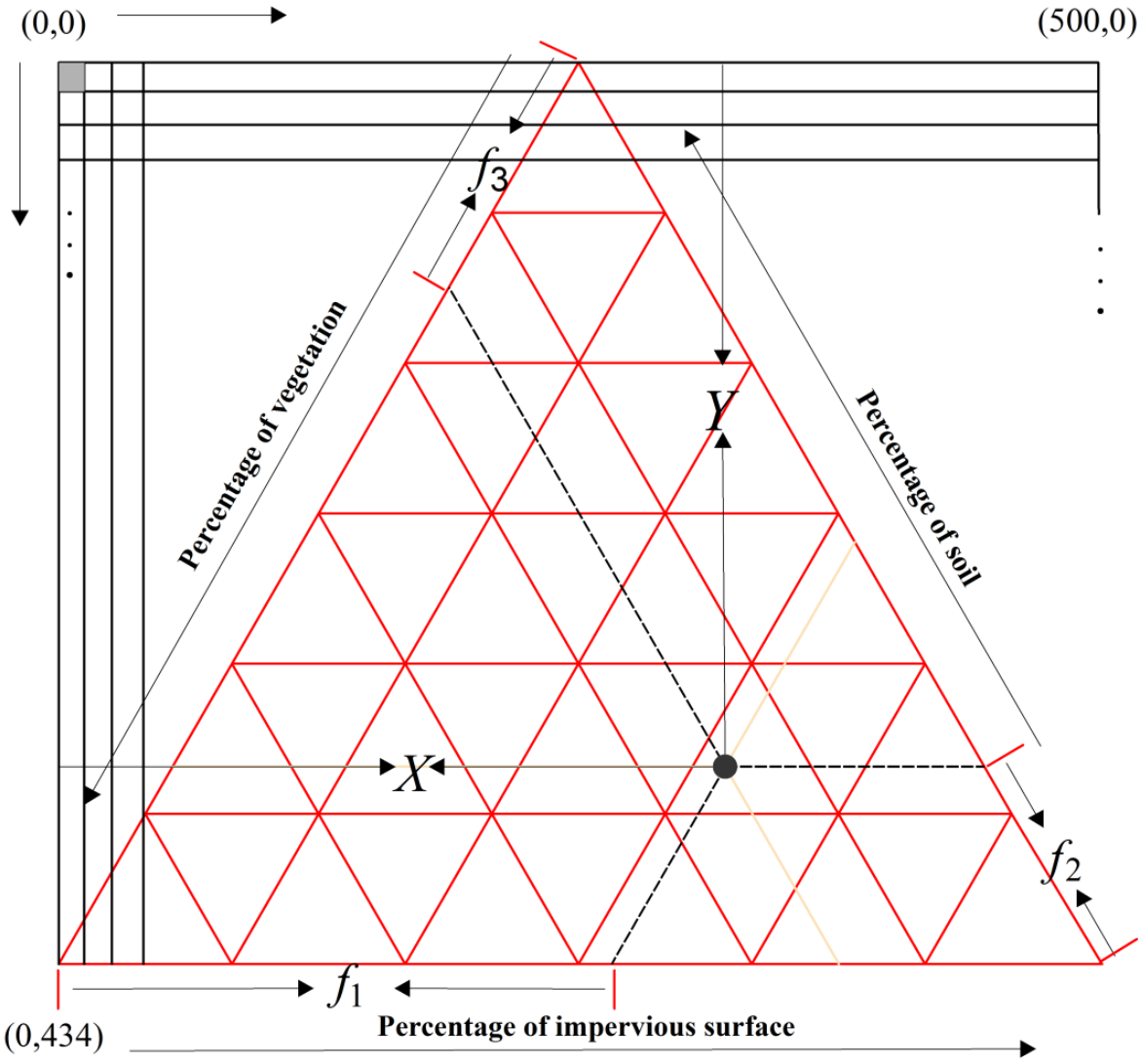

Figure 4-3 Rasterization of the V-I-S feature space .The grid is composed of 500×434 pixels. The black dot represents a given TM pixel with f_1 as the Impervious Surface fraction and f_2 as the Soil fraction being mapped to the gird. The origin of the grid is set to the upper left. The value of a pixel in this grid is the frequency of TM pixel being mapped to the considered pixel's location.

In the watershed segmentation algorithm, each local minima corresponds to a watershed and serve as the seeds to grow the watershed. However, due to random noise and complexity nature of the V-I-S feature space, there is still significant number of irrelevant local maxima other than the four major peaks corresponding to four LULC

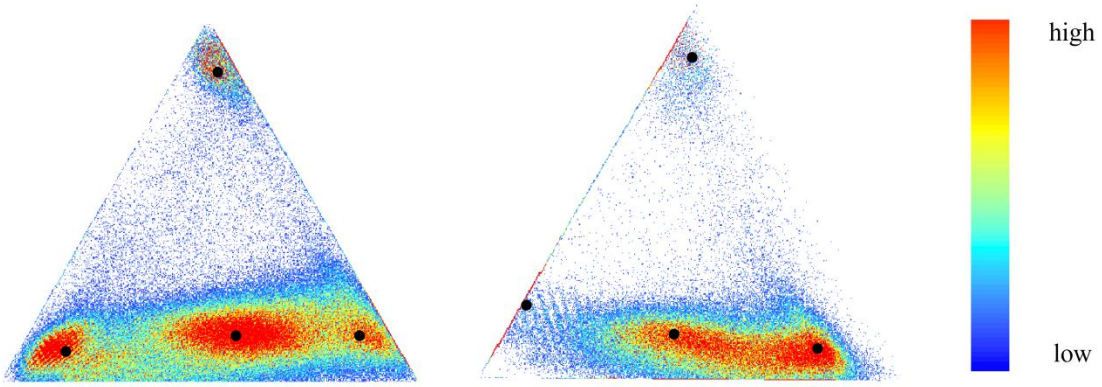

(*a*) (*b*)

Figure 4-4 (*a*) V-I-S feature space rasterization for New Orleans data; (*b*) V-I-S feature space rasterization for Baton Rouge data. The black dots in represent the underlying centers for peaks (LULC classes).

centers. Over-segmentation would result due to these spurious local maxima (Figure 4.5). Hence, to suppress the over-segmentation and to honor the pattern of the four clusters in the V-I-S feature space, WS need to be controlled by markers via the maxima imposition, which can be implemented through a series of morphological operations, including geodesic dilation and morphological reconstruction (Soille 2002, Vincent 1993). Both operations involve marker image (I_m) defined as the following:

$$I_m(\mathbf{x}) = 255, \text{ if } \mathbf{x} \text{ is the marker location}$$

$$I_m(\mathbf{x}) = 0, \text{ otherwise} \qquad (2)$$

where **x** is location in the V-I-S feature space triangle grid system.

Geodesic Dilation

Here I denote ∧ as the maximum operator, ∨ as the minimum operator, I as the grey image and I_m as the marker image. Geodesic dilation of size 1 of the marker image I_m with respect to I (denoted by $\delta_I^1(I_m)$) is defined as the pixel-wise minimum between the I

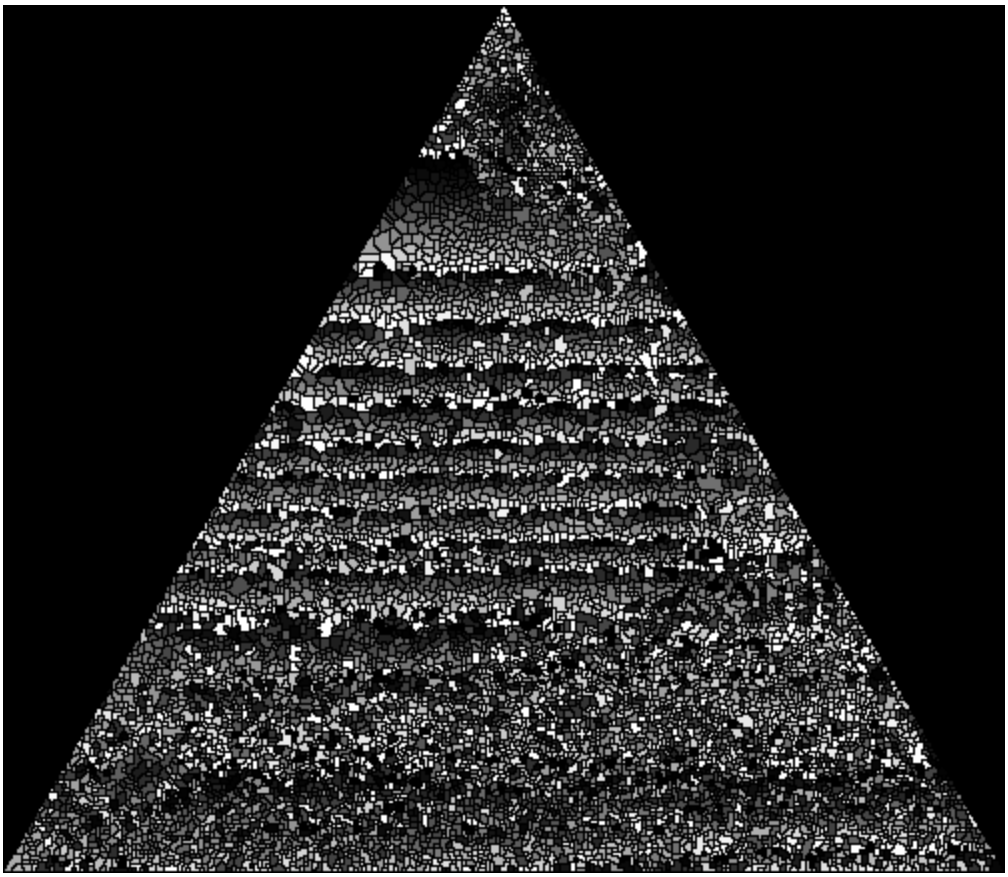

Figure 4-5 Over segmentation of the V-I-S feature space for the New Orleans case, if the WS process is not marker controlled.

and the elementary dilation of the image I_{m} (Soille 2002, Vincent 1993) as the following:

$$\delta_I^1(I_{\mathrm{m}}) = \delta^1(I_{\mathrm{m}}) \vee I \tag{3}$$

where $\delta^1(I_{\mathrm{m}})$ denotes the dilation operation on the marker image. Figure 4.6 illustrates the geodesic dilation for a simplified 1-D case.

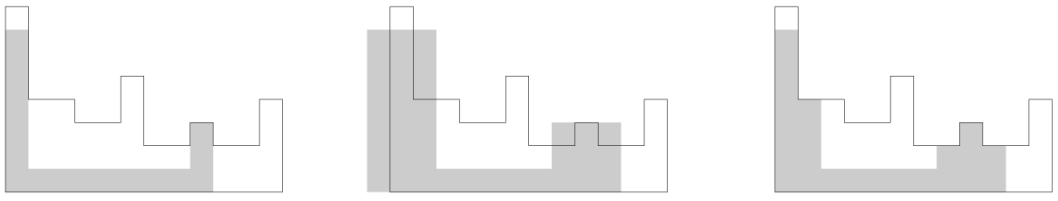

Figure 4-6 Illustration of geodesic dilation of size 1. (*a*) the maker image I_{m} is in grey and the image *I* is in white; (*b*) the elementary dilation of marker image I_{m}, e.g., $\delta^1(I_{\mathrm{m}})$,

in grey; (*c*) the point-wise minimum between the grey and the white in (*b*), e.g., the geodesic dilation. The hypothetic grey image is the courtesy of Soille (2002, page 298).

The $(i+1)^{th}$ iteration of geodesic dilation of the marker image I_m with respect to I is defined as:

$$\delta_I^{i+1}(I_m) = \delta_I^1(\delta_I^i(I_m)) = \delta_I^1(\delta_I^1((\delta_I^{i-1}(I_m)) = \delta_I^1(\delta_I^1(\delta_I^1(\delta_I^1 \dots \dots (\delta_I^1(I_m)) \quad (4)$$

Morphological Reconstruction by Dilation

Morphological reconstruction by dilation of the marker image I_m with respect to I (denoted by $R_I^\delta(I_m)$) is iterative geodesic dilation until convergence is achieved (Soille 2002, Vincent 1993). It follows that:

$$R_I^\delta(I_m) = \delta_I^i(I_m), \text{ such that } \delta_I^i(I_m) = \delta_I^{i+1}(I_m) \quad (5)$$

R stands for reconstruction. The superscript δ indicates that the reconstruction is through dilation as there is a counterpart called morphological reconstruction by erosion, which is used for minima imposition.

In this research, image maxima are imposed by utilizing the aforementioned morphological reconstruction by dilation. First, locations of initial markers are digitized through a user graphic interface as the approximate watershed centers in the V-I-S feature space image to represent the underlying LULC centers. Then, assuming the V-I-S feature space image is scaled over 8 bits (0~255), the marker image (I_m) is constructed using equation (2), and is thereby used to supress irrelevant local maxima. The maxima imposition is then defined as the morphological reconstruction by dilation of I_m with respect to $I_m \wedge I$, namely, $R^{\delta}_{I_m \wedge I}(I_m)$. The reconstruction by dilation is illustrated in Figure 4.7 for a simplified case.

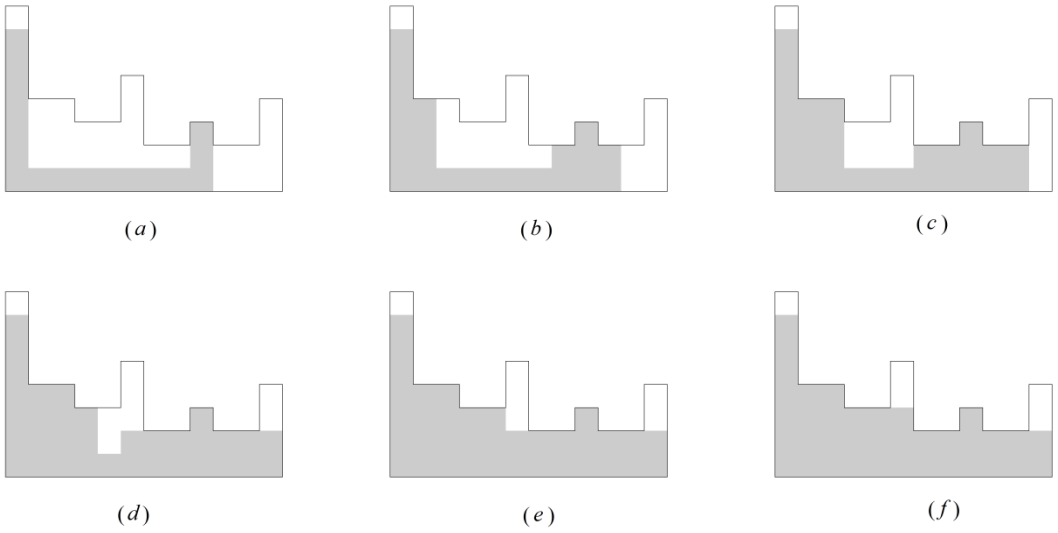

Figure 4-7 Illustration of morphological reconstruction by dilation. (*a*) the maker image I_m is in grey and the image I is in white (with three local minima); (*b*) the geodesic dilation of size 1; (*c)* the 2nd geodesic dilation; (*d*) the 3rd geodesic dilation; (*e*) the 4th geodesic dilation; (*f*) the 5th geodesic dilation, also the reconstruction by dilation as the convergence is achieved. The hypothetic grey image is the courtesy of Soille (2002, page 298).

Maxima imposition removes the local irrelevant minima and only keeps the maxima defined in the marker image. In Figure 4.7, the middle one of the three local maxima, which is not marked in the marker image, is filtered out and removed.

4.3.3 Classification and accuracy assessment

Vincent (1993) and Soille (2002) showed that maxima imposition removed all local maxima except for the location where initial markers are defined. In our study, the complement of the V-I-S feature space image after the maxima imposition has only four local minima and is then segmented by watershed segmentation. The pixels in the same watershed are assigned a certain watershed label (namely, A, B, C and D in Figure 4.8(*a*) and Figure 4.8(*b*)). The pixels belonging to watershed boundaries are assigned the label of the most prevalent watershed among their neighbors using a majority filter.

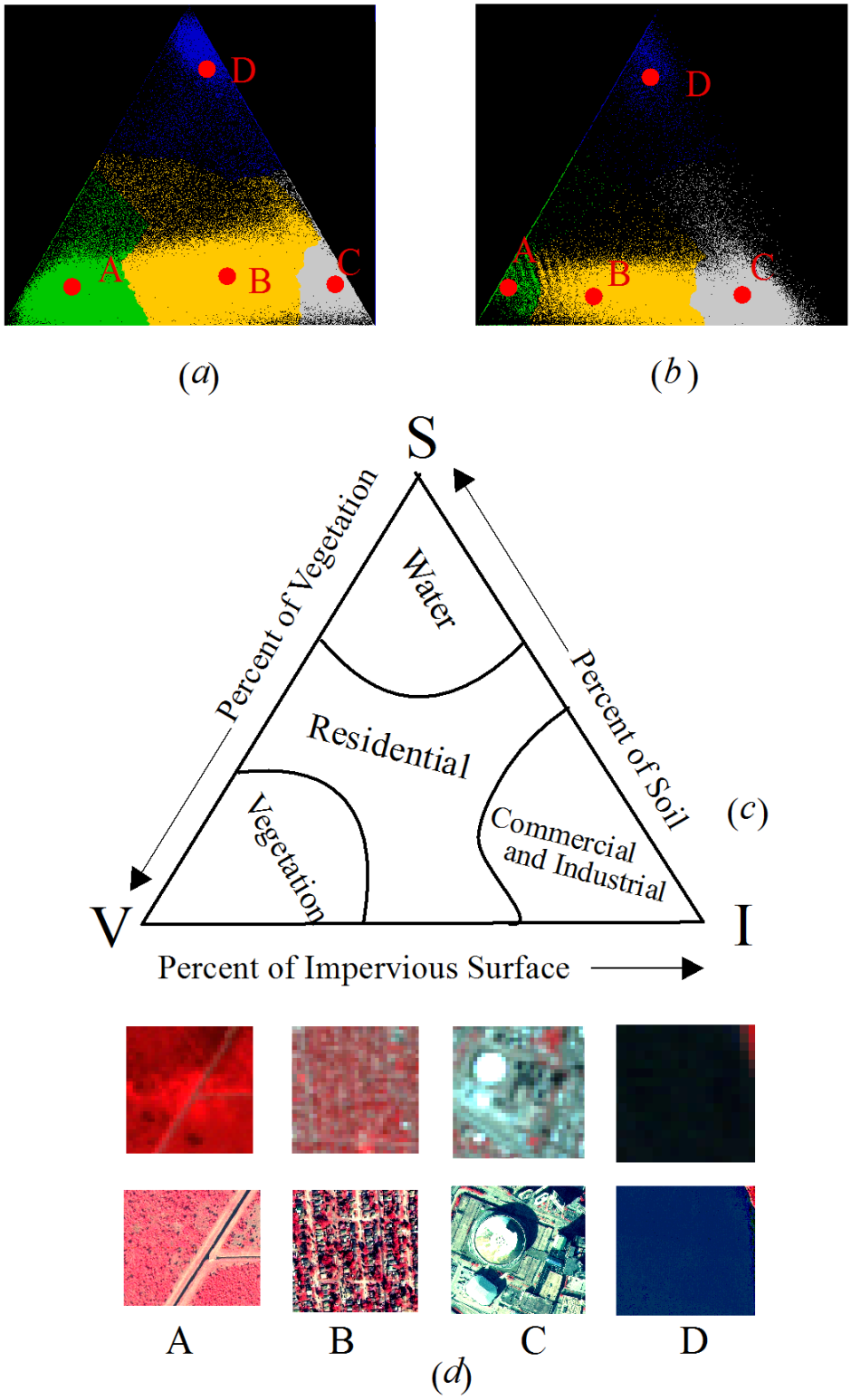

Figure 4-8 Watershed segmentation on the V-I-S feature space image derived from Landsat TM. (a) WS result of New Orleans. Black regions are areas with frequency of zero-occurrence; (b) TM (left) and DOQQ (right) (A = Vegetation; B= Residential; C = Commercial and Industrial; D =Water).

The corresponding four LULC classes in the watershed segmentation are Vegetation (A), Residential (B), Commercial and Industrial (C) and Water (D), according to Lu-Weng's triangle (Figure 4.8(*c*) and reference data from DOQQ (Figure 4.8(*d*)). As a result, all the original TM pixels are classified to one of these four classes based on their V-I-S feature space locations in the watersheds.

A simple random sampling was used for accuracy assessment for both test sites, and 397 points for New Orleans and 117 points for Baton Rouge were visually interpreted from the DOQQ and assigned the LULC class as the reference. A maximum likelihood classification (MLC) was also performed on the TM spectral bands to be used as the benchmark to evaluate the performance of our new method.

4.4 Results and discussion

4.4.1 Comparison between the new method and MLC

The maps of LULC classification from the WS-based method are displayed in Figure 4.9. The new method achieves slightly higher accuracy compared to MLC. The accuracy is improved from 69.5% to 72.8% for New Orleans (Table 4.1) and from 69.8% to 71.4% for Baton Rouge (Table 4.2). The kappa coefficient increases from approximately 0.55 to 0.60 for both sites after using the new method. The new method has higher producer's accuracy for the Vegetation class and the Water class for both test sites, as well as the higher producer's accuracy for the Commercial and Industrial class for Baton Rouge area and the Residential class for New Orleans area.

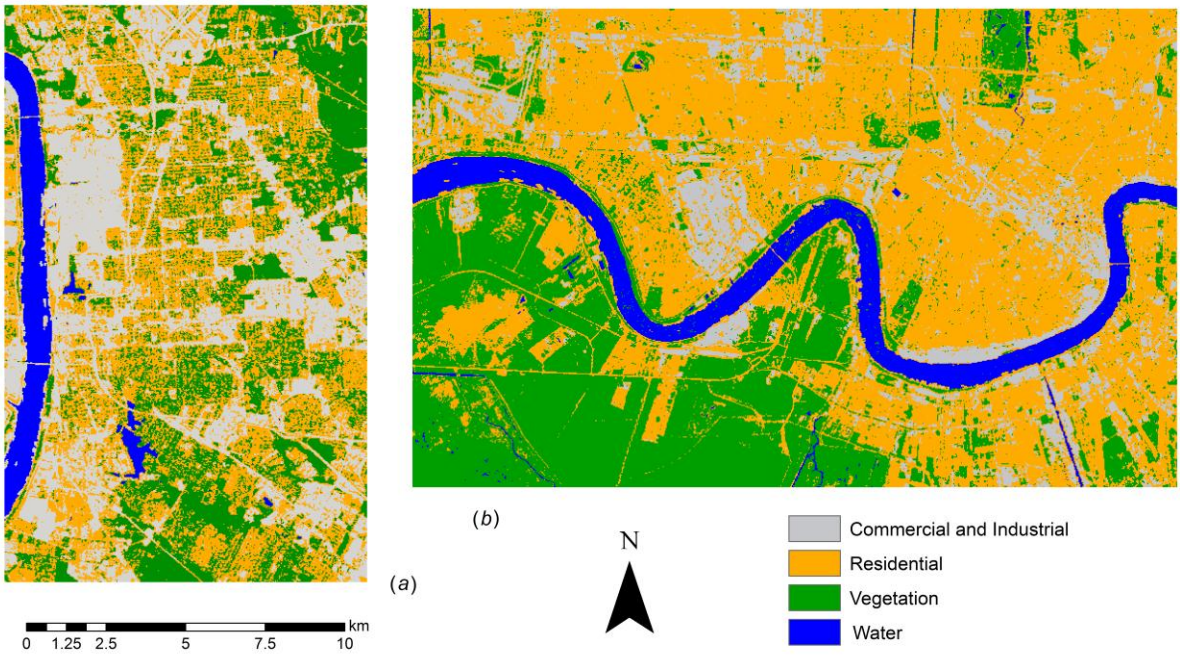

Figure 4-9 Classification results with WS method for (*a*) Baton Rouge and (*b*) New Orleans.

Table 4.1 Error Matrix for New Orleans test site. (*a*) Classification with MLC where Kappa=0.56 with overall accuracy as 69.5%; (*b*) Classification with WS and Kappa=0.60 with overall accuracy as 72.8% (UA = user's accuracy and PA = producer's accuracy).
(*a*)

Classified Data	Reference Data					UA (%)
	Commercial and Industrial	Residential	Vegetation	Water	Total	
Commercial and Industrial	52	7	9	2	70	71
Residential	39	110	48	1	198	56
Vegetation	8	6	98	0	112	88
Water	0	0	1	16	17	94
Total	99	123	156	19	397	
PA (%)	53	90	63	84		

(Table 4.1 Continued)
(*b*)

Classified Data	Reference Data					UA (%)
	Commercial and Industrial	Residential	Vegetation	Water	Total	
Commercial and Industrial	40	1	1	0	42	95
Residential	49	115	37	1	202	57
Vegetation	8	7	116	0	131	89
Water	2	0	2	18	22	82
Total	99	123	156	19	397	
PA (%)	40	94	74	95		

Table 4.2 Error Matrix for Baton Rouge test site. (*a*) Classification with MLC and Kappa=0.55 with overall accuracy as 69.8%; (*b*) Classification with WS and Kappa=0.59 with overall accuracy as 71.4% (UA = user's accuracy and PA = producer's accuracy).
(*a*)

Classified Data	Reference Data					UA (%)
	Commercial and Industrial	Residential	Vegetation	Water	Total	
Commercial and Industrial	21	2	1	0	24	88
Residential	8	41	22	1	72	57
Vegetation	0	2	17	0	19	90
Water	0	0	0	4	4	100
Total	29	45	40	5	119	
PA (%)	72	91	43	80		

(*b*)

Classified Data	Reference Data					UA (%)
	Commercial and Industrial	Residential	Vegetation	Water	Total	
Commercial and Industrial	28	7	3	0	38	74
Residential	1	29	14	0	44	66
Vegetation	0	9	23	0	32	72
Water	0	0	0	5	5	100
Total	29	45	40	5	119	
PA (%)	97	64	58	100		

Both WS-based classification and MLC honor the shape, orientation and size of classes for LULC classification, but in different ways. To be specific, MLC considers the

center of the class and the variance-covariance matrix of the normal distribution through parametric fitting, e.g., the maximum likelihood estimation (MLE). The watershed segmentation considers the class center via initial markers specified by users; the flooding process grows the watersheds by following the natural shapes of LULC clusters in the V-I-S feature space.

Although MLC is one of the most used image classification methods, WS has a number of advantages over it: (1) MLC is a mathematically parametric classifier based on the assumption of multivariate normality. The training data samples should be representative enough for parametric fitting for every LULC class. In reality, the normality assumption can only be approximated, which leads to biased class decision boundaries. Watershed segmentation is a non-parametric method; namely, it has no assumptions about the shape or distribution of the classes as long as the histogram displays clustering patterns (representing underlying watersheds). (2) A paradox of MLC is that the decision boundaries will be different if a different sample set from an extended or clipped input image is used to train the classifier because the MLE would be altered. WS has no such an issue because the class decision boundary fits locally to the dataset, so extending or clipping the input image will not affect the segmentation boundary. (3) WS requires minimal user input – just initial markers; hence, the chance to introduce uncertainty and subjectivity from the training dataset is reduced. MLC, on the contrary, needs separable training samples for different LULC classes.

4.4.2 Sensitivity to the initial marker specification

One important (and the only) input from the user is the imposition of initial markers for watershed segmentation. Theoretically, initial markers should be defined as the

watershed centers to partition the V-I-S feature space. However, since I employ manual on-screen digitizing in our study, this might introduce human subjectivity and error if the segmentation is sensitive to the marker locations. Therefore, this research tested the tolerance of the WS algorithm to human-imposed digitization error. The test was based on 50 randomized initial marker sets, which were generated by introducing a random perturbation of 30 pixels off from the LULC class centers in the V-I-S feature space. In addition, we added one more test scenario by using the geometric centers (mean) of the training data used in the MLC. The results show that the segmentation is not sensitive to the markers locations. All these different initial marker specifications lead to the same watershed segmentation result, which consequentially leads to the same labeling and classification. This test result validates the approach to the marker imposition by user on-screen digitizing. As long as the digitized markers are located inside the underlying watersheds, the segmentation algorithm will produce exactly the same result. Therefore, human subjectivity is not an issue in this method.

Figure 4.10 also gives a simplified (1-D) illustration. Figure 4.10(*a*) is the feature space image represented by the height of the columns. The two black columns represent two markers. Figure 4.10 (*b*) is the image imposed by the makers. Figure 4.10(*c*) is the final maxima imposition result using the morphological reconstruction. Two inverse watersheds are grown and met at the red dot as their boundary (figure 4.10(*c*)). Figure 4.10(*d*)~(*f*) showed the process of a different maxima imposition. Starting from figure 4.10 (*d*), the same maxima imposition was processed, however, with two different marker locations in the vicinity of the ones in figure 4.10(*a*). Figure 4.10(*f*) is the final maxima imposition and the watershed boundary (red dot) is located at the same location.

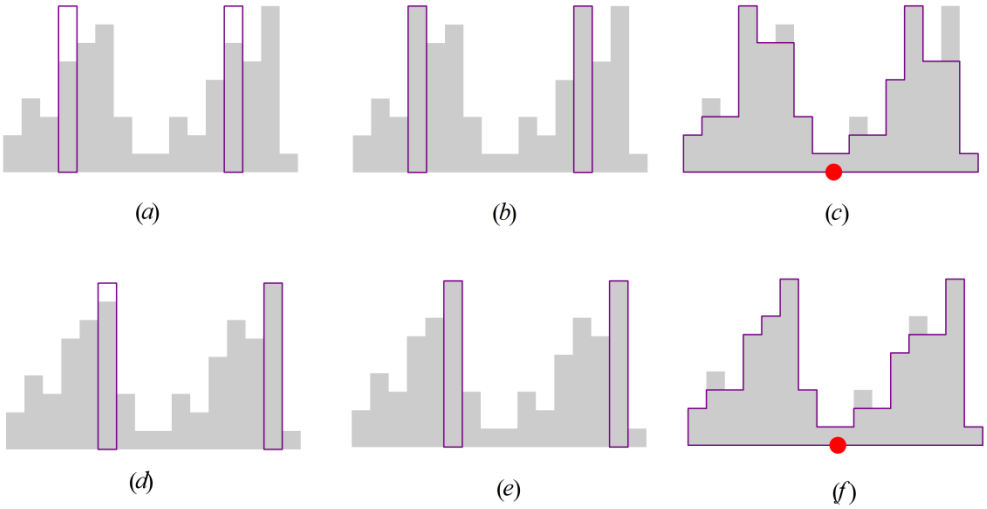

Figure 4-10 Sensitivity analysis of the location of markers. (*a*)–(*c*) are the maximum imposition from an imperfectly located maker as compared to (*d*).(*f*). The resultant watershed boundaries (red dot) are same. The hypothetic grey image is the courtesy of Soille (2002, page 298).

Other methods such as the nearest neighbor method (Richards and Jia 2006, p. 263~264) can also perform feature space segmentation. However, the nearest neighbor method only partitions the feature space according to the distance to the markers, without regarding to the shape, size, orientation, height (density) of the features. The nearest neighbor method fails if the adjacent land use regions in the V-I-S feature space are different in size (Figure 4.11), which is very likely to occur in real-world data. In contrast, the watershed segmentation is based on morphologic feature of the surface described by the V-I-S feature space image, and follows the natural divides of the clusters to define the classes. Figure 4.11 compares the partition results from the two methods illustrated in 1-D case.

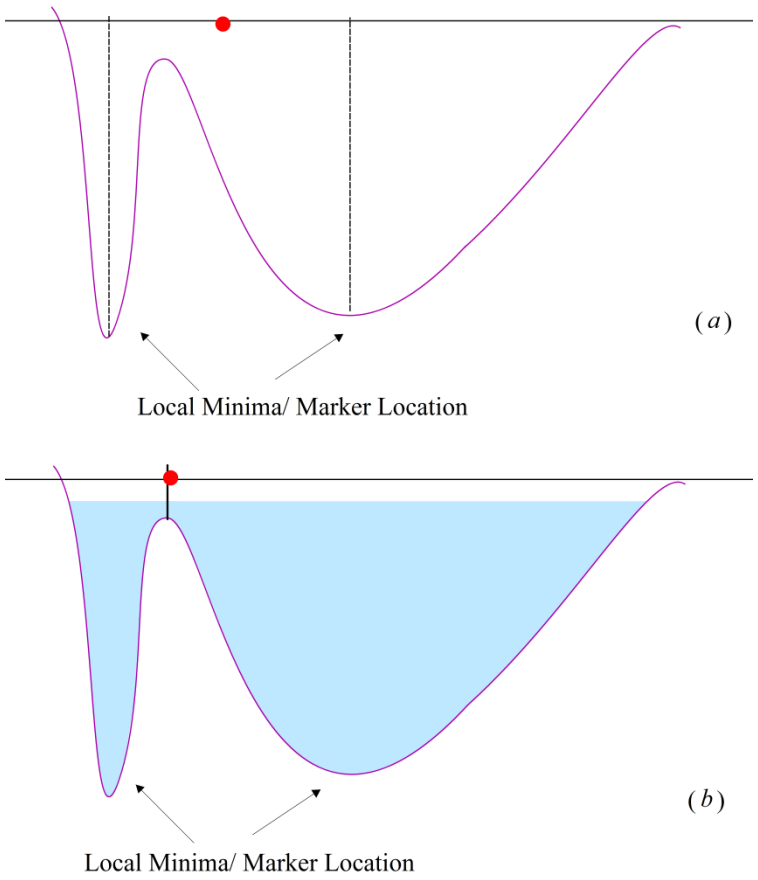

Figure 4-11 Comparison of two feature space partition methods. The red dot is the partition boundary. (*a*) Erroneous partition from the nearest neighbor method which defines the boundary by its distance to the markers. (*b*) Watershed segmentation results in the expected boundary.

4.5 Conclusion

This chapter introduced and tested an innovative urban LULC classification method of applying the WS in the V-I-S feature space. WS exploits the natural gaps between LULC classes and has no strict assumption on the distribution of classes in the V-I-S feature space. Compared to the conventional method, maximum likelihood classification, our new method requires less user input and improves classification accuracy. The study also shows that WS is tolerant to the human induced subjectivity and error; therefore, on-screen digitizing is the feasible way of imposing initial markers to guide the segmentation.

It is worth noting that there is variability in land use land cover conditions other than the two cases we presented in this letter. For instance, if vegetation (e.g. forested areas) is very limited in the scene, it may not stand out as a significant LULC cluster; so it could be submerged and suppressed in the watershed segmentation process and mixed with other classes. In some other areas, residential areas could show a pattern of multiple clusters (such as, high density residential and low density residential areas). In this case, additional initial markers would be needed to separate these classes. Hence, our new method is data driven and the number of initial marker has no preconceived knowledge. Currently, this method is only applicable to urban studies because it is based on the V-I-S model and the Lu-Weng urban triangle model. In the future, applying this method to other environments and classification purposes is possible and expected.

Chapter 5 Investigation of urban population distribution in New Orleans with the sub-pixel and land use characterization

5.1 Introduction

A large body of literature has been established to report the use of remotely sensed signals to investigate the urban population distribution. Derived indicators for the population process from remote sensing data included spectral reflectance (Hsu 1973, Iisaka and Hegedus 1982, Lo 1995), night-time illumination (Dobson et al. 2000, Lo 2001, Sutton 1997), vegetation indices (Li and Weng 2005), land use and land cover (Dobson et al. 2000, Langford et al. 1991, Lo 1995, Mennis 2003, Yuan et al. 1997), sub-pixel fractions (Joseph et al. 2012, Li and Weng 2005, Lu and Weng 2006, Morton and Yuan 2009, Wu and Murray 2007), textures (Li and Weng 2005, Liu et al. 2006), temperature (Li and Weng 2005) and spatial metrics (Liu 2003).

The V-I-S model (Ridd 1995) is a success in urban remote sensing. The V-I-S model reveals the fractional composition of vegetation and impervious surface, two major components of an urban area, which were frequently used to regress the population (population density) and its transforms. Joseph et al. (2012) used sub-pixel information to model the population in the Port-au-Prince, Haiti and highlighted three inputs that greatly contributes to a successful population model for Port-au-Prince, namely, the fraction of housing, the fraction of vegetation and the standard deviation of vegetation fractions. Morton and Yuan (2009) used power function fitting to establish the relationship between population density and the %ISA (percentage of impervious surface area). Other examples using V-I-S sub-pixel information in population regression could be found at Li

and Weng (2005) and Wu and Murray (2007). Land use and land cover (LULC) provides another input for population models. Langford et al. (1991) for the first time used multivariate regression with the land use information as a dasymetric mapping method to investigate the urban population. The application of using LULC as input for population regression was followed by many others with success, including Langford and Unwin (1994), Lo (1995), Yuan et al. (1997) and Lo (2008). Li and Weng (2010) compared these two types of input in investigating the population density of Marion County, Indiana with Landsat ETM image and termed them as "spectral response method" and "land use based method", respectively. The result showed that the latter input was superior as it achieved smaller mean relative error.

Recently, there is a growing interest of using local models to address the spatial dependency and spatial nonstationarity. Application of local models of population is also seen in the literature, examples are the regional models (Langford 2006, Yuan et al. 1997), GWR model (Liu et al. 2006, Lo 2008, Yu and Wu 2004) and spatial autoregressive regression (Griffith and Wong 2007).

Such population regression analysis is not seen for the city of New Orleans. The purpose of this study is straightforward: to use the regression models to link the urban population distribution and the V-I-S fraction and the urban land use classes for the city of New Orleans. Specifically, this research focuses on two analyses. One is the "spectral response method": to use the V-I-S sub-pixel information as the input. The spatial configuration of V-I-S may reveal the underlying land use and thus can be related to the population process. The spatial fragmentation level of vegetation fractions is believed to relate to population. Hence, the V-I-S fractions and their standard deviation are used as

explanatory variable to model the population. The second analysis is the "land use based method" that employs the regular dasymetric mapping by using the land use information as the regression input. I hope to see how these physical environment measures could contribute to the population model for the case of New Orleans. The chapter answers the research question 6.

5.2 Data source

The census 2010 data (Summary File 1, SF1) has been released in the public domain and downloadable from the United State Census Bureau website (http://www2.census.gov/census_2010/04-Summary_File_1/Louisiana/). The census tract level population data for two major parishes in the New Orleans Metropolitan Area: the Orleans Parish and the Jefferson Parish are obtained from the Census Bureau. The 2010 census tract boundary is available in the Topologically Integrated Geographic Encoding and Referencing (TIGER) files. Several large census tracts that cover the southern area and are out of the metropolitan are removed. These have resulted in totally 299 census tracts being included in the analysis (Figure 5.1).

The environment variables for population modeling are extracted from remotely sensed images. A Landsat Thematic Mapper (TM) image (Path/Row 39/22) acquired on 10/07/2010 is downloaded from USGS Glovis website (http://glovis.usgs.gov/) to derive the V-I-S fraction images and the LST image. The 1-m resolution Digital Orthophoto Quarter Quadrangles (DOQQs) acquired in the time of the year were used for reference.

Figure 5-1 299 selected census tracts in Orleans Parish and Jefferson Parish.

5.3 Methods

5.3.1 Regression Analyses

This study conducts two analyses to investigate the relationship between the urban population and the physiogeographic conditions. The two analyses differ from each other in terms of the type of explanatory variable being used. The first analysis uses the V-I-S sub-pixel fractions and their spatial variations to explain the population distribution. The second model is based on the land use information extracted from V-I-S configurations considering the Lu-Weng's urban triangle model. A previous study by Tang et al. (2012) shows that the synergy of V-I-S fractions and LST could improve both the accuracy and stability of classifier and also meet the normality assumptions of maximum likelihood

classifier (MLC). Hence, we used V-I-S fractions in conjunction with LST to train a MLC classifier to classify the TM image. A four-class schema is adopted considering the major land use classes in Lu-Weng's urban triangle model, e.g., Residential, Commercial and Industrial, Vegetation and Water. The area of land use classes for each census tract is used as the explanatory variable in the second analysis. Both analyses used Ordinary Least Square (OLS) regression and Geographically Weighted Regression (GWR) method due to their popularity in recent population modeling. GWR model is used to examine the spatial nonstationarity. Figure 5.2 illustrates the data flow and the analytical procedures.

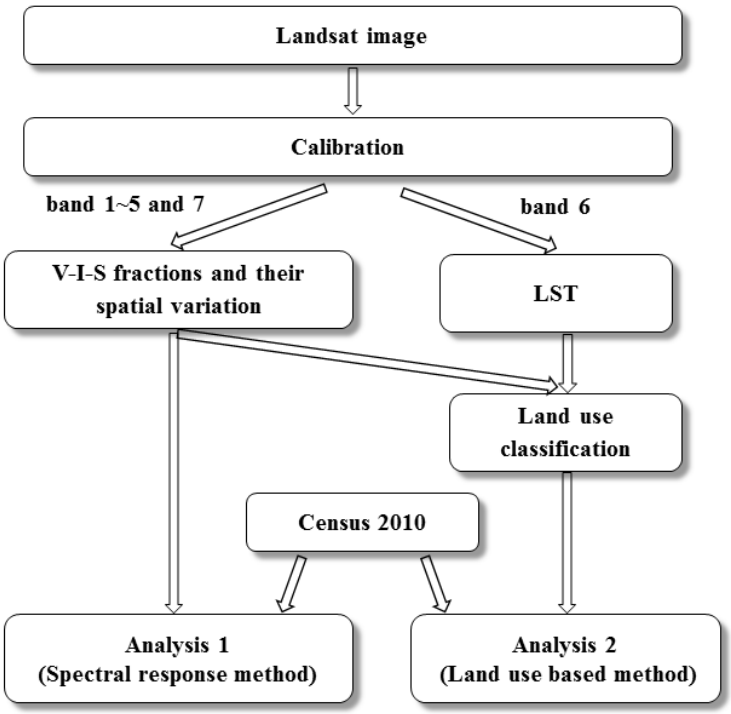

Figure 5-2 Procedures of population modeling using two types of input.

5.3.2 GWR

Geographically Weighted Regression (GWR) allows the regression coefficients to vary over space to investigate the spatial nonstationarity. The model can be expressed as:

$$y = \beta_{0i} + \beta_{1i}x_1 + \beta_{2i}x_2 + \cdots \beta_{ni}x_n + \varepsilon \quad (1)$$

Notice that the βs have the subscripts i, indicating that the coefficients are location variant. GWR performs weighted regressions locally at every observation location using weighted least square approach and the solution is given by

$$\beta_i = (X'W_iX)^{-1}XW_iY \quad (2)$$

Where W_i is the diagonal matrix with diagonal elements being weight of observations for location i, and β_i is the coefficient set for location i. The weighted regression employs weighting functions (usually monotone decreasing functions of the distance) to assign weights to observations. The closer observations play more important roles than distant ones in each local regression. In this research, we adopted the commonly-used Gaussian kernel to calculate spatial weights. The Gaussian kernel is defined as:

$$w_j(i) = e^{-(\theta d_{ij}^2)} \quad (3)$$

The parameter of θ determines the shape of the kernel function that controls how fast weights are decreasing with the distance. The parameter θ is determined by the leave-one-out cross-validation:

$$cv = \sum_{i=1}^{N}[y_i - \hat{y}_{(i)}(\theta)]^2 \quad (4)$$

where $\hat{y}_{(i)}(\theta)$ is the fitted value of y_i with the observation at location i omitted from the model calibration process. θ is the parameter of the weighting kernel. GWR chooses the desired θ parameter such that cv is a minimum.

A good aspect of GWR is that the local coefficients, local t-test and local R^2 can be calculated and mapped to investigate their spatial variations. Once the GWR is fitted, two following questions are often of the interest (Brunsdon et al. 1998, Fotheringham et al. 2002, Leung et al. 2000, Yu 2006):

- Does the GWR model describe the data significantly better than the OLS model?
- Does each set of parameters exhibit significant variation over the study region, e.g., the test of spatial nonstationarity?

Statistical tests were developed to address these two questions. Model fit comparisons are usually dealt with by employing the sum of squared residuals (SSE) and pivotal-method based hypothesis testing (Casella and Berger 2002). The distribution of the GWR's sum of square residuals was proven to be related to an approximate χ^2 distribution with non-integer degree of freedom, which becomes the basis to construct the likelihood ratio (LR) tests (F test here) to compare the goodness-of-fit between the GWR and OLS model. It is analogous to the conventional F-test to compare nested OLS models. The only difference is that the F-test for OLS model comparison has integer degree of freedom and the distribution is exact; however, in the F-test for OLS and GWR model comparison, the degree of freedom is non-integer and the distribution is approximate (Brunsdon et al. 1999). Two specific F-tests (Brunsdon et al. 1999, Fotheringham et al. 2002) and two others (Leung et al. 2000) were developed in this manner to compare GWR model with its OLS counterpart. The spatial nonstationarity can be examined by Monte Carlo (MC) randomization tests (see Brunsdon et al. 1999, Brunsdon et al. 1998, Fotheringham et al. 2002 page. 93 for details). However, its computational burden is overwhelming. An approximate F-test was developed to test the spatial nonstationarity of

parameters, see Leung et al. (2000) for detailed mathematical deduction. The R package **spgwr** has implemented the GWR algorithm and all these statistical tests.

5.3.3 Model comparison

To compare the model fit and their performance on predictions, the 299 census tracts were splitting into the training dataset and the validation dataset. The training part contained 80% of original census tracts and the rest went to the validation dataset.

Models are compared with one another in terms of prediction accuracy. I use two goodness-of-fit indicators in this research: Root Mean Square Error (RMSE) and Mean Absolute Percentage Error (MAPE) defined as the following.

$$RMSE = \sqrt{\frac{\sum_{i=1}^{N}(\hat{y}_i - y_i)^2}{N}} \tag{5}$$

$$MAPE = \sqrt{\frac{\sum_{i=1}^{N}\left|\frac{\hat{y}_i - y_i}{y_i}\right|}{N}} \tag{6}$$

5.4 Analysis and result

5.4.1 Population and sub-pixel configurations

Input feature for analysis-1 include the V-I-S fractions and their standard deviation at the census tract level. The standard method for extracting V-I-S fractions introduced in section 3.2 was applied to the TM image that is subset to the New Orleans area. The Zonal Statistics tool was used to aggregate the V-I-S fractions of the pixel level to the census tract level. The mean and the standard deviation of V-I-S fractions were calculated.

Due to the fact that the V-I-S sub-pixel fractions sum up to one, throwing them all to the regression model would cause the linear dependency (multicolinearity) problem. Hence, only the Vegetation fraction and the Impervious Surface fraction are used in the

regression model as different composition of V and I fractions are related to different land use patterns in urban that may be associated with the underlying population process.

I also considered the standard deviation of vegetation fractions because the vegetation fragmentation level is found to be related the population distribution. Instead of the absolute population value, the population density (PD) and its logarithm transform and square root transform were selected as dependent variables. These transforms served the purpose of removing the skewness and reducing the heterogeneity. Table 5.1 indicates that the population density and its square root transform are more related to the V-I-S sub-pixel information than its logarithm transform.

Table 5.1 Correlation between transforms of population density and explanatory variables.

	Mean Imperviousness	Mean Vegetation	Std of V fraction
Population Density (PD)	0.27	-0.19	-0.41
Logarithm of PD	0.13	-0.12	-0.39
Square root of PD	0.26	-0.16	-0.47

The best OLS model among the three favors the square root transform of PD as the dependent variable; however, the regression model gives a poor fit. The R^2 was only 0.2420 (the other two inferior models have R^2 of 0.19 and 0.16). The model also suggested that the fraction of vegetation was not significantly related with the population (Table 5.2). The GWR model was also poor. The local R^2 ranged from 0.19~0.28. Compared to similar studies that were conducted in other places, such as Port-au-Prince (Joseph et al. 2012), Columbus, Ohio(Wu and Murray 2007), and the seven counties in Twin Cities Metropolitan Area, Minnesota (Morton and Yuan 2009), etc, the relationship between the remote sensing sub-pixel configurations and population distribution was not statistical significant. This indicates the inadequacy of the V-I-S fraction input to model the population in New Orleans. Reason could be that the New Orleans is a complicated

area; the population is not only directed by the physiogeographic variables but also the socioeconomic process.

Table 5.2 OLS model fit of population density and sub-pixel information

Variable	DF	Parameter Estimate	Standard Error	t Value	Pr > |t|
Intercept	1	80.07599	9.37107	8.55	<.0001
Impervious surface fraction	1	-42.69073	18.45390	-2.31	0.0214
Vegetation fraction	1	-2.24136	13.15354	-0.17	0.8648
Std of vegetation fraction	1	-225.41501	25.15871	-8.96	<.0001

5.4.2 Population and land use

Input features for analysis-2 are mainly the area of different land use classes of census tracts. In this research, I only considered the classification schema adopted used in Chapter 3 and 4, namely, 1) Residential; 2) Commercial and Industrial; 3) Vegetation; 4) Water. I used V-I-S fraction and LST along with a maximum likelihood classifier to produce the land use classification result (Figure 5.3). The classification accuracy was 78.0% indicated by 300 test samples that were generated by a random sampling method.

Due to the fact that "Water" class is not an inhabitable land use class, it is excluded from the model. Hence, the final regression model is as the following:

$$P = \beta_0 + \beta_1 Com + \beta_2 Res + \beta_3 Veg \quad (7)$$

Where Com, Reg, and Veg are the area of the commercial and industrial, residential and vegetation land use with in a census tract.

There will be no population if there is no land use for any of these three classes. So the regression model without the intercept seems to be more appropriate.

$$P = \beta_1 Com + \beta_2 Res + \beta_3 Veg \quad (8)$$

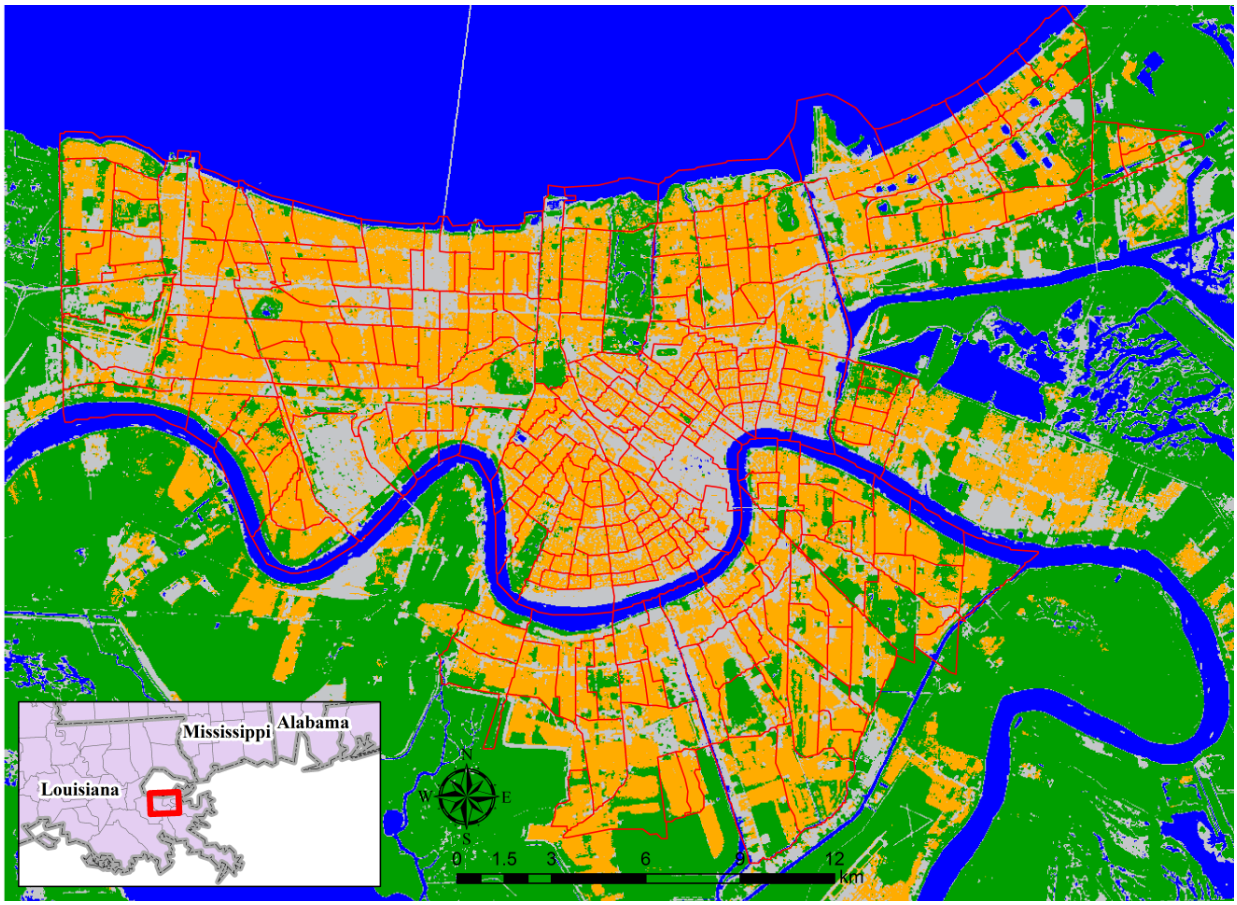

Figure 5-3 The land use map of study area, 2010, produced using V-I-S fractions and LST as the input and a MLC classifier.

The model fit with and without the intercept term is shown in table 5.3 and table 5.4 respectively. Both models achieved a much better fit than the model fitted with the sub-pixel fraction information.

Table 5.3 Model fit using land use information with intercept (R^2=0.6392)

Variable	DF	Parameter Estimate	Standard Error	t Value	Pr > |t|
Intercept	1	901.50	90.45	9.966	<.0001
Commercial and Industrial	1	42.39	113.06	0.375	0.7080
Residential	1	2227.25	104.88	21.237	<.0001
Vegetation	1	-238.96	121.76	-1.963	0.0506

Table 5.4 Model fit using land use information without intercept (R^2=0.8811)

Variable	DF	Parameter Estimate	Standard Error	t Value	Pr > |t|
Commercial and Industrial	1	366.15	125.00	2.929	0.00366
Residential	1	2963.66	85.91	34.498	<.0001
Vegetation	1	-444.72	138.50	-3.211	0.00147

Based on both models, it is shown that the strongest relationship with the population was the residential land use. Vegetated land use imposes a negative effect on the population distribution. Y is the population, not population density as the x is in terms of area already. This model has a good R^2. There is no significant multicollinearity problem.

The GWR model returns an adjusted R^2= 0.75. The F-test suggested that the GWR achieved a much improvement over OLS model. All three input parameters had spatial nonstationarity pattern as seen in Table 5.5.

Table 5.5 Spatial nonstationarity test results

Parameter	F statistic	Num d.f.	Den d.f.	*p* value
Commercial and Industrial	2.9868	22.1471	278.47	<0.001
Residential	6.9566	63.3263	278.47	<0.001
Vegetation	2.7962	28.2279	278.47	<0.001

High local coefficients for commercial and industrial land use could be found at the Metairie community and CBD (Figure 5.4), where there were constructed with shopping center and mall that attracted people occupation or the other way . In the contrary, the relation is reversed in the East New Orleans, lower 9th Ward and the south. Although ANOVA test suggested that the spatial-nonstationarity exists for the residential land use, the coefficient did not change the sign over space (Figure 5.5). The region with small value of coefficients could be founded at the City Park area and its southern

neighborhood. Lower 9th ward, East New Orleans and the mid-city also had relatively smaller coefficients. These areas with small local estimated parameter for the residential land use were majorly located in the Orleans Parish that was badly flooded during the Hurricane Katrina. The Jefferson's Parish, such as Metairie community had higher estimated coefficients for the residential land use. This spatial discrepancy highlighted that the population are more crowded in the residential area that were less exposed to the potential flooding. The local model agrees with the global model in terms of the sign of the vegetation land use for the majority part of the study area (Figure 5.6). The sign is reversed in the East New Orleans and the southeastern Jefferson Parish. This also indicates the strong spatial nonstationarity of this variable.

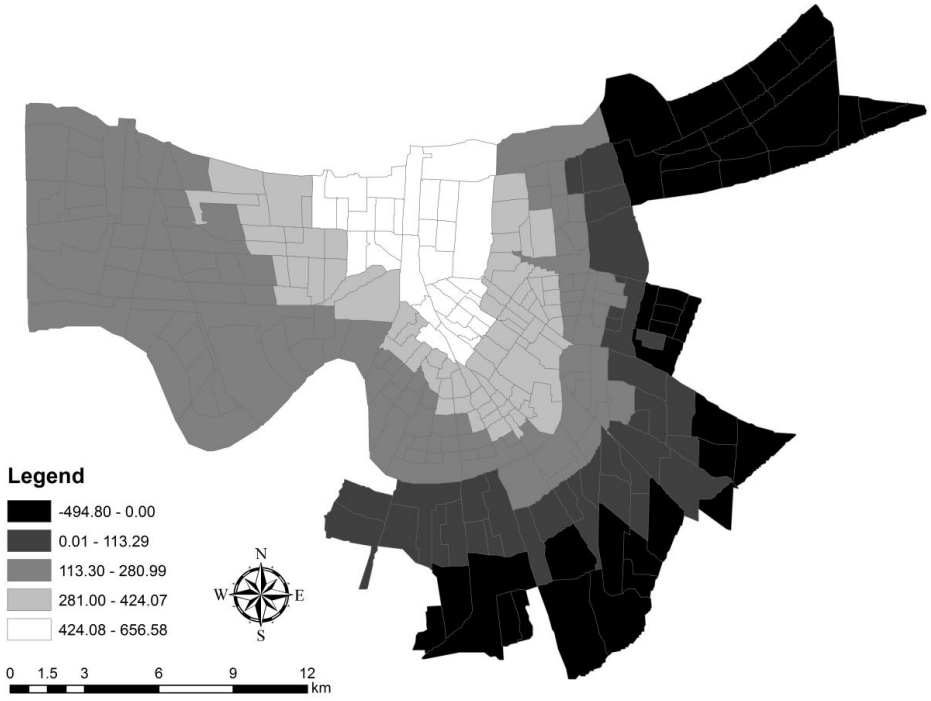

Figure 5-4 Spatial variation of the regression coefficient for "commercial and industrial" land use.

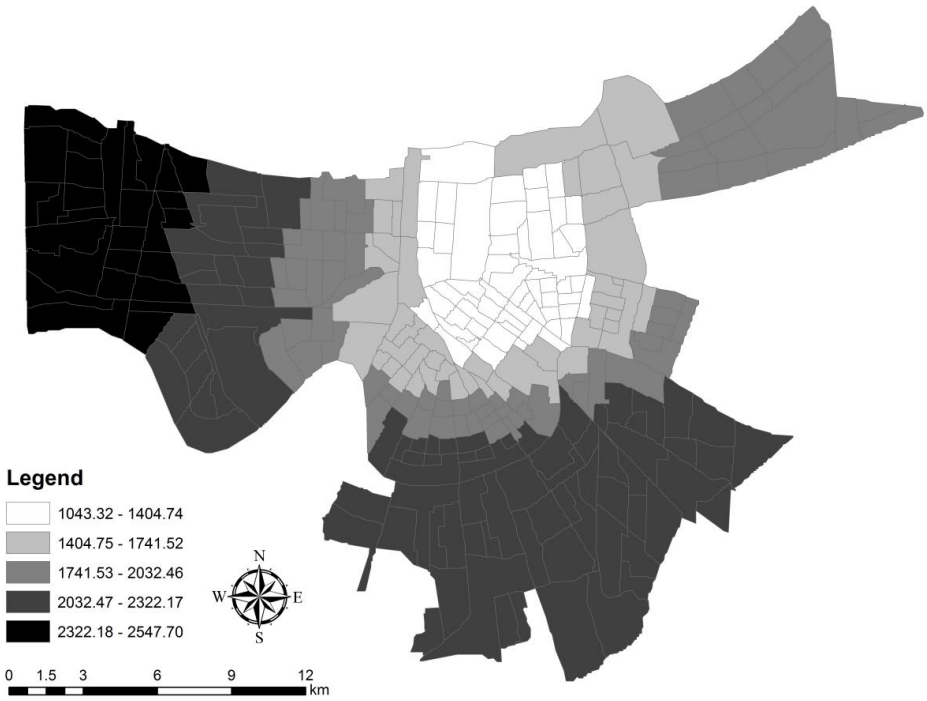

Figure 5-5 Spatial variation of the regression coefficient for “residential” land use.

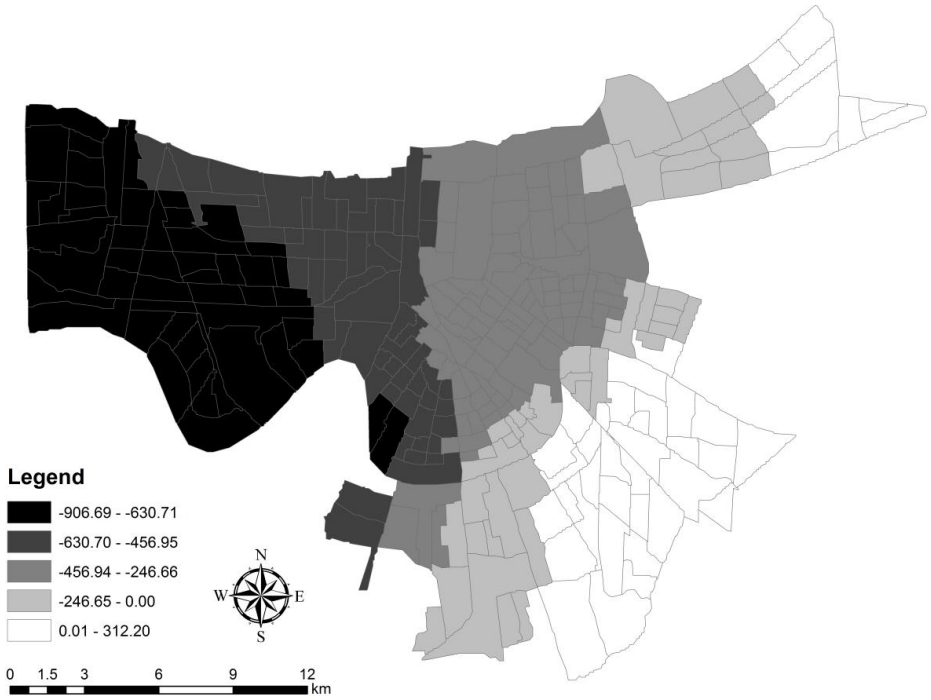

Figure 5-6 Spatial variation of the regression coefficient for “vegetation” land use.

The use of GWR model make possible to map the local model fit in terms of R^2 (Figure 5.7). It is shown that the model fit was the poorest in the city-core and becomes better as the distance from the city-core increases. The pattern of R^2 displays a concentric pattern, which is a classic urban spatial pattern of Chicago school.

Table 5.6 displays the comparison result between the OLS model and GWR model for the land use based population regression. The GWR just achieved a slightly higher prediction power than the OLS model. Generally speaking, both the OLS and GWR model failed to achieve an adequate prediction accuracy, which indicated that the population in New Orleans could not be fully modeled by just considering physiogeographic indicators.

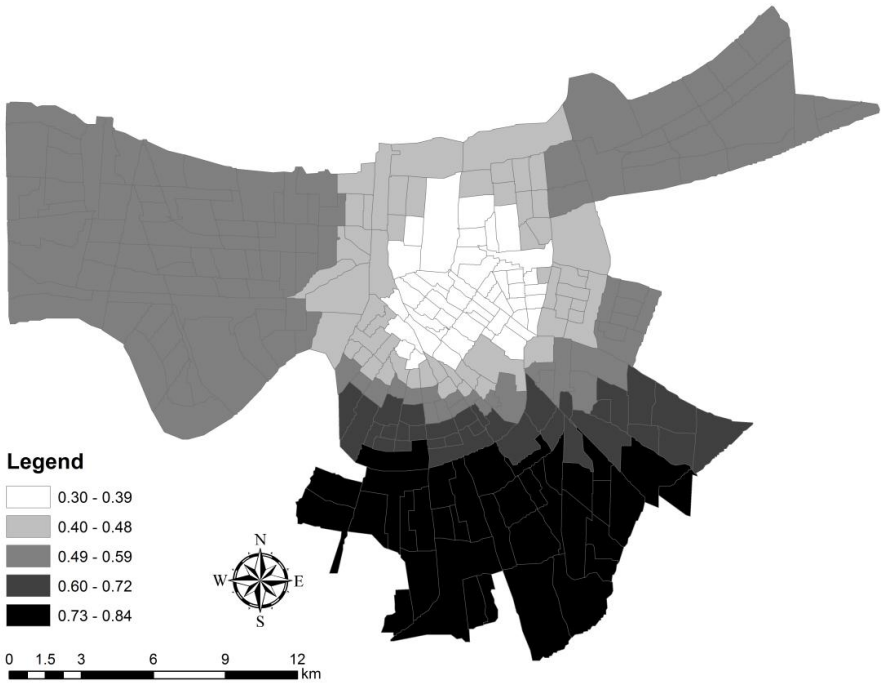

Figure 5-7 Spatial variation of the local R^2

Table 5.6 Comparison of regression model performance

Model	RMSE(TEST)	MAPE(TEST)	RMSE(TRAINING)	MAPE(TRAINING)
OLS	951.7712	0.6408385	845.0236	0.5228068
GWR	910.7484	0.6332819	725.1055	0.4791138

5.5 Conclusion

The urban population distribution could be modeled by using the physiogeographic measures derived from remote sensing. This study used two types of variables that can be derived from remotely sensed images that reflect the urban physical environment conditions: the V-I-S fractions and the land use class. OLS model and GWR model were fitted using these two types of input to examine the association between population and these inputs.

The relationship between population and the V-I-S fractions is not strong or significant. Both the global and the local model had poor model goodness-of-fit. This indicates that the direct use of V-I-S fractions to model the population is not adequate in New Orleans, although the similar applications were proven success in other urban area. The land use map extracted from the V-I-S fractions and LST achieved an overall accuracy of 78.4% and demonstrated its strength in population modeling for New Orleans. I considered the three-class model, embracing the Residential land use, Vegetation land use and the Commercial and industrial land use and exclude the water class. The OLS model returned a model with R^2=0.64. The model fitted with no intercept parameter returned a high R^2=0.89. The relationship also exhibits spatial nonstationarity. The local model fit is relatively poor in the city core and the model fit improves as the distance from the city center increases, depicting a classic concentric urban pattern.

Chapter 6 Summary

This dissertation focuses on the advances in urban environment remote sensing methodology, urban population regression model, and spatial analysis of urban population decline. Specifically, this dissertation addresses the inadequacies of previous research in the understanding of 1) the superiority of the V-I-S model and LST used in land use classification; 2) urban population modeling from the V-I-S components and other environment measurements, e.g., land use. This research chooses New Orleans, LA as the key study area, for its unique geographic settings and history of hurricane related disasters. Baton Rouge, the capital of Louisiana, is used to test the generalization of the knowledge learned from this research about remote sensing and urban study methodology.

The tasks of this research include: 1) to develop an evaluation framework for assessing and comparing classifiers and input features with an emphasize on the stability discussions; 2) to apply the proposed evaluation framework on the urban land use classification for investigating the superiorly of the V-I-S model and LST used as the classification input; 3) to implement and test the idea of urban land use classification by partitioning the V-I-S feature space using marker-controlled watershed segmentation and explore the property and advantage of this new method; and 4) to establish the relationship between the population distribution of New Orleans and physiogeographic conditions derived from remote sensing data.

6.1 Summary of findings

(1) I propose a comprehensive evaluation framework to investigate the performance of classifiers and input features for urban environment remote sensing. The framework utilizes the randomization technique to quantify the stability of classifiers, which was

generally ignored in previous remote sensing classification applications. The decision tree method is used to compare the importance and relevance of input features for a given classification context. This evaluation framework is applied in the context of the urban land use classification. Four modern classifiers are evaluated by this framework, benchmarked by the standard MLC method.

(2) In the light of a general improvement to the classifiers when the V-I-S model and LST is used in urban land use classification, some guidelines for urban remote sensing are inferred. The V-I-S fractions and LST input not only improves the accuracy, but more importantly, also improves the stability of classifiers. The tree classifier has been shown as an unstable and weak classifier when being used with conventional spectral based classification. The randomization in the tree-based ensembles improves the stability of tree classifier. V-I-S fractions and LST display more importance and relevance to urban land use classes than the conventional band reflectance as they are favored by tree and tree-based ensembles for branch splitting. The use of them also leads to less complex trees than band spectral reflectance as the classification input. These conclusions apply to the cases of both pixel-based classification and object-oriented classification. The distribution of V-I-S fractions in the feature space is close to the normal distribution which makes the normality assumption more realistic, hence, the MLC classifier, although being criticized in the literature, works well with the input of V-I-S fractions fraction and LST. The object oriented classification further improves the accuracy but not much significantly improvement is found in stability. SVM classifier is the most robust classifier for all cases. A general guideline for urban land use classification inferred from this research is that the remote sensing analyst can choose to use either object-oriented

method or the transformation from band reflectance to V-I-S images + LST to perform an adequately accurate and reliable classification. They are suggested to be used with MLC. If none of them is used, then the SVM classifier is strongly recommended.

(3) This research invented a new land use classification method. Land use classes form clusters in the V-I-S feature space. If viewed upside down, these clusters resemble topographic water catchments. Hence, a marker-controlled watershed segmentation method is explored to partition the V-I-S feature space into LULC regions to assist a semi-unsupervised classification. The result shows that when compared to a traditional MLC-based approach with V-I-S fractions, the watershed segmentation method achieves slightly higher accuracy. The markers that are used for controlling the watershed segmentation process can be specified by using on-screen digitizing and can be casually selected as long as they are close to the underlying watershed centers. This successful method adds new knowledge to the methodology of urban remote sensing and digital image processing.

(4) Regression models are employed to map the link the urban physiogeographic conditions and the population in New Orleans from the 2010 Census. Two types of input are considered: V-I-S sub-pixel fractions and land use information. The result shows that the population distribution could not be directly explained by the sub-pixel fractions in New Orleans. The land use information extracted from V-I-S fractions and LST produces a reasonable regression model with high R^2. However, neither OLS nor GWR predict the population adequately. The GWR analysis suggests the spatial nonstationarity of the relationship which displays a concentric pattern, namely, the model fit is the lowest in the city core and increases with the distance from the city center. This study indicates that

New Orleans is a sophisticated city and the population models fitted with only physiogeographic variables still have room to improve.

6.2 Suggestions for future research

In addition to V-I-S and LST, textual variables could be included as input data for image classification and evaluated in the evaluation framework. The commonly used texture algorithms are: GLCM-based textural statistics, fractal dimensions, spatial metrics, and Gabor filter. Both the fractional variables and textural variables can enhance the performance of urban LULC classification by providing the spatial information. An interesting future research track would be conducting a comparison between them with emphasize on the discussion of the classification stability.

It is necessary to test more study areas for the new watershed-segmentation-based image classification method developed in this research. The areas should cover a variety of urban types that could result in a different look in the V-I-S feature space (e.g., more/less clustering centers).

More research efforts could be devoted to consider the incorporation of the socioeconomic data collected from census survey in the urban analysis. For example, it is desirable to include socioeconomic data in the population regression model in addition to the physiogeographic measurements used in this research. The historical population can also be used to model and predict the present population. The socioeconomic data (such as the parcel data) can also be considered in the urban LULC mapping and urban land characterization. These suggest other future research tracks.

References

Adams, J. B., Sabol, D. E., Kapos, V., Almeida Filho, R., Roberts, D. A., Smith, M. O., and Gillespie, A. R., 1995, Classification of multispectral images based on fractions of endmembers: Application to land-cover change in the Brazilian Amazon. *Remote Sensing of Environment*, **52**, pp. 137-154.

Anderson, J. R., Hardy, E. E., Roach, J. T., and Witmer, R. E., 1976, A land use and land cover classification system for use with remote sensor data. *U.S. Geological Survey, Professional Paper 964*.

Anselin, L., 1988, Spatial econometrics: methods and models (Dordrecht: Kluwer Academic Publisher).

Baatz, M., and Schäpe, A., 1999, Object-oriented and multi-scale image analysis in semantic networks: In Proceedings of *2nd International Symposium: Operationalization of Remote Sensing*.

Baatz, M., and Schäpe, A., 2000, Multiresolution Segmentation: an optimization approach for high quality multi-scale image segmentation. In Angewandte Geographische Informationsverarbeitung XII. , edited by J. Strobl, T. Blaschke, and G. Griesebner (Heidelberg: Wichmann-Verlag).

Baller, R. D., Anselin, L. U. C., Messner, S. F., Deane, G., and Hawkins, D. F., 2001, Structural covariates of U.S county homicide rates: incorporating spatial effects *Criminology*, **39**, pp. 561-588.

Benz, U. C., Hofmann, P., Willhauck, G., Lingenfelder, I., and Heynen, M., 2004, Multi-resolution, object-oriented fuzzy analysis of remote sensing data for GIS-ready information. *ISPRS Journal of Photogrammetry and Remote Sensing*, **58**, pp. 239-258.

Berberoglu, S., Lloyd, C. D., Atkinson, P. M., and Curran, P. J., 2000, The integration of spectral and textural information using neural networks for land cover mapping in the Mediterranean. *Computers & Geosciences*, **26**, pp. 385-396.

Berk, A., Bernstein, L. S., and Robertson, D. C., 1989, MODTRAN: A moderate resolution model for LOWTRAN 7.

Boardman, J. W., Kruse, F. A., and Green, R. O., 1995, Mapping target signatures via partial unmixing of AVIRIS data: In Proceedings of *Summaries of 5th JPL Airborne Earth Science Workshop*.

Breiman, L., 1996, Bagging predictors. *Machine Learning*, **24**, pp. 123-140.

Breiman, L., 2001, Random forests. *Machine Learning*, **45**, pp. 5-32.

Brown, M., Gunn, S. R., and Lewis, H. G., 1999, Support vector machines for optimal classification and spectral unmixing. *Ecological Modelling*, **120**, pp. 167-179.

Brunsdon, C., Fotheringham, A. S., and Charlton, M., 1999, Some notes on parametric significance tests for geographically weighted regression. *Journal of Regional Science*, **39**, pp. 497-524.

Brunsdon, C., Fotheringham, S., and Charlton, M., 1998, Geographically weighted regression-modelling spatial non-stationarity. *Journal of the Royal Statistical Society. Series D (The Statistician)*, **47**, pp. 431-443.

Bruzzone, L., and Carlin, L., 2006, A multilevel context-based system for classification of very high spatial resolution images. *IEEE Transactions on Geoscience and Remote Sensing*, **44**, pp. 2587-2600.

Burges, C. J. C., 1998, A tutorial on support vector machines for pattern recognition. *Data Mining and Knowledge Discovery*, **2**, pp. 121-167.

Carr, J. R., 1996, Spectral and textural classification of single and multiple band digital images. *Computers & Geosciences*, **22**, pp. 849-865.

Casella, G., and Berger, R. L., 2002, Statistical inference (Pacific Grove, CA: Thomson Learning).

Chan, J., and Paelinckx, D., 2008, Evaluation of random forest and Adaboost tree-based ensemble classification and spectral band selection for ecotope mapping using airborne hyperspectral imagery. *Remote Sensing of Environment*, **112**, pp. 2999-3011.

Chan, J. C.-W., Huang, C., and DeFries, R., 2001, Enhanced algorithm performance for land cover classification from remotely sensed data using bagging and boosting. *IEEE Transactions on Geoscience and Remote Sensing*, **39**, pp. 693-695.

Chen, Q., and Gong, P., 2004, Automatic variogram parameter extraction for textural classification of the panchromatic IKONOS imagery. *IEEE Transactions on Geoscience and Remote Sensing*, **42**, pp. 1106-1115.

Chi, G., and Zhu, J., 2008, Spatial regression models for demographic analysis. *Population Research and Policy Review*, **27**, pp. 17-42.

Chica-Olmo, M., and Abarca-Hernández, F., 2000, Computing geostatistical image texture for remotely sensed data classification. *Computers & Geosciences*, **26**, pp. 373-383.

DeFries, R. S., and Chan, J. C.-W., 2000, Multiple criteria for evaluating machine learning algorithms for land cover classification from satellite data. *Remote Sensing of Environment*, **74**, pp. 503-515.

Dietterich, T. G., 2000, An experimental comparison of three methods for constructing ensembles of decision trees: Bagging, Boosting, and Randomization. *Machine Learning*, **40**, pp. 139-157.

Dobson, J. E., Brlght, E. A., Coleman, P. R., Durfee, R. C., and Worley, B. A., 2000, LandScan: a global population database for estimating populations at risk. *Photogrammetric Engineering & Remote Sensing*, **66**, pp. 849-857.

Eicher, C. L., and Brewer, C. A., 2001, Dasymetric mapping and areal interpolation: implementation and evaluation. *Cartography and Geographic Information Science*, **28**, pp. 125-138.

Emerson, C. W., Lam, N. S.-N., and Quattrochi, D. A., 2005, A comparison of local variance, fractal dimension, and Moran's I as aids to multispectral image classification. *International Journal of Remote Sensing*, **26**, pp. 1575 - 1588.

Foody, G. M., 2003, Geographical weighting as a further refinement to regression modelling: An example focused on the NDVI-rainfall relationship. *Remote Sensing of Environment*, **88**, pp. 283-293.

Foody, G. M., Boyd, D. S., and Sanchez-Hernandez, C., 2007, Mapping a specific class with an ensemble of classifiers. *International Journal of Remote Sensing*, **28**, pp. 1733 - 1746.

Foody, G. M., and Mathur, A., 2004a, A relative evaluation of multiclass image classification by support vector machines. *IEEE Transactions on Geoscience and Remote Sensing*, **42**, pp. 1335-1343.

Foody, G. M., and Mathur, A., 2004b, Toward intelligent training of supervised image classifications: directing training data acquisition for SVM classification. *Remote Sensing of Environment*, **93**, pp. 107-117.

Fotheringham, A. S., Brunsdon, C., and Charlton, M., 2002, Geographically weighted regression: the analysis of spatially varying relationships (West Sussex: Wiley).

Fotheringham, A. S., Charlton, M. E., and Brunsdon, C., 1998, Geographically weighted regression: a natural evolution of the expansion method for spatial data analysis. *Environment and Planning A*, **30**, pp. 1905-1927.

Fotheringham, S., Brunsdon, C., and Charlton, M., 2000, Quantitative geography: perspective on spatial data analysis (Thousand Oaks, CA: SAGE Publications Ltd).

Franklin, S. E., Hall, R. J., Moskal, L. M., Maudie, A. J., and Lavigne, M. B., 2000, Incorporating texture into classification of forest species composition from airborne multispectral images. *International Journal of Remote Sensing*, **21**, pp. 61-79.

Franklin, S. E., and Peddle, D. R., 1989, Spectral texture for improved class discrimination in complex terrain *International Journal of Remote Sensing*, **10**, pp. 1437-1443.

Franklin, S. E., and Peddle, D. R., 1990, Classification of SPOT HRV imagery and texture features *International Journal of Remote Sensing*, **11**, pp. 551-556.

Freund, R. J., and Wilson, W. J., 2002, Statistical methods, 2nd edition (Boston: Academic Press).

Friedl, M. A., and Brodley, C. E., 1997, Decision tree classification of land cover from remotely sensed data. *Remote Sensing of Environment*, **61**, pp. 399-409.

Fussell, E., Sastry, N., and VanLandingham, M., 2010, Race, socioeconomic status, and return migration to New Orleans after Hurricane Katrina. *Population Environment*, **31**, pp. 20-42.

Geneletti, D., and Gorte, B. G. H., 2003, A method for object-oriented land cover classification combining Landsat TM data and aerial photographs. *International Journal of Remote Sensing*, **24**, pp. 1273-1286.

Gislason, P. O., Benediktsson, J. A., and Sveinsson, J. R., 2006, Random forests for land cover classification. *Pattern Recognition Letters*, **27**, pp. 294-300.

Gong, P., Marceau, D. J., and Howarth, P. J., 1992, A comparison of spatial feature extraction algorithms for land-use classification with SPOT HRV data. *Remote Sensing of Environment*, **40**, pp. 137-151.

Goodchild, M. F., Anselin, L. U. C., and Deichmann, U., 1993, A framework for the areal interpolation of socioeconomic data. *Environment and Planning A*, **25**, pp. 383-397.

Goodchild, M. F., and Lam, N., 1980, Areal interpolation: a variant of the traditional spatial problem. *Geo-Processing*, **1**, pp. 297-312.

Griffith, D., and Wong, D., 2007, Modeling population density across major US cities: a polycentric spatial regression approach. *Journal of Geographical Systems*, **9**, pp. 53-75.

Groen, J. A., and Polivka, A. E., 2009, Going home after hurricane Katrina: determinants of return migration and changes in affected areas, *U.S. Bureau of Labor Statistics*.

Gruninger, J., Ratkowski, A. J., and Hoke, M. L., 2004, The sequential maximum angle convex cone (SMACC) endmember model. *Proceedings of SPIE, Algorithms for Multispectral and Hyper-spectral and Ultraspectral Imagery*, **5425-1**.

Guo, B., Gunn, S. R., Damper, R. I., and Nelson, J. D. B., 2008a, Customizing kernel functions for SVM-based hyperspectral image classification. *IEEE Transactions on Image Processing*, **17**, pp. 622-629

Guo, Q., Du, G., Liu, Y., and Liu, D., 2008b, Integrating object-based classification with one-class support vector machines in mapping a specific land class from high spatial resolution images. *The International Archives of the Photogrammetry, Remote Sensing and Spatial Information Sciences*, **XXXVII**.

Gustafson, E. J., 1998, Quantifying landscape spatial pattern: what Is the state of the art? *Ecosystems*, **1**, pp. 143-156.

Ham, J., Yangchi, C., Crawford, M. M., and Ghosh, J., 2005, Investigation of the random forest framework for classification of hyperspectral data. *IEEE Transactions on Geoscience and Remote Sensing*, **43**, pp. 492-501.

Haralick, R. M., Shanmugam, K., and Dinstein, I. h., 1973, Textural features for image classification. *IEEE Transactions on Systems, Man, and Cybernetics*, **6**, pp. 610-621.

Harvey, J. T., 2002a, Estimating census district populations from satellite imagery: Some approaches and limitations. *International Journal of Remote Sensing*, **23**, pp. 2071-2095.

Harvey, J. T., 2002b, Population estimation models based on individual TM pixels. *Photogrammetric Engineering & Remote Sensing*, **68**, pp. 1181-1192.

Hastie, T., Tibshirani, R., and Friedman, J., 2009, The elements of statistical learning, data mining, inference, and prediction, 2nd edition (New York, NY: Springer).

Herold, M., Liu, X., and Clarke, K. C., 2003, Spatial metrics and image texture for mapping urban land use. *Photogrammetric Engineering & Remote Sensing*, **69**, pp. 991-1001.

Herold, M., Scepan, J., and Clarke, K. C., 2002, The use of remote sensing and landscape metrics to describe structures and changes in urban land uses. *Environment and Planning A*, **34**, pp. 1443-1458.

Hsu, S.-Y., 1973, Population estimation from ERTS imagery - Methodology and evaluation In Proceedings of *American Society of Photogrammetry, Annual Meeting, 39th*, pp. 583-591.

Hu, X., and Weng, Q., 2009, Estimating impervious surfaces from medium spatial resolution imagery using the self-organizing map and multi-layer perceptron neural networks. *Remote Sensing of Environment*, **113**, pp. 2089–2102.

Hu, X., and Weng, Q., 2010a, Estimation of impervious surfaces of Beijing, China, with spectral normalized images using LSMA and ANN. *Geocarto International*, **25**, pp. 231-253.

Hu, X., and Weng, Q., 2010b, Impervious surface area extraction from IKONOS imagery using an objectbased fuzzy method. *Geocarto International*, **26**, pp. 3-20.

Huang, C., Davis, L. S., and Townshend, J. R. G., 2002, An assessment of support vector machines for land cover classification. *International Journal of Remote Sensing*, **23**, pp. 725-749.

Ifarraguerri, A., and Chang, C.-I., 1999, Multispectral and hyperspectral image analysis with convex cones. *IEEE Transactions on Geoscience and Remote Sensing*, **37**, pp. 756-770.

Iisaka, J., and Hegedus, E., 1982, Population estimation from Landsat imagery. *Remote Sensing of Environment*, **12**, pp. 259-272.

Jensen, J. R., 2007, Remote rensing of the environment: an earth resource perspective, 2nd edition (N.J.: Prentice Hall).

Jiménez-Muñoz, J. C., and Sobrino, J. A., 2003, A generalized single-channel method for retrieving land surface temperature from remote sensing data. *Journal of Geophysical Research*, **108**, pp. 4688.

Joelsson, S. R., Benediktsson, J. A., and Sveinsson, J. R., 2005, Random forest classifiers for hyperspectral data: In Proceedings of *Geoscience and Remote Sensing Symposium, 2005. IGARSS '05. Proceedings. 2005 IEEE International*, pp. 160-163.

Joseph, M., Wang, L., and Wang, F., 2012, Using Landsat ETM Imagery for population estimation in Port-au-Prince, Haiti. *GIScience & Remote Sensing*, **49**, pp. 228-250.

Kaplan, D., Wheeler, J. O., and Holloway, S., 2008, Urban geography, 2nd edition (New York, NY: Wiley, John & Sons, Inc).

Kaya, S., Llewellyn, G., and Curran, P. J., 2004, Displaying earthquake damage: an urban area using a vegetation-impervious-soil model and remotely sensed data: In Proceedings of *International Society for Photogrammetry and Remote Sensing Conference*, pp. 634-638.

Kim, H. H., 1992, Urban heat island. *International Journal of Remote Sensing*, **13**, pp. 2319 - 2336.

Laliberte, A. S., Rango, A., Havstad, K. M., Paris, J. F., Beck, R. F., McNeely, R., and Gonzalez, A. L., 2004, Object-oriented image analysis for mapping shrub encroachment from 1937 to 2003 in southern New Mexico. *Remote Sensing of Environment*, **93**, pp. 198-210.

Lam, N., 1983, Spatial interpolation methods: a review. *The American Cartographer*, **10**, pp. 129-149.

Landsat Project Science Office, 2002, Landsat 7 science data user's handbook.

Langford, M., 2006, Obtaining population estimates in non-census reporting zones: An evaluation of the 3-class dasymetric method. *Computers, Environment and Urban Systems*, **30**, pp. 161-180.

Langford, M., Maguire, D. J., and Unwin, D. J., 1991, The areal interpolation problem: estimating population using remote sensing in a GIS framework. In Handling Geographical Information: Methodology and Potential Applications, edited by I. Masser, and M. Blakemore (New York, NY: Wiley).

Langford, M., and Unwin, D. J., 1994, Generating and mapping population density surfaces within a geographical information system. *The Cartographic Journal*, **31**, pp. 21-26.

Lark, R. M., 1996, Geostatistical description of texture on an aerial photograph for discriminating classes of land cover. *International Journal of Remote Sensing*, **17**, pp. 2115-2133.

Lawrence, R., Bunn, A., Powell, S., and Zambon, M., 2004, Classification of remotely sensed imagery using stochastic gradient boosting as a refinement of classification tree analysis. *Remote Sensing of Environment*, **90**, pp. 331-336.

Lawrence, R. L., Wood, S. D., and Sheley, R. L., 2006, Mapping invasive plants using hyperspectral imagery and Breiman Cutler classifications (randomForest). *Remote Sensing of Environment*, **100**, pp. 356-362.

Lawrence, R. L., and Wright, A., 2001, Rule-based classification systems using classification and regression tree (CART) analysis. *Photogrammetric Engineering & Remote Sensing*, **67**, pp. 1137-1142.

Leung, Y., Mei, C. L., and Zhang, W. X., 2000, Statistical tests for spatial nonstationarity based on the geographically weighted regression model. *Environment and Planning A*, **32**, pp. 9-32.

Li, G., and Wan, Y., 2010, Remote sensing image classification based on improved watershed segmentation and fuzzy support vector machine: In Proceedings of *International Conference on Computer Design and Applications*.

Li, G., and Weng, Q., 2005, Using Landsat ETM+ imagery to measure population density in Indianapolis, Indiana, USA. *Photogrammetric Engineering and Remote Sensing*, **71**, pp. 947-958.

Li, G., and Weng, Q., 2010, Fine-scale population estimation: how Landsat ETM+ imagery can improve population distribution mapping? *Canadian Journal of Remote Sensing*, **36**, pp. 155-165.

Li, J., and Zhao, H. M., 2003, Detecting urban land-use and land-cover changes in Mississauga using Landsat TM images. *Journal of Environmental Informatics*, **2**, pp. 38-47.

Li, P., Guo, J., Song, B., and Xiao, X., 2010a, A multilevel hierarchical image segmentation method for urban impervious surface mapping using very high resolution imagery. *Journal of Selected Topics in Applied Earth Observations and Remote Sensing*, **4**, pp. 103-116.

Li, P., and Xiao, X., 2007, Multispectral image segmentation by a multichannel watershed-based approach. *International Journal of Remote Sensing*, **28**, pp. 4429 - 4452.

Li, P., and Xu, H., 2010, Land-cover change detection using one-class support vector machine. *Photogrammetric Engineering and Remote Sensing*, **76**, pp. 255-263.

Li, P., Xu, H., and Guo, J., 2010b, Urban building damage detection from very high resolution imagery using OCSVM and spatial features. *International Journal of Remote Sensing*, **31**, pp. 3393-3409.

Li, W., and Guo, Q., 2010, maximum entropy approach to one-class classification of remote sensing imagery. *International Journal of Remote Sensing*, **31**, pp. 2227-2235.

Li, W., Guo, Q., and Elkan, C., 2011, A positive and unlabeled learning algorithm for one-class classification of remote sensing data. *IEEE Transactions on Geoscience and Remote Sensing*, **49**, pp. 717 - 725.

Liaw, A., and Wiener, M., 2002, Classification and regression by randomForest. *R News*, **2/3**, pp. 18-22.

Liu, X., 2003, Estimation of the spatial distribution of urban population using high spatial resolution satellite imagery. *Dissertation, University of California, Santa Barbara*.

Liu, X., Clarke, K., and Herold, M., 2006, Population density and image texture: a comparison study. *Photogrammetric Engineering & Remote Sensing*, **72**, pp. 187-196.

Liu, Z. H., Wang, J., and Liu, W. P., 2005, Building extraction from high resolution imagery based on multi-scale object oriented classification and probabilistic Hough transform: In Proceedings of *IEEE International Geoscience and Remote Sensing Symposium*, pp. 2250–2253.

Lloyd, C. D., 2006, Local models for spatial statistics (Boca Raton: CRC Press, Taylor & Francis Group).

Lo, C. P., 1995, Automated population and dwelling unit estimation from high-resolution satellite images: a GIS approach. *International Journal of Remote Sensing*, **16**, pp. 17 - 34.

Lo, C. P., 2001, Modeling the population of China using DMSP operational linescan system nighttime data. *American Society for Photogrammetry and Remote Sensing*, **67**, pp. 1037-1047.

Lo, C. P., 2003, Zone-based estimation of population and housing units from satelittle-generated land use/land cover maps. In Remotely Sensed Cities edited by V. Mesev(New York: Taylor & Francis Inc), pp. 368.

Lo, C. P., 2008, Population estimation using geographically weighted regression *GIScience & Remote Sensing*, **45**, pp. 131-148.

Lo, C. P., Quattrochi, D. A., and Luvall, J. C., 1997, Application of high-resolution thermal infrared remote sensing and GIS to assess the urban heat island effect. *International Journal of Remote Sensing*, **18**, pp. 287 - 304.

Lu, D., Hetrick, S., and Moran, E., 2010, Land cover classification in a complex urban-rural landscape with QuickBird imagery. *Photogrammetric Engineering & Remote Sensing*, **76**, pp. 1159-1168.

Lu, D., Moran, E., and Batistella, M., 2003, Linear mixture model applied to Amazonian vegetation classification. *Remote Sensing of Environment*, **87**, pp. 456-469.

Lu, D., and Weng, Q., 2004, Spectral mixture analysis of the urban landscape in Indianapolis with Landsat ETM+ imagery. *Photogrammetric Engineering & Remote Sensing*, **70**, pp. 1053-1062.

Lu, D., and Weng, Q., 2005, Urban classification using full spectral information of Landsat ETM+ imagery in Marion County, Indiana. *Photogrammetric Engineering and Remote Sensing*, **71**, pp. 1275-1284.

Lu, D., and Weng, Q., 2006, Use of impervious surface in urban land-use classification. *Remote Sensing of Environment*, **102**, pp. 146-160.

Maantay, J. A., Maroko, A. R., and Herrmann, C., 2007, Mapping population distribution in the urban environment: the cadastral-based expert dasymetric system (CEDS). *Cartography and Geographic Information Science*, **34**, pp. 77-102.

Madhavan, B. B., Kubo, S., Kurisaki, N., and Sivakumar, T. V. L. N., 2001, Appraising the anatomy and spatial growth of the Bangkok Metropolitan area using a vegetation-impervious-soil model through remote sensing. *International Journal of Remote Sensing*, **22**, pp. 789-806.

Maillard, P., 2003, Comparing texture analysis methods through classification. *Photogrammetric Engineering & Remote Sensing*, **69**, pp. 357-367.

Margineantu, D. D., and Dietterich, T. G., 1997, Pruning adaptive boosting: In Proceedings of *Fourteenth International Conference on Machine Learning*, pp. 211-218.

Mark, D. P., Dan, S. R., Kamar, A., and Olfert, M. R., 2008, The geographic diversity of U.S. nonmetropolitan growth dynamics: a geographically weighted regression approach. *Land Economics*, **84**, pp. 241-266.

Martin, D., 1989, Mapping population data from zone centroid locations. *Transactions of the Institute of British Geographers*, **14**, pp. 90-97.

Mathur, A., and Foody, G. M., 2008, Crop classification by support vector machine with intelligently selected training data for an operational application. *International Journal of Remote Sensing*, **29**, pp. 2227-2240.

Mayor's Office of Environment Affairs, 2001, City of New Orleans baseline greenhouse gas emissions profile. pp. 1-11.

McGarigal, K., Cushman, S., Neel, M., and Ene, E., 2002, RAGSTATS: spatial pattern analysis program for categorical maps.

Melgani, F., and Bruzzone, L., 2004, Support vector machines for classification of hyperspectral remote-sensing images *IEEE Transactions on Geoscience and Remote Sensing*, **42**, pp. 1778 - 1790.

Mennis, J., 2003, Generating surface models of population using dasymetric mapping. *The Professional Geographer*, **55**, pp. 31-42.

Mesev, V., 2010, Classification of urban areas: inferring land use from the interpretation of land cover. In Remote Sensing of Urban and Suburban Areas, Remote Sensing

and Digital Image Processing 10, edited by T. Rashed, and C. Jürgens(New York: Springer), pp. 144.

Morton, T. A., and Yuan, F., 2009, Analysis of population dynamics using satellite remote sensing and US census data. *Geocarto International*, **24**, pp. 143 - 163.

Mountrakis, G., Im, J., and Ogole, C., 2010, Support Vector Machines in Remote Sensing: A Review. *ISPRS Journal of Photogrammetry and Remote Sensing*.

Mũnoz-Marí, J., Bovolo, F., Gómez-Chova, L., Bruzzone, L., and Camp-Valls, G., 2010, Semisupervised one-class support vector machines for classification of remote sensing data *IEEE Transactions on Geoscience and Remote Sensing*, **48**, pp. 3188-2892.

Myint, S. W., 2003, Fractal approaches in texture analysis and classification of remotely sensed data: Comparisons with spatial autocorrelation techniques and simple descriptive statistics. *International Journal of Remote Sensing*, **24**, pp. 1925-1947.

Myint, S. W., Giri, C. P., Wang, L., Zhu, Z., and Gillette, S. C., 2008, Identifying mangrove species and their surrounding land use and land cover classes using an object-oriented approach with a lacunarity spatial measure. *GIScience & Remote Sensing*, **45**, pp. 188-208.

Myint, S. W., Gober, P., Brazel, A., Grossman-Clarke, S., and Weng, Q., 2011, Per-pixel versus object-based classification of urban land cover extraction using high spatial resolution imagery. *Remote Sensing of Environment*, **115**, pp. 1145-1161.

Myint, S. W., and Lam, N., 2005a, A study of lacunarity-based texture analysis approaches to improve urban image classification. *Computers, Environment and Urban Systems*, **29**, pp. 501-523.

Myint, S. W., and Lam, N. S.-N., 2005b, Examining lacunarity approaches in comparison with fractal and spatial autocorrelation techniques for urban mapping. *Photogrammetric Engineering & Remote Sensing*, **71**, pp. 927-937.

Myint, S. W., Mesev, V., and Lam, N. S.-N., 2006, Urban textural analysis from remote sensor data lacunarity measurements based on the differential box counting method. *Geographical Analysis*, **38**, pp. 371-390.

Pal, M., and Foody, G. M., 2010, Feature selection for classification of hyperspectral data by SVM. *IEEE Transactions on Geoscience and Remote Sensing*, **48**, pp. 2297-2307.

Pal, M., and Mather, P. M., 2003, An assessment of the effectiveness of decision tree methods for land cover classification. *Remote Sensing of Environment*, **86**, pp. 554-565.

Phinn, S., Stanford, M., Scarth, P., Murray, A. T., and Shyy, P. T., 2002, Monitoring the composition of urban environments based on the vegetation-impervious surface-soil (VIS) model by subpixel analysis techniques. *International Journal of Remote Sensing*, **23**, pp. 4131 - 4153.

Powell, R. L., Roberts, D. A., Dennison, P. E., and Hess, L. L., 2007, Sub-pixel mapping of urban land cover using multiple endmember spectral mixture analysis: Manaus, Brazil. *Remote Sensing of Environment*, **106**, pp. 253-267.

Qin, Z., Karnieli, A., and Berliner, P., 2001, A mono-window algorithm for retrieving land surface temperature from Landsat TM data and its application to the Israel-Egypt border region. *International Journal of Remote Sensing*, **22**, pp. 3719 - 3746.

Rase, W.-D., 2001, Volume-preserving interpolation of a smooth surface from polygon-related data. *Journal of Geographical Systems*, **3**, pp. 199-213.

Rashed, T., Weeks, J. R., Gadalla, M. S., and Hill, A. G., 2001, Revealing the anatomy of cities through spectral mixture analysis of multispectral satellite imagery: A case study of the Greater Cairo Region, Egypt. *Geocarto International*, **16**, pp. 7-18.

Rashed, T., Weeks, J. R., Roberts, D., Rogan, J., and Powell, R., 2003, Measuring the physical composition of urban morphology using multiple endmember spectral mixture models. *Photogrammetric Engineering & Remote Sensing*, **69**, pp. 1011-1020.

Ravikumar, R., 2008, Multi-scale texture analysis of remote sensing images using Gabor filter banks and wavelet transforms. Thesis: Texas A&M University, College City, 127 pp.

Richards, J. A., and Jia, X., 2006, Remote sensing digital image analysis: an introduction, 4th edition (Berlin: Springer).

Ridd, M. K., 1995, Exploring a V-I-S (vegetation-impervious surface-soil) model for urban ecosystem analysis through remote sensing: comparative anatomy for cities. *International Journal of Remote Sensing*, **16**, pp. 2165 - 2185.

Roberts, D. A., Gardner, M., Church, R., Ustin, S., Scheer, G., and Green, R. O., 1998, Mapping chaparral in the Santa Monica Mountains using multiple endmember spectral mixture models. *Remote Sensing of Environment*, **65**, pp. 267-279.

Sanchez-Hernandez, C., Boyd, D. S., and Foody, G. M., 2007, One-class classification for mapping a specific land cover class: SVDD classification of Fenland. *IEEE Transactions on Geoscience and Remote Sensing*, **45**, pp. 1062-1073.

Schmugge, T., Hook, S. J., and Coll, C., 1998, Recovering surface temperature and emissivity from thermal infrared multispectral data. *Remote Sensing of Environment*, **65**, pp. 121-131.

Schölkopf, B., and Smola, A. J., 2002, Learning with kernels: support vector machines, regularization, optimization, and beyond, 1st edition (Cambridge, MA: MIT Press).

Settle, J. J., and Drake, N. A., 1993, Linear mixing and the estimation of ground cover proportions. *International Journal of Remote Sensing*, **14**, pp. 1159-1177.

Shackelford, A. K., and Davis, C. H., 2003, A combined fuzzy pixel-based and object-based approach for classification of high-resolution multispectral data over urban areas. *IEEE Transactions on Geoscience and Remote Sensing*, **41**, pp. 2354 - 2363

Small, C., 2001, Estimation of urban vegetation abundance by spectral mixture analysis. *International Journal of Remote Sensing*, **22**, pp. 1305-1334.

Small, C., and Lu, J. W. T., 2006, Estimation and vicarious validation of urban vegetation abundance by spectral mixture analysis. *Remote Sensing of Environment*, **100**, pp. 441-456.

Sobrino, J. A., Jiménez-Muñoz, J. C., and Paolini, L., 2004, Land surface temperature retrieval from LANDSAT TM 5. *Remote Sensing of Environment*, **90**, pp. 434-440.

Soille, P., 2002, Morphological image analysis: principles and applications, 2nd edition (Berlin: Springer).

Souza, C. M., Roberts, D. A., and Cochrane, M. A., 2005, Combining spectral and spatial information to map canopy damage from selective logging and forest fires. *Remote Sensing of Environment*, **98**, pp. 329-343.

Sutton, P., 1997, Modeling population density with night-time satellite imagery and GIS. *Computers, Environment and Urban Systems*, **21**, pp. 227-244.

Tang, Q., 2008, Research on remote sensing software system development methodology and cases using IDL & ENVI redevelopment technology. Thesis: Chinese Academy of Sciences, Beijing.

Tang, Q., Wang, L., Li, B., and Yu, J., 2012, Towards a comprehensive evaluation of V-I-S sub-pixel fractions and land surface temperature for urban land-use classification in the USA. *International Journal of Remote Sensing*, **33**, pp. 5996-6019.

Tax, D. M. J., and Duin, R. P. W., 2004, Support vector data description. *Machine Learning*, **54**, pp. 45-66.

Tobler, W. R., 1979, Smooth pycnophylactic interpolation for geographical regions. *Journal of the American Statistical Association*, **74**, pp. 519-530.

Van Coillie, F. M. B., Verbeke, L. P. C., and De Wulf, R. R., 2007, Feature selection by genetic algorithms in object-based classification of IKONOS imagery for forest mapping in Flanders, Belgium. *Remote Sensing of Environment*, **110**, pp. 476-487.

Vincent, L., 1993, Morphological grayscale reconstruction in image analysis: applications and efficient algorithms. *IEEE Transactions on Image Processing*, **2**, pp. 176-201.

Vincent, L., and Soille, P., 1991, Watersheds in digital spaces: an efficient algorithm based on immersion simulations. *IEEE TRansactions on Pattern Analysis and Machine Intelligence*, **13**, pp. 583-598.

Voogt, J., 2003, Thermal remote sensing of urban climates. *Remote Sensing of Environment*, **86**, pp. 370-384.

Voorde, T. V. d., Vlaeminck, J., and Canters, F., 2008, Comparing different approaches for mapping urban vegetation cover from Landsat ETM+ data: A case study on Brussels. *Sensors*, **8**, pp. 3880-3902.

Walter, V., 2004, Object-based classification of remote sensing data for change detection. *ISPRS Journal of Photogrammetry and Remote Sensing*, **58**, pp. 225-238.

Wang, C., Du, Z., Liu, Z., and Liu, Y., 2008, Study on decision tree land cover classification based on MODIS data: In Proceedings of *Earth Observation and Remote Sensing Applications, 2008. EORSA 2008. International Workshop on*, pp. 1-6.

Wang, L., Sousa, W. P., and Gong, P., 2004, Integration of object-based and pixel-based classification for mapping mangroves with IKONOS imagery. *International Journal of Remote Sensing*, **25**, pp. 5655-5668.

Ward, D., Phinn, S. R., and Murray, A. T., 2000, Monitoring growth in rapidly urbanizing areas using remotely sensed data. *The Professional Geographer*, **52**, pp. 371-386.

Weng, Q., 2001, A remote sensing-GIS evaluation of urban expansion and its impact on surface temperature in the Zhujiang Delta, China. *International Journal of Remote Sensing*, **22**, pp. 1999-2014.

Weng, Q., 2009, Thermal infrared remote sensing for urban climate and environmental studies: Methods, applications, and trends. *ISPRS Journal of Photogrammetry and Remote Sensing*, **64**, pp. 335-344.

Weng, Q., and Hu, X., 2008, Medium spatial resolution satellite imagery for estimating and mapping urban impervious surfaces using LSMA and ANN. *IEEE Transactions on Geoscience and Remote Sensing*, **46**, pp. 2397-2406.

Weng, Q., Liu, H., and Lu, D., 2007, Assessing the effects of land use and land cover patterns on thermal conditions using landscape metrics in city of Indianapolis, United States. *Urban Ecosystems*, **10**, pp. 203-219.

Weng, Q., Lu, D., and Liang, B., 2006, Urban surface biophysical descriptors and land surface temperature variations. *Photogrammetric Engineering and Remote Sensing*, **72**, pp. 1275-1286.

Weng, Q., Lu, D., and Schubring, J., 2004, Estimation of land surface temperature-vegetation abundance relationship for urban heat island studies. *Remote Sensing of Environment*, **89**, pp. 467-483.

Weng, Q., and Quattrochi, D. A., 2007, Urban remote sensing, 1st edition (Boca Raton, FL: Taylor & Francis Group, LLC).

Winter, M. E., 1999, N-FINDER: an algorithm for fast autonomous spectral end-member determination in hyperspectral data. *Proceedings of SPIE*, **3753**, pp. 226-275.

Wright, J. K., 1936, A method of mapping densities of population: with Cape Cod as an example. *Geographical Review*, **26**, pp. 103-110.

Wu, C., 2004, Normalized spectral mixture analysis for monitoring urban composition using ETM+ imagery. *Remote Sensing of Environment*, **93**, pp. 480-492.

Wu, C., and Murray, A. T., 2003, Estimating impervious surface distribution by spectral mixture analysis. *Remote Sensing of Environment*, **84**, pp. 493-505.

Wu, C., and Murray, A. T., 2005, A cokriging method for estimating population density in urban areas. *Computers, Environment and Urban Systems*, **29**, pp. 558-579.

Wu, C., and Murray, A. T., 2007, Population estimation using Landsat Enhanced Thematic Mapper imagery. *Geographical Analysis*, **39**, pp. 26-43.

Wu, S., Qiu, X., and Wang, L., 2006, Urban land-use classification using variogram-based analysis with an aerial photograph. *Photogrammetric Engineering & Remote Sensing*, **72**, pp. 813-822.

Xu, H., and Li, P., 2010, Urban land cover classification from very high resolution imagery using spectral and invariant moment shape information *Canadian Journal of Remote Sensing*, **36**, pp. 248-260.

Yang, L., Chengquan, H., Homer, C. G., Wylie, B. K., and Coan, M. J., 2003a, An approach for mapping large-area impervious surfaces synergistic use of Landsat-7 ETM+ and high spatial resolution imagery. *Canadian Journal of Remote Sensing*, **29**, pp. 230-240.

Yang, L., Xian, G., Klaver, J. M., and Deal, B., 2003b, Urban land-cover change detection through sub-pixel imperviousness mapping using remotely sensed data. *Photogrammetric Engineering & Remote Sensing*, **69**, pp. 1003-1010.

Yu, D., and Wu, C., 2004, Understanding population segregation from Landsat ETM+ imagery: a geographically weighted regression approach. *GIScience & Remote Sensing*, **41**, pp. 187-206.

Yu, D. L., 2006, Spatially varying development mechanisms in the Greater Beijing Area: a geographically weighted regression investigation. *The Annals of Regional Science*, **40**, pp. 173-190.

Yuan, F., and Bauer, M. E., 2006, Mapping impervious surface area using high resolution imagery: a comparison of object-sased and per pixel classification: In Proceedings of *Annual Conference of American Society of Photogrammetry and Remote Sensing*.

Yuan, F., and Bauer, M. E., 2007, Comparison of impervious surface area and normalized difference vegetation index as indicators of surface urban heat island effects in Landsat imagery. *Remote Sensing of Environment*, **106**.

Yuan, Y., Smith, R. M., and Limp, W. F., 1997, Remodeling census population with spatial information from LandSat TM imagery. *Computers, Environment and Urban Systems*, **21**, pp. 245-258.

Zhou, W., and Troy, A., 2008, An object-oriented approach for analysing and characterizing urban landscape at the parcel level. *International Journal of Remote Sensing*, **29**, pp. 3119-3135.

Zhou, Y., and Wang, Y. Q., 2008, Extraction of impervious surface areas from high spatial resolution imagery by multiple agent segmentation and classification. *Photogrammetric Engineering & Remote Sensing*, **74**, pp. 857–868.

Vita

Quan Tang was born in Wuhu City, Anhui Province, China. He went to Beijing for college on August, 2001 (one month after Beijing won the bid for hosting 2008 Summer Olympics). After exposure to information system and information science, he attended Chinese Academy of Sciences for study of GIS and remote sensing starting 2005 fall. He traveled to the United States for Ph.D study just two days prior to the opening ceremony of 2008 Beijing Olympics. In the last four years, he has been working for Department of Geography and Anthropology as a teaching assistant and a GIS developer and analyst for Office of Parking, Traffic and Transportation at LSU. His research concentrated on the analysis of urban land use and population distribution with a variety of tools, including remote sensing, GIS and (spatial) statistics. While pursuing the Ph.D, he obtained Master Degree in Applied Statistics from Department of Experimental Statistics at LSU in 2011.